

Modeling an EDC Cracker using Computational Fluid Dynamics (CFD)

Torbjørn Herder Kaggerud

Master of Science in Energy and Environment
Submission date: June 2007
Supervisor: Truls Gundersen, EPT

Problem Description

The main objective of this Master's thesis is to develop a model for EDC cracking by integrating a CFD model for the firebox with a reactor model for the cracking reaction in the coils.

The work is divided into three parts:

1. Establish a Fluent model for the firebox based on a simplified representation of the burners. The burners are represented as source terms for heat and flue gas based on the simulations of a single burner conducted through the project work.
2. Include the reactor coil in the model with heatflux as the interface. The model is simplified by assuming homogenous temperature over the cross section of the coil, and that the firebox is symmetrical in a plane parallel to the coils. The heatflux along the reaction coil is calculated using EDC CRACK.
3. Integrate the CFD model with the Matlab model for the reaction coil, including: (a) understand how interfaces are defined in Fluent, (b) evaluate alternative solutions for the EDC cracking model, (c) develop the model, (d) compare the results with corresponding simulations conducted with EDC CRACK, and (e) suggest further work for refining the model. The third part is regarded as very challenging and it will be regarded as a plus if the candidate attains this target.

Assignment given: 15. January 2007

Supervisor: Truls Gundersen, EPT

Preface

This report is the result of the course TEP 4900 Heat and Energy Processes, Specialisation. The work has been conducted during the period January to June 2007, as a cooperation between Hydro's Oil and Energy Research Centre in Porsgrunn, and the department of Energy and Process Engineering at the Norwegian University of Science and Technology in Trondheim.

I would like to thank my supervisor at the university, professor Truls Gundersen, for his support and guidance. I would also like to thank my supervisors at Hydro, Terje Fuglerud, for introducing me to the details of the VCM process, and Eirik Manger for numerous tips and tricks in Fluent. I would also like to thank Petter Saxegaard for his many instructive tips and input during the spring. The possibility to run the Fluent simulations on Hydro's multiple compute node mainframe has reduced computation times significantly.

A thanks also to the entire petrochemicals department at the Research Centre, and especially head of department Steinar Kvisle, for making me feel very welcome.

Finally, thank you to my girlfriend Siw-Christin Aaserud, for always believing in me, and of course for finding more misprints than I thought possible.

Norsk Hydro's Research Centre, Porsgrunn/Department of Energy and Process Engineering, Trondheim, 07.06.2007

Torbjørn Herder Kaggerud

Abstract

The process used by the Norwegian company Hydro for making Vinyl Chloride Monomer (VCM) from natural gas and sodium chloride has been studied. A three dimensional CFD model representing the firebox of the EDC cracker has been developed using the commercial CFD tool Fluent. Heat to the cracker is delivered by means of combustion of a fuel gas consisting of methane and hydrogen. In the developed CFD model used in this work, the combustion reaction itself is omitted, and heat is delivered by hot flue gas. With the combustion reaction left out, the only means of tuning the CFD model is through the flue gas inlet temperature. With the flue gas inlet temperature near the adiabatic flame temperature, the general temperature level of the EDC cracker was reported to be too high. The outer surface temperature of the coil was reported to be 3-400 K higher than what was expected. By increasing the mass flow of flue gas and decreasing the temperature, the net delivered heat to the firebox was maintained at the same level as the first case, but the temperature on the coil was reduced by 100-150 K. Further reductions in the flue gas inlet temperature and modifications in the mass flow of flue gas at the different burner rows, eventually gave temperature distributions along the reaction coil, and flue gas and refractory temperatures, that resemble those in the actual cracker.

The one-dimensional reactor model for the cracking reaction represents the actual cracker in a satisfactorily manner. The cracking reaction was simulated using a simple, global reaction mechanism, thus only the main components of the process fluid, EDC, VCM and HCl, can be studied. The model is written in a way suitable for implementation of more detailed chemical reaction mechanisms. The largest deviation in temperature between measured and simulated data are about 5%. At the outlet the temperature of the process fluid is equal to the measured data. The conversion of EDC out of the firebox is assumed to be 50 wt-%, this value is met exactly by the model.

Contents

1	Introduction	1
2	Hydro Polymers Stenungsund	3
2.1	VCM production	3
2.1.1	Chlorine production	3
2.1.2	EDC production	4
2.1.3	VCM production	4
2.2	Simplified representation of the EDC cracker	6
2.3	Thermographic reference data	8
3	CFD Simulation	10
3.1	Geometry	10
3.1.1	Grid design	11
3.2	Overview of equations	13
3.3	Equation solving	15
3.3.1	Numerical methods and schemes	15
3.3.2	Convergence control	17
3.3.3	Under-relaxation	18
3.4	Simulation setup	18
3.4.1	Burner inlet boundary conditions	18
3.4.2	Heatflux profiles	20
4	Radiation modeling	23
4.1	General	23
4.2	Radiative transfer equation	23
4.3	Discrete Ordinates radiation model	26
4.3.1	Gas radiation	27
4.3.2	Wall radiation	28
5	Process side simulation	30
5.1	Governing equations	30
5.2	Coupling Fluent and Matlab	31
5.2.1	Calculation of outer surface temperature	32
5.3	Procedure for coupling Fluent and Matlab simulations	33
5.3.1	Preparing Fluent data for Matlab calculations.	34
5.4	Simulation setup	35
6	Results	38
6.1	Matlab simulation with EDC Crack heatflux profile	38
6.2	CFD simulation with EDC Crack heatflux profile	40
6.2.1	Original boundary conditions	40
6.2.2	Modified boundary conditions	43
6.2.3	Inlet temperature 1800 K	43
6.2.4	Inlet temperature 1700 K	45
6.2.5	Modified firing profile	47
6.3	Refractory	50
7	Discussion	51
7.1	Reaction coil temperature	51
7.1.1	Molar flow	53

7.2	Firebox properties	54
7.2.1	Flue gas temperature	54
7.2.2	Flow pattern	56
7.2.3	Refractory temperature	56
7.3	Sources of computational instability	58
8	Conclusions and further work	60
	Bibliography	65
A	Acronyms	66
B	Basic equations	67
B.1	Reynolds averaged Navier-Stokes equations	67
B.2	Closure of the equations	69
C	Plug Flow Reactor model	71
C.1	Original equation set	71
C.2	Modified equation set	71
D	Thermophysical data	73
D.1	Refractory materials	73
D.2	Coil material	74
D.3	Process fluid properties	75
D.4	Flue gas properties	76

Nomenclature

$\bar{\Phi}$	Generic, time averaged property
\bar{R}	Universal gas constant, 8.314 kJ/kmolK
δ_{ij}	Kronecker delta
\dot{m}	Mass flow (kg/s)
λ	Thermal conductivity (W/mK) or normalized air to fuel ratio
λ_t	Turbulent thermal conductivity (W/mK)
\mathcal{D}	Mass diffusivity coefficient (m ² /s)
μ	Dynamic viscosity (Pa s)
μ_t	Turbulent viscosity (Pa s)
ν	Stoichiometric coefficient (1) or kinematic viscosity (m ² /s)
Ω'	Solid angle, refers to in-scattering
Φ	Phase function, used for in-scattering
Φ'	Generic, fluctuating property
Φ''	Generic, flux
ρ	Density (kg/m ³)
σ	Stefan-Boltzmann constant (5.672·10 ⁻⁸ W/m ² K ⁴)
σ_t	Turbulent Prandtl number
σ_Y	Turbulent Schmidt number
τ_{ij}	Stress tensor
ε	Dissipation rate of turbulent kinetic energy (m ² /s ³) or emissivity (1)
ε_w	Wall emissivity (1)
ζ	Tube bend friction factor (1)
f_d	Diffuse fraction, radiation at opaque wall (1)
L_M	Mean beam length (m)
q''	Heat flux (W/m ²)
σ_s	Scattering coefficient (1/m)
τ_{opt}	Optical thickness (1)
ε_g	Gas emissivity (1)
S_h	Source term in the energy equation
$[X_k]$	Molar concentration of species k (mol/m ³)
A	Area (m ²)
a	Absorption coefficient (1/m)

a_ϵ	Emissivity correction coefficient, WSGGM (1)
c_p	Constant pressure specific heat (J/kgK)
c_v	Constant volume specific heat (kJ/kgK)
d_t	Inner diameter of PFR (m)
E	Total energy (J)
f	Straight tube friction factor (1)
F_k	Molar flow rate of component k (mol/s)
H	Enthalpy (J)
h	Convection heat transfer coefficient(W/mK)
I	Radiation intensity
k	Turbulent kinetic energy (m^2/s^2)
k_f	Forward reaction rate constant
k_r	Reverse reaction rate constant
L	Characteristic length (m)
MW	Molecular weight (kg/kmol)
n	Number of moles (1) or refractive index (1)
Nu_D	Nusselt number based on tube diameter (1)
p	Pressure (Pa)
Pr	Prandtl number (1)
Q	Heat (W)
r_b	Tube bend diameter, PFR (m)
r_i	Production rate of species i ($\text{mol}/\text{m}^3\text{s}$)
R_k	Rate of reaction k ($\text{mol}/\text{m}^3\text{s}$)
Re_D	Reynolds number based on tube diameter (1)
s	Pathlength WSGGM (m)
T	Temperature (K or °C)
t_w	PFR wall tube thickness (m)
u	Velocity
V	Volume (m^3)
Y_i	Mass fraction of component i

1 Introduction

Commercial production of Polyvinyl Chloride (PVC) was started in 1926 by the American company B.F. Goodrich. From the discovery of PVC almost 100 years earlier and until then PVC was regarded not useful since the polymer was too brittle for real life applications. By blending the raw PVC with additives Goodrich managed to plasticize the polymer, yielding a material that was easy to process, and soon the commercial usage of PVC was widespread. Today PVC is the second most abundant plastic in the world, second only to polyethylene. The annual worldwide consumption of PVC is over 25 million tonnes, over half of this is used in construction applications such as pipes, fittings and flooring. Other applications of PVC is in the medical sector as gloves, tubes and blood bags and in consumer products such as furniture, clothing and sports equipment.

Production of PVC is basically the construction of long chains of the monomer Vinyl Chloride Monomer (VCM), this is usually done in pressurized batch reactors known as autoclaves. PVC production follows the principal chemical reaction:



During the reaction the double bond between the carbon atoms of the VCM is broken making it possible to link together the molecules. The n in reaction (1.1) is the number of VCM molecules in the PVC chain, called the chain length, this value is normally around 1000 [1].

This work is focused on the process used by Hydro for making the monomer VCM, more than 95% of the VCM produced worldwide is used in PVC production, the rest is used to make other chlorinated hydrocarbons. The most common way of producing VCM today is by thermal decomposition, or cracking, of 1,2-dichloroethane also known as Ethylene Dichloride (EDC). This is the process used by Hydro at both the VCM plant at Rafnes and in Stenungsund. Cracking requires addition of heat to the reactants, this is usually done by combustion of oil or natural gas.

Modeling and simulation of process equipment have received an increased interest over the last years. As computer power has become more readily available, detailed three-dimensional models can be run even on personal computers. While the earlier simulation models focused on predicting run-lengths and process gas composition, today's sophisticated CFD models can give detailed representations of temperature- and flow fields. This gives the opportunity to use simulations not only for prediction of the operating parameters of a reactor, but also to optimize the operation.

Objective

The objective in this work is to make a Computational Fluid Dynamics (CFD) model of the firebox side of an EDC cracker and to combine this with an existing computer model for the cracking reaction.

The commercial CFD program Fluent will be used for CFD simulations, and the EDC cracking computer model is written in Matlab. The Matlab model is a one-dimensional model that represents the reaction coil as a Plug Flow Reactor (PFR). The input to the model is a heatflux profile over the entire length of the reactor. Based on this profile the model integrates a set of governing equations, and the result is a reactor temperature profile, a process fluid composition profile and a velocity profile. From these profiles the outer wall temperature of the reaction coil can be computed. Using CFD modeling, the outer surface temperature can be computed based on the fired heat and the same heatflux profile along the reaction coil. The two models converge when the two temperature profiles are similar, that is when the temperature profile based on the extent of the cracking reaction equals the profile based on fired heat. The basis for this work is the Matlab code for the process side simulation and CFD simulations of the burners delivering heat to the reaction. The burners

will be simplified by omitting the combustion reaction, and representing the burners as streams of hot combustion products.

2 Hydro Polymers Stenungsund

At the industrial site in Stenungsund, Sweden, Hydro Polymers has a fully integrated PVC operation, converting raw materials into PVC. The VCM plant has a capacity of about 140 000 tonnes per year, and the annual turnaround for the entire operation is approximately 2 billion Swedish Kroner.

2.1 VCM production

VCM is produced by thermal decomposition of EDC, a block diagram with the main steps in the VCM production is shown in Figure 2.1

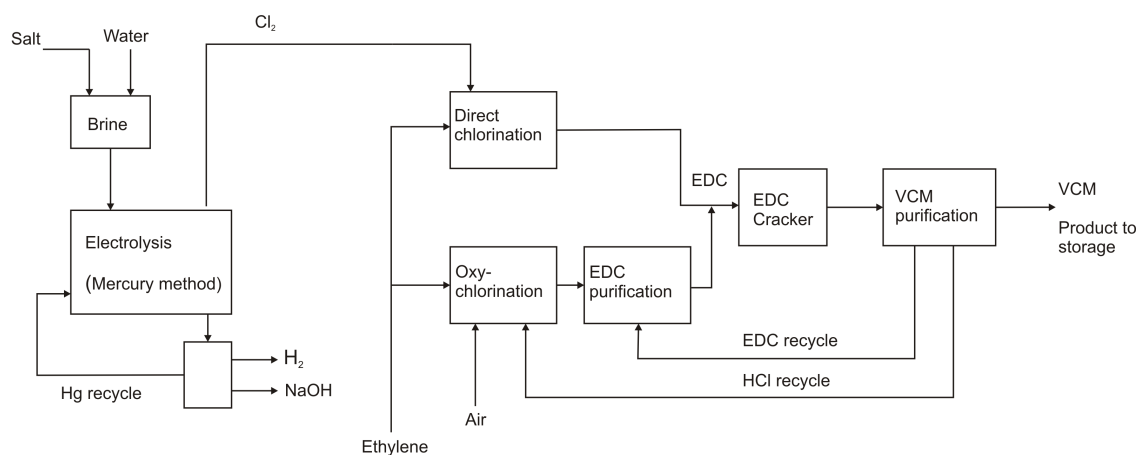


Figure 2.1: Block Diagram. VCM Production at Hydro Polymers Stenungsund

2.1.1 Chlorine production

Chlorine is produced from sodium chloride through electrolysis in the on-site chlorine plant. Sodium chloride is dissolved in water to form a brine, and this brine is fed to the electrolysis cells. The cathode reaction is production of hydrogen gas from hydrogen ions in the brine:



The anode reaction is production of chlorine gas from chloride ions in the brine:



Combining equation (2.1) and (2.2) and introducing the sources of H^+ and Cl^- ions, namely water and salt, respectively, the overall equation for electrolysis of the sodium chloride brine is:



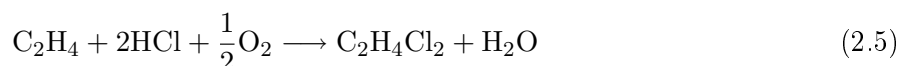
As can be seen from the above equations, production of chlorine also yields sodium hydroxide and hydrogen gas. The sodium hydroxide is sold as a product, while the hydrogen is mixed with methane to give fuel gas.

2.1.2 EDC production

As can be seen from Figure 2.1 there are two different reactors that are used to produce EDC. The first is the direct chlorination reactor, where ethylene and chlorine are reacted directly giving EDC:



Oxychlorination is a means of using the Hydrogen chloride (HCl) produced in the thermal dehydrochlorination of EDC. After the EDC cracker, the produced VCM and HCl are separated and the HCl recirculated to the oxychlorination reactor. Oxychlorination follows the principal reaction:



The source of oxygen in reaction (2.5) is air, as indicated in Figure 2.1. Using both direct- and oxy chlorination, results in a balanced VCM production unit, where the amounts of byproducts are kept at a minimum.

2.1.3 VCM production

The heart of the VCM plant is the furnace, or cracker, where VCM is produced from thermal dehydrochlorination of EDC following the highly endothermic overall reaction:



The process is typically operated at 480-530°C and pressures from 6-35 atm, with the conversion level of EDC usually kept between 50-65 wt-% [2]. Choice of operating conditions will be based on a trade-off between cost of utilities, production rate and maintenance intervals among others. Due to the operating parameters and the composition of the process fluid, the cracking process is highly susceptible to formation of solid deposits (coke) and components inhibiting the process. The higher the conversion level, the more coke and byproducts are formed, and thus both the maintenance (de-coking) intervals and ease of separation of the product stream decrease with increased conversion.

Figure 2.2 gives a side view schematic of an EDC cracker, indicating that the cracker has four different zones. The lower part of the cracker is referred to as the firebox, where gas burners are placed along the wall of the cracker. Heat transfer in the firebox is mainly done by radiation from the walls and the flue gas due to the high temperatures in this section. The hot flue gas rise up through the cracker, and in the shock section heat transfer to the process is both radiation from the firebox and convective heat transfer from the flue gas. In the convection section heat transfer is mainly convective, the damper in the top of the cracker directs the flue gas either to the stack or a heat recovery steam generator. Due to the installation of the steam generator the flue gas exits the convection section at about 450-500°C. Reaction (2.6) takes place inside the reactor represented as circles in Figure 2.2. The reactor is a tube with an outer diameter of 15 cm and an overall length of about 300 m, and each cracker has two tubular reactors in parallel. As opposed to the EDC cracker operated by Hydro Polymers at Rafnes, where the flow direction of the process fluid in the firebox is from bottom to top, or counter current mode, the cracker in Stenungsund is operated in co-current mode. The product stream is taken out in the bottom of the cracker.

In the convection section the fed EDC is heated from approximately 110°C at the inlet, to 195°C at the outlet. Evaporation is carried out externally in a steam driven evaporator. The phase

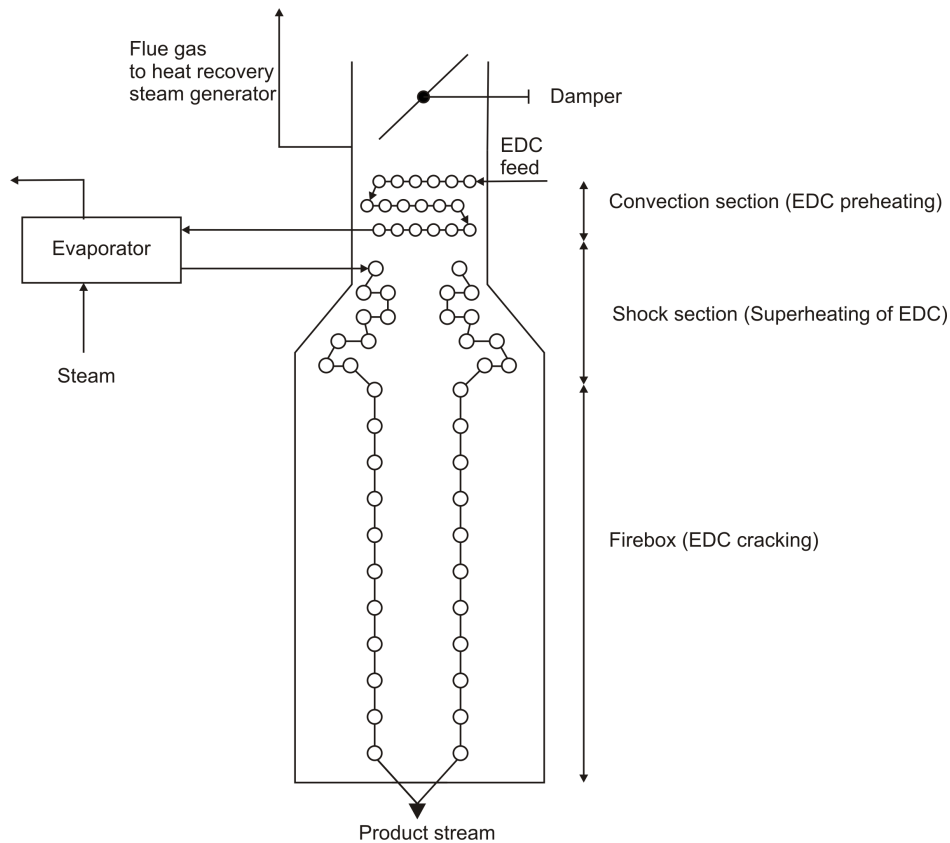


Figure 2.2: Side view schematic of the VCM cracker

transition from liquid to vapour is believed to be a source of coke formation, especially if the tube wall temperature is much higher than the fluid temperature [3]. In the steam driven external evaporator, however, the tube wall temperature is controlled by the steam temperature, and coking rates can be kept at a minimum. The temperature of the available steam, however, limits the temperature at which evaporation can be carried out. Thus the evaporator may become a bottleneck in the cracker. When entering the shock zone the EDC is in a saturated vapour state at approximately 205°C and 14.5 bars. Through the shock section the EDC is superheated to about 420°C . The EDC cracking reaction is known to start at temperatures of about 430°C [2], hence the cracking reaction should, theoretically, not start until the process fluid has exited the shock coil.

2.2 Simplified representation of the EDC cracker

To study the amounts of energy consumed in the distinct parts of the cracker, a simplified flow sheet representation is made. The convection and shock zones are represented as heat exchangers, while the coil in the firebox is represented as a reactor.

The simplified flow sheet shown in Figure 2.3 is used for calculation of the energy balance in the EDC cracker. The indicated temperature indicators (TI) and temperature indicator and control (TIC), refer to temperature measurement points in the actual plant [4].

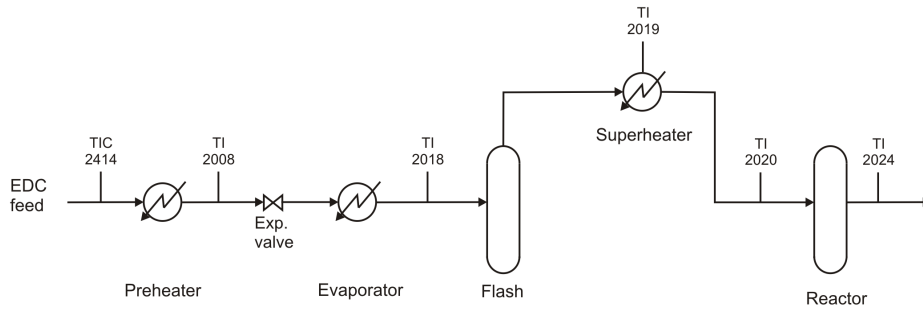


Figure 2.3: Simplified flow sheet used for energy balance calculations

Temperature readings averaged over a period of three months, which is a normal operating time between de-cokings, are given in Table 2.1 [5]. In Figure 2.3, the preheater represents the convection coil, the evaporator the external evaporator, and the superheater represents the shock coil. The coil in the firebox is represented by a reactor. To ensure that only EDC vapour enters the shock coil, a flash chamber is fitted after the evaporator, the liquid stream from this chamber is recycled to the evaporator. The temperature indicator TI-2020 is believed to not give the correct temperature, the reason for this is not known [6]. TI-2019 is placed at the outlet of the fifth of a total of nine tubes in the shock section. TI-2021 to TI-2023 are placed along the coil in thermo pockets. TI 2024 is placed at the outlet of the second to lowest tube in the firebox. The accumulated reactor length refers to the distance covered by the process fluid after entering the reaction coil. In the preheating section, the pressure is about 22 bars, but before the evaporator the pressure is lowered to about 14 bars to avoid flashing of the EDC. Pressure reduction is accomplished by a set of expansion valves, but for simplicity only one is shown in Figure 2.3.

Table 2.1: Measured temperatures in the EDC cracker

Tag #	\bar{T} [°C]	Accumulated reactor length [m]	Phase
TIC 2414	115		Liquid
TI 2008	193		Liquid
TI 2018	206		Vapour
TI 2019	390		Vapour
TI 2020	315	0	Vapour
TI 2021	437	40.23	Vapour
TI 2022	465	80.46	Vapour
TI 2023	498	120.69	Vapour
TI 2024	502	147.51	Vapour

The capacity of each coil in the cracker is about 9 tonnes of VCM per hour. The average conversion level of EDC is 50wt-% out of the firebox, which corresponds to a mass flow rate of 23.7 tonnes per hour or 6.6 kg/s of EDC into the cracker. With the given conversion level and flow rate the duty in each of the heat exchangers and the reactor can be calculated using the first law of thermodynamics for a control volume at steady state [7]:

$$\dot{Q} = \dot{m}\Delta h \quad (2.7)$$

In equation (2.7), the effects of kinetic and potential energy is neglected, no work is delivered from the control volume, and there is one inlet and one outlet.

Change in thermal enthalpy is calculated using the definition of specific heat, equation (2.8), combined with the ideal gas equation of state, which states that enthalpy is a function of temperature alone. The change in enthalpy is therefore found by integrating the expression for specific heat.

$$c_p \equiv \frac{\partial h}{\partial T} \quad (2.8)$$

For the superheater, data from Ranzi et al. [8] can be used readily, since the specific heat is given in a polynomial form. For the preheater data for EDC as a liquid is needed, and for the evaporator, the heat of vaporization is needed. Heat of vaporization, ΔH_{vap} , at a given temperature can be calculated using the thermodynamical relation [9]:

$$\Delta H_{vap}(T_2) = \Delta H_{vap}(T_1) + \int_{T_1}^{T_2} \Delta_{vap} C_p dT \quad (2.9)$$

In equation (2.9) $\Delta_{vap} C_p$ is the change in specific heat in going from liquid to the vapour phase. Using data from Manion, the heat of vaporization of EDC at 206°C is calculated to 25321.7 kJ/kmol [9]. For the liquid phase, specific heat values are taken from Chemical Properties Handbook [10]. Because this is a highly simplified calculation, the specific heat of EDC liquid is taken as constant over the preheater and expansion valve. For the superheater the duty is calculated by integrating the polynomial expressions for specific heat found in Ranzi et al [8]. The calculated duty for each of the heat exchangers are listed in table Table 2.2.

Table 2.2: Simple energy balance for one half of the EDC cracker

Unit	Duty [kW]	T _{out} [°C]
Fired heat	6830	
Preheater (Convection section)	675	473
Evaporator	1821 ¹	
Superheater (Shock section)	1613	636
Reaction heat (Firebox)	2541	1007
To heat recovery	2271	

The fired heat is based on the consumption of fuel gas in the EDC cracker in February 2007, data are taken from the monthly operational report for February 2007 [11]. The heat of reaction is calculated using data from Ranzi et al. Since the reaction takes place at elevated temperatures, the heat of reaction for the dehydrochlorination of EDC is:

¹Externally driven, not taken from fired heat

$$\frac{\dot{Q}}{\dot{m}} = Y_{VCM,e}(h_f^o + \Delta h)_{VCM} + Y_{HCl,e}(h_f^o + \Delta h)_{HCl} + Y_{EDC,e}(h_f^o + \Delta h)_{EDC} - Y_{EDC,i}(h_f^o + \Delta h)_{EDC} \quad (2.10)$$

In equation (2.10) h_f^o is the heat of formation, and the indices e and i refer to the exit and the inlet of the reactor, respectively. In the simplified calculations, the reactor feed is assumed to be pure EDC. Δh the thermal enthalpy departure from the reference state, calculated as:

$$\Delta h = h(T) - h(T_{ref}) = \int_{T_{ref}}^T c_p dT \quad (2.11)$$

Specific heat polynomials from Ranzi et al. [8] are used in calculating the thermal enthalpy departure, T_{ref} is 298 K. Heats of formation are also taken from Ranzi et al.

T_{out} in Table 2.2 is the flue gas temperature out of the distinct sections. Except the temperature out of the convection section, which is taken from a temperature measurement probe in the cracker, the temperatures are estimates. The flue gas temperatures are estimated using specific heat data from Moran and Shapiro [7]. These temperatures can be used to tune the CFD model as the temperature of the flue gas is directly proportional to the amount of heat absorbed by the reaction coil. The mass flow of flue gas is set to 3.3 kg/s throughout the calculations.

2.3 Thermographic reference data

Thermographic measurements of the cracker have been conducted in order to obtain a better understanding of the actual temperature distribution on the cracker's surfaces. No discussion of the underlying principles of thermographic measurements will be given in this work, more details are given e.g. in the thermographic report [12]. Data from the thermographic control will be used as reference data, an example of a thermographic picture and corresponding temperature profiles is given in Figure 2.4. The thermographic control was conducted on March 16, 2007, at this time a de-coking of the cracker was impending.

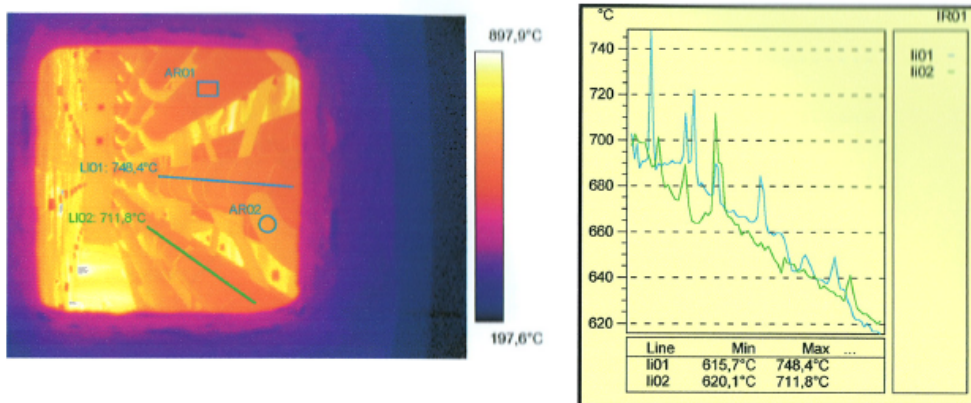


Figure 2.4: Thermographic picture (left) and corresponding temperature profiles along the coil (right) [12]

The blue and green line shown in Figure 2.4 are added in a post processing computer program. The corresponding temperature profiles are drawn by the same program. The direction of the lines is

from the center and out towards the short wall, thus the temperature is lower near the short walls than near the center.

Unfortunately the thermographic report does not contain the raw data used in drawing the temperature profiles on the right in Figure 2.4. To be able to compare the thermographic data with simulated data, a manual data extraction from the report is necessary. The result of such data extraction is shown in Figure 2.5 To arrive at the profiles shown in Figure 2.5 an estimation of both line length and position is performed. Hence the drawn profiles can only be taken as approximate values.

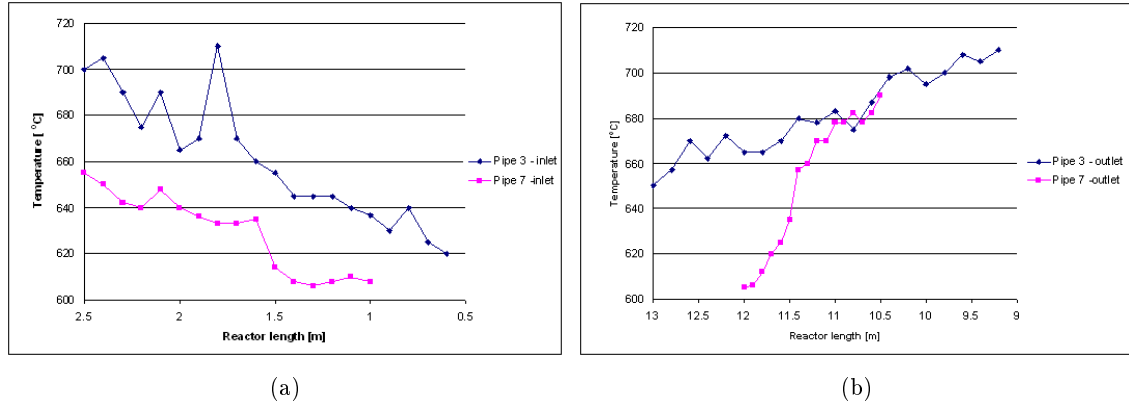


Figure 2.5: Extracted data from thermographic measurements; Profiles near pipe inlet (a); Profiles near outlet (b)

The reactor length in Figure 2.5 refers to the distance from the inlet of the given pipe. A general trend from the thermographic report is that the temperature is lower on the upper tubes than on the lower, and that the peak temperature on each tube is near its center. The outer surface temperature increases approximately 100°C from the upper tubes in the coil to the lower. The surface temperature on the tubes also seems to be higher at the flow outlets of the tube than at the flow inlets. And there seems to be a «shadow effect» which means that the temperature on the side of the tubes not facing the burners is lower than on the opposite side. The temperature on the side of the tube facing the burners is as much as 50-60°C higher than on the side facing the center of the firebox.

3 CFD Simulation

A simulation model of the EDC cracker is developed by extracting data from the technical drawings of the cracker. The computational network, or mesh, is generated using the graphical preprocessor Gambit.

3.1 Geometry

The cracker is built up in several layers, the innermost is made from insulating fire bricks known as MPK-125. Outside the bricks are two layers of calcium silicate insulating boards, and the entire cracker is enclosed in a steel shell. The burners are cast in special burner tiles measuring 39×39 cm, and made from Rodarox. Figure 3.1 shows a detail from the refractory, with the burner tile in the centre, bricks on the sides, and insulation boards on the outer surface.

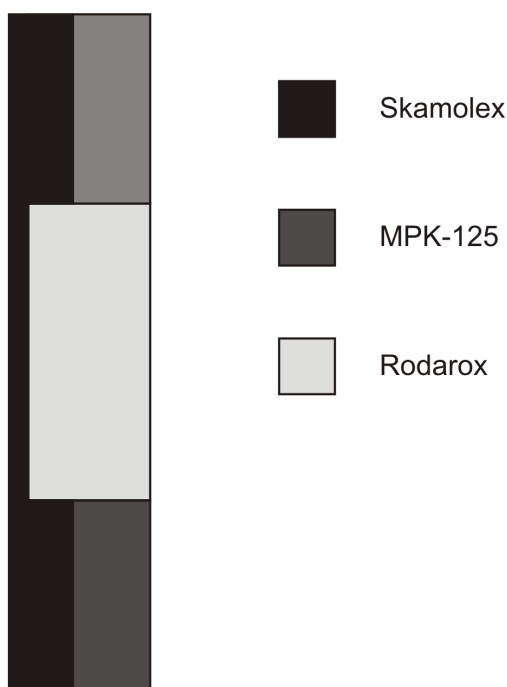


Figure 3.1: Detail of cracker wall

The inner dimensions of the cracker are given in Figure 3.2, all measurements are given in meters.

For the reactor coil the pipe bends are omitted, and the coil is thus represented as 11 straight tubes with a length of 13.41 m. The distance from the symmetry plane to the center of the coil tubes is 14.3 cm, the distance from the cracker floor to the lowest tube is 50 cm, and there is 32.5 cm between each tube. The coil in the shock- and convection section is omitted altogether. By leaving the pipe bends out of the model, the overall reactor length is shortened by approximately 5 m. With the overall length of the reaction coil being over 150 m, the pipe bends only make up approximately 3% of the total coil length.

A graphical three dimensional representation of the cracker is given in Figure 3.3. As can be seen from the figure, the cracker coil is represented by 11 straight tubes.

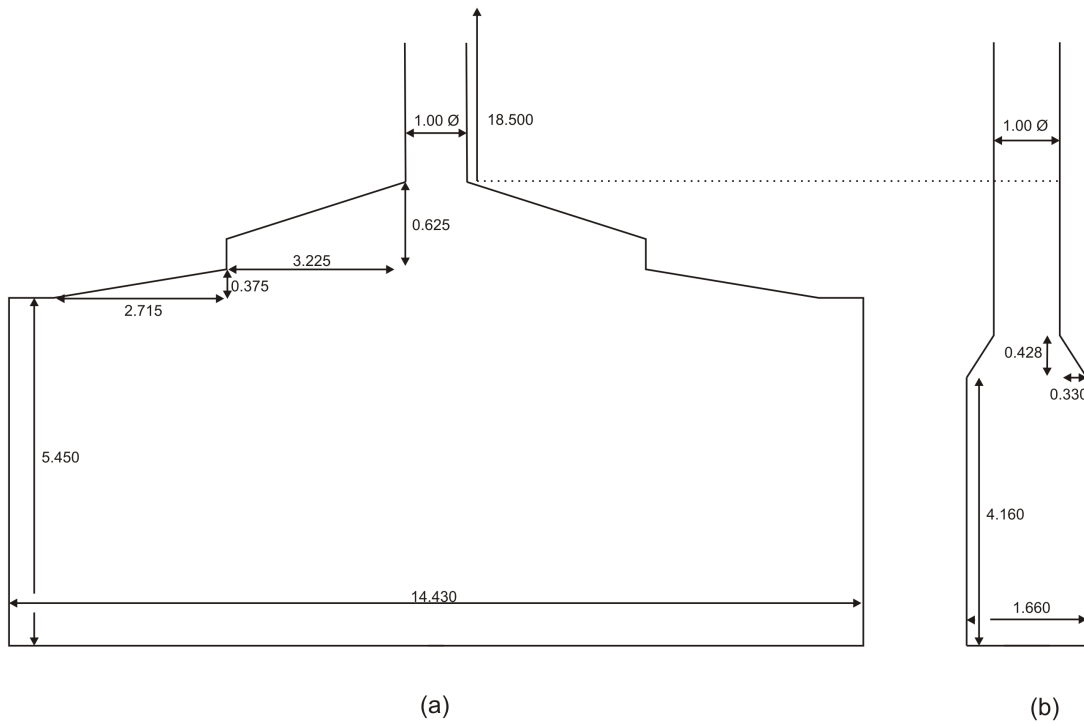


Figure 3.2: Cracker geometry, side wall (a) and end wall (b). All measurements in meters

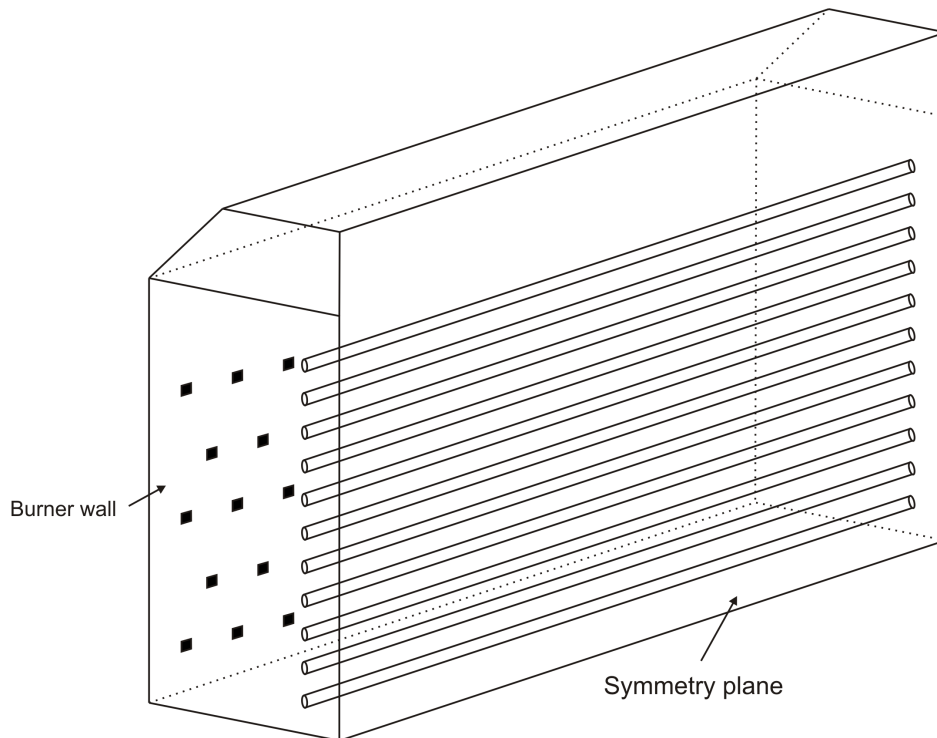


Figure 3.3: Three dimensional simplified representation of the EDC cracker

3.1.1 Grid design

The grid is designed by using a series of primitive geometric shapes, such as bricks and cylinders, to represent the measurements of the actual cracker. The grid is made in Fluent's graphical pre-

processor, Gambit. Using primitive geometric shapes to make the grid is usually referred to as a top-down design method. The computational network is designed with non-uniform hexagonal cells. In order to increase the grid resolution in certain areas, such as around the coil and burner outlets, size functions are used. Size functions allow the grid size to grow from a given entity and outwards. The growth rate of the grid is a user defined value. An example of the use of size functions in the grid is given in Figure 3.4(a). Here a cross section of the cracker is shown, the coil is represented by the horizontal cylinders. As can be seen the grid is substantially finer around the coil than in the rest of the cracker. The grid in this part of the cracker is made by meshing one short end wall with a Pave scheme, and then using the Cooper algorithm to draw this face mesh along the length of the coil [13].

Furthermore, the burner wall is made by repeating one module including 5 burners 12 times. The repeated module is shown in Figure 3.4(b)

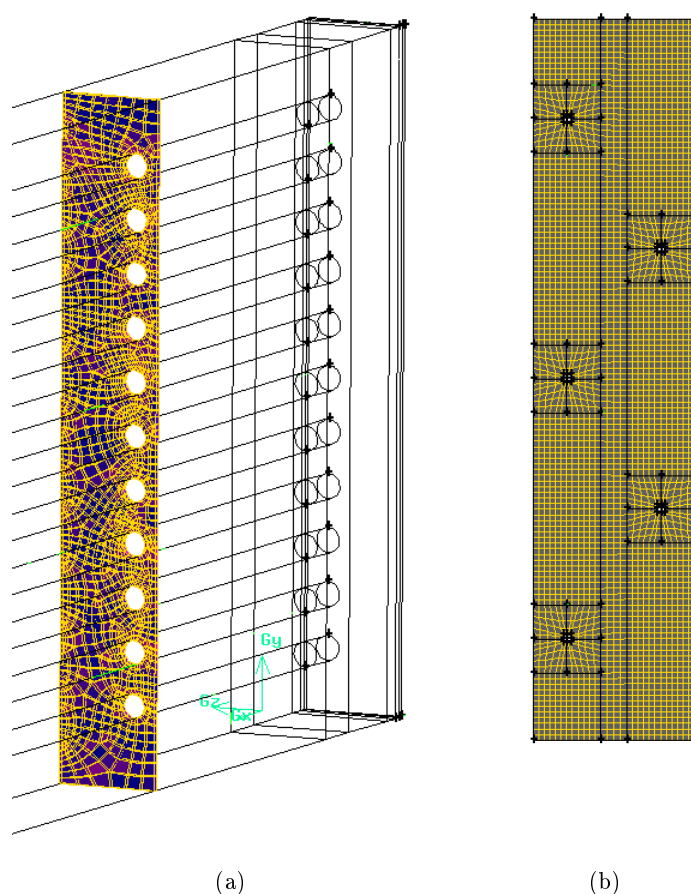


Figure 3.4: Details of the grid: Cross section of the grid around the coil (a); Repeated module used for burner wall (b)

The tube wall in the coil can be represented in two different ways. The simplest is to model the wall as infinitely thin, and then use Fluent's «Shell Conduction» possibility. By enabling shell conduction, a one dimensional heat conduction equation is solved for the wall. A wall thickness must be given, but there is no need to construct a grid to represent the wall. To avoid using shell conduction, which can cause instability when running parallel simulations, the tube wall must be included in the grid. Usually two adjoining cells should have similar size in a computational grid, and as the cell size around the tube walls are about 5 cm long, this could lead to problems when meshing the 8 mm thick tube wall. Fortunately, this limitation does not apply when meshing two distinct zones. At

the tube wall, the cracker volume or fluid zone, and a solid zone representing the wall meet. The tube wall can therefore be meshed independently of the mesh in the cracker volume. The latter representation of the coil is used in the grid in this work. Due to the dimensions of the cracker, and the wish to maintain a high level of detail, the final computational grid has approximately two million cells. Such a high number of cells indicates that the computational time for the model may be long, but by partitioning the grid into 16 zones, and running the calculations in parallel the grid size is manageable as each partition contains only about 125 000 cells. Partitioning is done using the Metis algorithm in Fluent [14].

In order to simplify the grid, the burner geometry is made less complex in the model than in the actual cracker. In the cracker the burners are circular tubes with eight rectangular burner outlets along the periphery. To make meshing of the model easier, the burners are simplified as square tubes with two rectangular outlets on each side. In Figure 3.5(a) the grid around one burner is shown. The burner tube is the quadratic «tube» in the center of the figure. Around the burner tube is the burner tile, which is made up from four sections. One of these sections is removed in Figure 3.5(a) to give a better view of the burner. The burner tile shown in Figure 3.5(a) corresponds to one of the five equal squares shown in Figure 3.4(b). For comparison, the grid used for simulation of one burner is shown in Figure 3.5(b) [15]. As can be seen from the two figures, the grid used in modeling the entire cracker is much coarser than that used for modeling one burner only. The size and shape of the burner outlets are, however, the same, and through the boundary conditions setup in Fluent the mass flow direction out of the burner outlets is maintained.

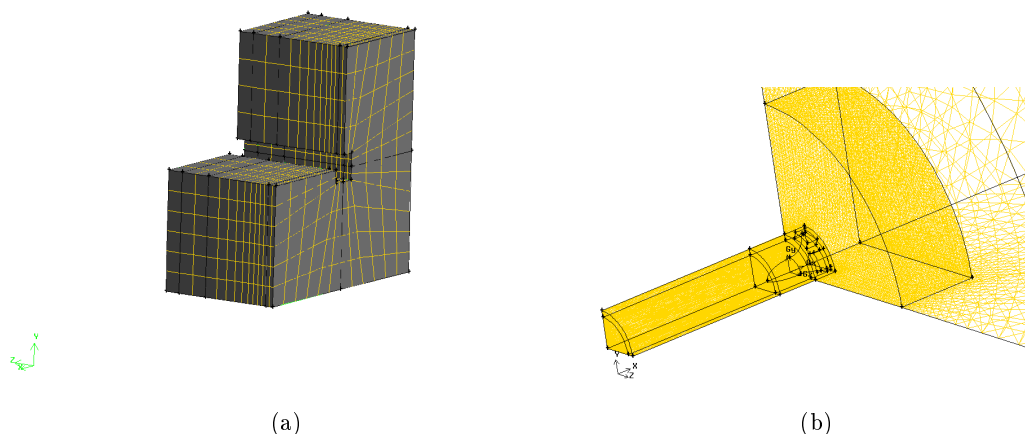


Figure 3.5: Burner representation: Coarse grid used in overall CFD model (a); Detailed grid used in CFD simulations of burners only [15] (b)

3.2 Overview of equations

CFD modeling is based on solving transport equations for momentum-, energy- and species conservation.

For laminar flows the basic equations can be solved quite readily, however most applications encountered in process equipment include turbulent flow. In applications including chemical reactions or heat transfer, or as in an EDC cracker both, turbulence is often desired as both chemical reactions and heat transfer can be enhanced by turbulence. From simulations of a single burner in the EDC cracker, it is known that the Reynolds number at the burner inlet is about 50000 [15]. This shows that the flow in the burners is fully turbulent. Turbulent flows are inherently more difficult to describe than laminar flows, and for practical applications modeling is required. One approach to

modeling a turbulent flow is to introduce Reynolds time-averaging concept, that is each property is divided into a mean value plus a fluctuation or deviation from this mean value. More details on Reynolds averaging is found in Appendix B, the resulting equations for momentum-, energy- and species conservation are given below.

By assuming constant density, the continuity equation takes the form:

$$\frac{\partial \bar{u}_j}{\partial x_j} = 0 \quad \text{and} \quad \frac{\partial \bar{u}'_j}{\partial x_j} = 0 \quad (3.1)$$

The Reynolds averaged transport equation for momentum is:

$$\frac{\partial}{\partial t}(\rho \bar{u}_i) + \frac{\partial}{\partial x_j}(\rho \bar{u}_i \bar{u}_j) = -\frac{\partial \bar{p}}{\partial x_i} + \frac{\partial}{\partial x_j}(\bar{\tau}_{ij} - \overline{u'_i u'_j}) + \rho \bar{f}_i \quad (3.2)$$

Closure of equation (3.2) is done by modeling of the term $\overline{u'_i u'_j}$. In Fluent a number of models for closing the equations are available. None of the models are universal, and for a given case a simple model might yield better results than a complicated one. In general, both turbulent velocity and length scales need to be determined independently in order to give a good representation of a turbulent flow. This means that minimum two transport equations are needed to have a «complete model» [14]. Launder and Spalding discuss different two-equation models, and conclude that equations with ε should be preferred [16]. The conclusion may be questioned [17], but the k- ε -model has been the most widely used turbulence model over the three last decades. Three different k- ε -models are available in Fluent, the standard, RNG and realizable. The two latter models result from improvements of the standard k- ε -models. In this work, the simplest and most computationally effective two equation model, the standard k- ε -model, is used. The model is described in more detail in Appendix B. More about turbulence models and a discussion of their applications can be found in Ertesvåg [17].

In Reynolds averaged form, conservation of species is determined by:

$$\frac{\partial}{\partial t}(\rho \bar{Y}_k) + \frac{\partial}{\partial x_j}(\rho \bar{Y}_k \bar{u}_j) = \frac{\partial}{\partial x_j}(\rho \mathcal{D} \frac{\partial \bar{Y}_k}{\partial x_j} - \rho \overline{Y'_k u'_j}) + \bar{R}_k \quad (3.3)$$

In Fluent the correlation $-\overline{Y'_k u'_j}$ is modeled using a gradient model:

$$-\overline{Y'_k u'_j} = \frac{\nu_t}{\sigma_Y} \frac{\partial \bar{Y}_k}{\partial x_j} \quad (3.4)$$

Equation (3.4) closes equation (3.3). Since the equation is now only dependent on average values, it is possible to solve numerically. σ_Y is known as the turbulent Schmidt number and is given a value of 0.7 as default in Fluent. ν_t is the kinematic turbulent viscosity defined by the chosen turbulence model.

Heat transport in turbulent flow is modeled using the equation:

$$\frac{\partial}{\partial t}(\rho E) + \frac{\partial}{\partial x_i}[\bar{u}_i(\rho E) + \bar{p}] = \frac{\partial}{\partial x_j} \left[(\lambda + \lambda_t) \frac{\partial \bar{T}}{\partial x_j} + \bar{u}_i(\tau_{ij})_{\text{eff}} \right] + \bar{S}_h \quad (3.5)$$

Where the effective stress tensor is defined as:

$$(\tau_{ij})_{\text{eff}} = \mu_t \left(\frac{\partial \bar{u}_j}{\partial x_i} + \frac{\partial \bar{u}_i}{\partial x_j} \right) - \frac{2}{3} \mu_t \frac{\partial \bar{u}_i}{\partial x_i} \delta_{ij} \quad (3.6)$$

The turbulent thermal conductivity, λ_t is defined as:

$$\lambda_t = \frac{c_p \mu_t}{\sigma_t} \quad (3.7)$$

σ_t is the turbulent Prandtl number, by default assigned a value of 0.85 in Fluent, other values can be given. The turbulent viscosity, μ_t , is calculated from the chosen turbulence model. In equation (3.5) E is the total energy, that is the sum of internal and kinetic energy. The source term, $\overline{S_h}$ accounts for any internal sources of heat, such as heat of reaction and radiative heat transfer.

3.3 Equation solving

In CFD simulations the conservation equations described above are solved numerical over a finite number of cells. The basics of the numerical methods employed in Fluent are given in this section.

3.3.1 Numerical methods and schemes

There are three basic steps in performing a CFD simulation of a given problem [14]:

1. Division of the domain into discrete control volumes using a computational grid
2. Integration of the governing equations on the individual control volumes to construct algebraic equations for the discrete dependent variables (“unknowns”) such as velocities, pressure, temperature, and conserved scalars
3. Linearization of the discretized equations and solution of the resultant linear equation system to yield updated values of the dependent variables.

Step 1 are the tasks related to extraction of geometry data from technical drawings and creating a mesh. Step 2 is the first task conducted by Fluent, in each of the control volumes (or cells) defined by the generated mesh, the governing equations are integrated. As the conservation equations are integrated numerically, they need to be discretized first. Fluent uses a control volume based technique, where the governing equations are integrated over each of the cells in the computational domain. This result in a set of discrete equations representing the conservation laws on a control volume (or cell) basis. For a generic scalar, Φ , the integral and corresponding dicretized governing equations are given by equation (3.8) and equation (3.9), respectively.

$$\int_V \frac{\partial \rho \Phi}{\partial t} dV + \oint \rho \Phi \vec{u} \cdot d\vec{A} = \oint \Gamma_\Phi \nabla \Phi \cdot d\vec{A} + \int_V S_\Phi dV \quad (3.8)$$

$$\frac{\partial \rho \Phi}{\partial t} V + \sum_f^{N_{\text{faces}}} \rho_f \vec{u}_f \Phi_f \cdot \vec{A}_f = \sum_f^{N_{\text{faces}}} \Gamma_\Phi \nabla \Phi_f \cdot \vec{A}_f + S_\Phi V \quad (3.9)$$

The time dependent, or transient, terms in equation (3.8) and (3.9) are handeled by temporal discretization. As the cases considered in this work are all asumed to be steady state, or time

independent, no further discussion of transient terms is given here. In equation (3.8) \vec{A} is a surface area vector, Γ_Φ a diffusion coefficient, and S_Φ a source term. In the discretized equation, the subscript f refers to the exchange of the scalar over the face f , cf. Figure 3.6. For instance $\rho_f \vec{u}_f \Phi_f \cdot \vec{A}_f$ represents the mass flux through the face. The sums are carried out over all the N faces enclosing the control volume, V is the cell volume.

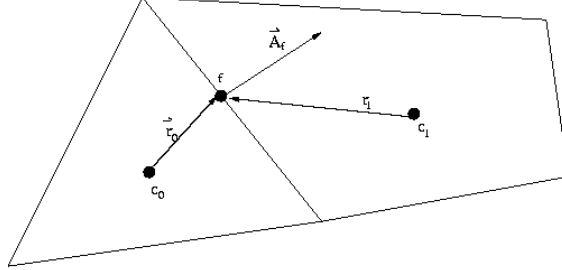


Figure 3.6: Arbitrary control volume used to describe discretization [14]

The discretized system, equation (3.9), is then linearized and solved to give a value for the unknown scalar, Φ . A linearized representation of equation (3.9) is given by:

$$a_P \Phi = \sum_{nb} a_{nb} \Phi_{nb} + b \quad (3.10)$$

Where a_P and a_{nb} are the linearized coefficients for Φ and Φ_{nb} , and the index nb refers to the neighbouring cells to the center cell (P). b represents any constant contributions, such as boundary conditions and constant source terms. Expressions such as equation (3.10) are written for each property considered in each of the cells making up the computational domain. This result in a set of algebraic equations with a sparse coefficient matrix. Fluent uses Gauss-Seidel iteration combined with an Algebraic multigrid method to solve the equation set [14].

As Fluent is designed to solve a wide range of problems, numerous different solution methods are available. There are two different solvers in Fluent, namely the pressure-based, and the density-based solvers. Both methods are applicable to all cases, the only differences between the two are the approach used to linearize and solve discretized equations. In this work the pressure based solver is used, because it has the opportunity of solving equations segregated. This solver uses a pressure correction equation to achieve the constraint of mass conservation, and belongs to a general class of methods called the projection method. The pressure based solver has two different solver algorithms, a coupled and a segregated one. This refers to how the resulting equation set after linearization is solved. In the segregated algorithm, the governing equations are solved one by one decoupled from each other. Such an approach is quite slow with respect to convergence, since a large number of iterations is usually needed in order to reach convergence. However, the method is memory efficient, as there is only need for the storage of one variable at a time. The pressure based solver also has the opportunity that the user can choose which equations that are solved. This means that the equations of primary importance can be solved to convergence, while those regarded as less important can be run only until «reasonably well converged» [14]. The coupled algorithm, solves all equations simultaneously, hence convergence may be reached in fewer iterations. Solving the equations coupled requires significantly more memory than solving them segregated. In this work the segregated solver is used, as time for each iteration is quite low when running on multiple processors.

The methods discussed thus far relates to the values of the properties at the center of the cells, i.e. c_0 and c_1 in Figure 3.6. However, when the convective terms are calculated, the values at the cell faces

are used. These are interpolated from the cell center values, and numerous interpolation schemes are available. The default scheme used with the pressure based solver, is a first order upwind scheme for all scalars. Generally first order schemes are better with respect to convergence than second order ones, while second order schemes yield more accurate results than first order. This is mainly due to so-called numerical diffusion, or more correctly a numerical discretization error, which is larger in first order than second order schemes. The Fluent User's Guide recommends using second order accuracy for all other cases than laminar flows where the flow is aligned with the grid [14]. Higher order schemes may be employed after arriving at a converged solution with first order accuracy. All interpolation schemes used for scalars are of the upwind type. Upwinding means that values upstream, or upwind, of the cell at hand are used. In this work first order accuracy will be used for all equations except for energy and radiation where second order schemes are used. This choice is based on the fact that in this work, the heat transfer is regarded as more important than the flow field. The diffusion terms of equation (3.9), i.e. the $\nabla\Phi_f$ term in steady state cases, are always modeled using a second order central differencing term.

The pressure at the cell faces are interpolated from center values using special pressure interpolation schemes. According to the Fluent User's Guide, cases with strongly swirling flows and natural convection cases with a high Rayleigh number require special pressure interpolation schemes [14]. As this is not the case in the EDC cracker, the standard, linear interpolation scheme is used for pressure in this work. Pressure-velocity coupling is achieved through the SIMPLE (Semi-Implicit Pressure-Linked Equation) algorithm [14].

3.3.2 Convergence control

In general convergence in the CFD simulations is monitored by means of residuals. For the segregated solver used in this work the residual, R^Φ , is defined as the unbalance in equation (3.10) summed over all computational cells (P). This can be stated mathematically as:

$$R_u^\Phi = \sum_P \left| \sum_{nb} a_{nb}\Phi_{nb} + b - a_P\Phi \right| \quad (3.11)$$

The residual defined by equation (3.11) is referred to as the unscaled residual of the variable Φ . Usually the residuals are scaled by a scaling factor representative of the flow rate of Φ through the domain. In most cases scaled residuals are better to use when monitoring convergence than unscaled ones, and these are the ones used as default in Fluent [14]. Mathematically the scaled residual can be expressed as:

$$R_s^\Phi = \frac{\sum_P \left| \sum_{nb} a_{nb}\Phi_{nb} + b - a_P\Phi \right|}{\sum_P |a_P\Phi_P|} \quad (3.12)$$

With infinite precision in the calculations a converged solution would be reached when the residuals of all variables go to zero. On an actual computer convergence is reached when the residuals are below the smallest number allowed by the computer's precision. Single precision computers allow the residuals to drop by six orders of magnitude before being rounded off. The default convergence criterion in Fluent is that all scaled residuals decrease to 10^{-3} . The exceptions are the energy and the radiation equations, where the criterion is 10^{-6} . The default convergence criteria will be used in this work. It should be pointed out that a converged solution is not necessarily a correct solution. Even if all the scaled residuals are below the specified criterion, the solution should be examined carefully to avoid reporting unphysical data.

3.3.3 Under-relaxation

The value of the generic variable Φ in iteration n is given as:

$$\Phi_n = \Phi_{n-1} + \alpha\Delta\Phi \quad (3.13)$$

Where Φ_{n-1} is the value of the variable in the previous iteration and $\Delta\Phi$ is calculated from the numerical scheme used. α is the under-relaxation factor, it is used to dampen the effects of non-linearity in the equations. The under-relaxation factor can be given any value between zero and one. Usually the under-relaxation factors set as default in Fluent are sufficient to achieve convergence. In some cases, convergence may be sped up by adjusting the factors. Care should be taken, as one might end up with unphysical solutions by adjusting the factors too far from the default values. In the list below, the default under-relaxation factor for the equations considered in this work are given. For some of the equations, the Fluent User's Guide give some guidelines as to how much the factors could be adjusted [14]. A list of these default under-relaxation factors and some rules-of-thumb about their adjustment are given below.

Equation	Default α	Comments
Pressure	0.3	Can be reduced to 0.2 if unstable or divergent behavior is observed
Density	1	Can be reduced if there is a high density/temperature coupling
Body forces	1	-
Momentum	0.7	Can be reduced to 0.5 if unstable or divergent behavior is observed
Turbulence kinetic energy	0.8	Can be reduced to 0.5 if unstable or divergent behavior is observed
Turbulence dissipation rate	0.8	Can be reduced to 0.5 if unstable or divergent behavior is observed
Turbulent viscosity	1	-
Energy	1	Can be reduced if there is a high density/temperature coupling
Discrete ordinates	1	-

3.4 Simulation setup

The computational network represents the three lower sections of the cracker; the firebox, the shock section and the convection section. The stack is left out for simplicity. Before running the simulation, boundary conditions must be given. The boundary conditions at the burner inlets dictate the amount of heat delivered to the cracker, while the boundary conditions at the reaction coil dictates the heat delivered to the cracking reaction.

3.4.1 Burner inlet boundary conditions

Energy is supplied by means of hot flue gas with a composition governed by the reaction:



Reaction (3.14) describes complete combustion of a mixture of 90% methane and 10%² hydrogen with 10% excess air. When energy is supplied in this way, the combustion reaction is neglected, and the overall complexity of the simulation model is reduced. From earlier simulations of the burners only, it is known that the reaction zone for the combustion reaction is approximately 10 to 20 centimeters long [15]. In other words the combustion reaction is restricted to the close vicinity of the burner, and at a plane parallel to the burner wall and 10 cm from the burner cup, the combustion reaction is finished. This means that the gas composition is fairly uniform at all locations in the cracker, except those closest to the burner outlets. Temperature, mass flow and composition of the flue gas are taken from Kaggerud [15]. These are listed in Table 3.1.

Table 3.1: Boundary conditions for one burner

	Value	Unit
Temperature	2062	K
Y_{CO_2}	0.135	1
Y_{H_2O}	0.116	1
Y_{O_2}	0.020	1
Y_{N_2}	0.729	1
Mass flow	0.051	kg/s
Turbulence intensity	5	%
Hydraulic diameter	0.017	m

The value for mass flow in Table 3.1 is the mass flow through one burner. However, the simplified burner geometry used in this work has eight separate burner outlets on each burner. In addition all burner outlets with the same mass flow direction on each burner row are grouped together. The mass flow of flue gas for one such group of burner outlets is therefore 0.07638 kg/s. The hydraulic diameter is used, along with turbulence intensity, for turbulence specification and is taken as:

$$\text{Hydraulic diameter} = \frac{4 \cdot (\text{Length} \times \text{Width})}{2 \cdot (\text{Length} + \text{Width})}$$

Where length and width describe the dimensions of the rectangular burner outlets.

The fuel gas composition used by Kaggerud as a base case was 90% methane and 10% hydrogen [15]. The amount of excess air was assumed to be 10%, which is the suggested optimum by the burner supplier. Measurements of fuel gas consumption and flue gas composition suggests that the fuel gas only has about 4% of hydrogen, and that there is a 25% excess of air [18]. The change in fuel gas composition means that the heat of combustion of the fuel gas is lowered, and the mass flow of fuel must be increased in order to maintain the same amount fired heat. The increase in excess air leads to a significant increase in flue gas mass flow through the cracker. As more mass needs to be heated, the adiabatic flame temperature is lowered, and the maximum temperature of the flue gas is reduced accordingly. Adiabatic flame temperatures for different fuels and operating conditions can be calculated using the Fortran program HPFLAME [19]. In Table 3.2 the adiabatic flame temperature, T_{ad} for four different amounts of excess air are given. As can be seen, the adiabatic flame temperature is lowered by almost 150 K as the amount of excess air is increased from 10 to 25%.

The adiabatic flame temperature is the temperature achieved, by the reaction products, in a combustion process where all the released energy is transferred to the products. Thus the adiabatic flame temperature is the highest achievable temperature in a combustion reaction. An EDC cracker is, by nature, not an adiabatic combustion chamber. The purpose of the combustion in the cracker

²Molar basis

Table 3.2: T_{ad} at various levels of excess air

λ	T_{ad} [K]
1.0	2225.57
1.1	2144.86
1.2	2044.91
1.25	1996.09

is to deliver heat to the cracking reaction, and hence remove energy from the combustion reaction. In the flame zone, where the temperature is at its highest, the emitted radiation from the gas is also at its highest. In a steady state case, as this, radiation from the flame zone will result in a lower temperature in this area. To use the adiabatic flame temperature as the inlet condition for the flue gas can therefore lead to a too high temperature level in the cracker. When this is included in the model, the temperature at the mass flow inlet is introduced as a new variable suitable for tuning the model. The tuning parameters of the CFD model are outer tube temperature profile and flue gas temperature out of the firebox. By lowering the temperature, the delivered heat to the cracker is also lowered, to account for this the mass flow of flue gas must be increased to maintain the given amount of fired heat.

In addition to running simulations with the inlet conditions given in Table 3.1, simulations with a reduced temperature, and the mass flow increased accordingly, will be run. Although the composition of the flue gas will be affected by the change in operating conditions, this is believed to be only a minor contribution. The flue gas composition will therefore be kept as those given in Table 3.1.

3.4.2 Heatflux profiles

To obtain a temperature profile along the reaction coil a numerical value for the heat absorbed by the cracking reaction is needed. The absorbed heat is dictated by the extent of the cracking reaction, and a starting point could be to impose an even heat flux along the entire coil. However, the commercial EDC cracking simulation software «EDC Crack» calculates the heat absorbed in the reaction coil. Operating data from the Stenungsund EDC cracker is used to tune the «EDC Crack» model with respect to fired heat, conversion level and production rate among others [20]. The simulation printout is quite extensive, including both process- and firebox temperature profiles, heat flux distributions, process fluid composition etc. The heat flux is imported into Fluent as a profile, with different values for the heat flux depending on both tube number and axial position. The heat flux is assumed to be constant over the entire cross-section of the tube.

Boundary profiles are entered in Fluent in the form of an external file. The profile file contains information about which entity the boundary conditions apply to, spatial coordinates and a number of values (velocity, pressure, turbulent kinetic energy etc). The generic form of a profile file is given in the box below.

```
((profile-name point|line|radial number of entries (n)
(field_1-name
list of values for field_1)
(field_2-name
list of values for field_2)
:
(field_n-name
list of values for field_n)
```

To define the heat flux along the reaction coil, the numerical value for the heat flux plus the relevant coordinates must be given. All values must be given in SI units, as no unit conversion is possible. From the given set of data Fluent performs a zeroth order interpolation³ to give the heat flux value at the necessary points. This means that in order to get a good representation of a spatially varying quantity, a high number of points is needed. As the heat flux exported from «EDC Crack» only contains 15 values for the heat flux per tube, an interpolation using the «splines» method in Matlab is used to acquire 135 points for each tube. An excerpt from one of the heat flux boundary profiles used in this work is given in the box below. The minus sign in the heat flux part means that the heat flux direction is into the reaction coil.

```
((wall_p1 point 135
(x
0.51 0.61 0.71 ...))
(y
0.5762 0.5762 0.5762 ...))
(z
-0.69 -0.69 -0.69 ...))
(heat-flux -31402.64 -31363.76 -31318.90 ...))
```

The above profile is a point profile with 135 entries, it is attached to the entity «wall_p1» which is the lower of the tubes in the cracking coil. The profile assigns a numerical value for the heat flux at different positions along the tube. As the heat flux is assumed to be constant over the cross section in a given position, only the x-value needs to vary in the profile. The heat flux points exported from «EDC Crack» and the interpolated data from Matlab are shown in Figure 3.7 as circles and the drawn line respectively.

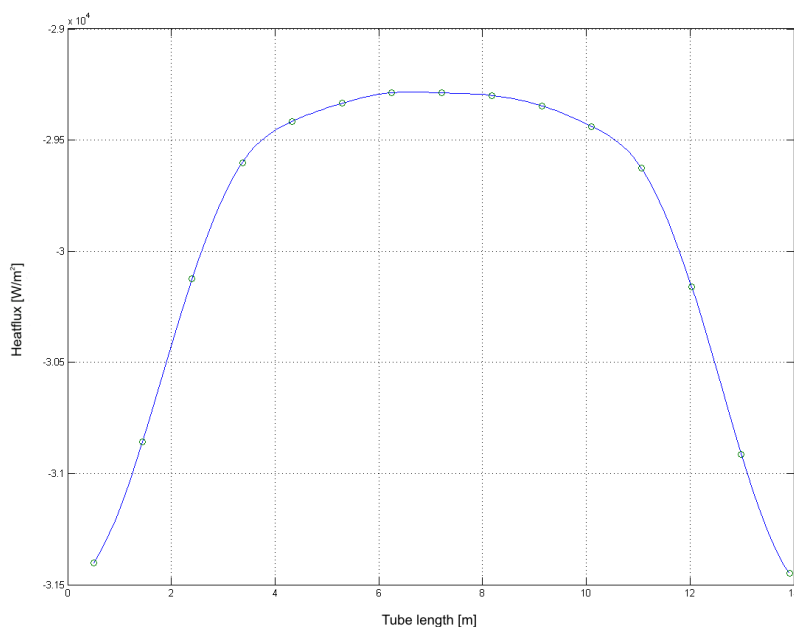


Figure 3.7: Heat flux profile exported data (circles) and interpolated data (drawn line)

The shock coil is left out of the model to make it simpler, this can be compensated for by adding a heat sink in the shock section of the cracker. In a three-dimensional case, groups of cells can

³Zeroth order interpolation implies using the value at the nearest data point

be separated into distinct zones. Inside this new zone, source terms for e.g. energy, mass or momentum can be defined. By making a separate zone of the grid in the part of the computational grid representing the shock section, an approximate representation of the shock coil can be made without having to modify the grid.

The boundary condition of the outer surface of the refractory wall is set to a constant temperature of 350 K. This is in agreement with the thermographic measurements and the fact that one can safely place one's hand on the outer steel shell of the cracker.

4 Radiation modeling

Due to the high temperatures of both the refractory, reaction coil and flue gas, radiation is the most important means of heat transfer in the firebox of the cracker.

4.1 General

Radiant heat transfer differs significantly from both conduction and convection. As radiative energy is transferred by means of electromagnetic waves, no participating medium is required. Radiation originates from oscillations in electrons inside the matter, and is therefore linked to internal energy, and further to temperature. Thermal radiation is assigned to the part of the electromagnetic spectrum with wavelengths ranging from 0.1 to 100 μm (approximately). This means that from the total electromagnetic radiation spectrum, only parts of the ultraviolet, and the entire visible and infrared components are pertinent to heat transfer. Two fundamentally different modes of radiative heat transfer exist, namely surface (or body) radiation, and gas radiation. While surfaces absorb and emit radiation at all wavelengths, gases absorb and emit radiation only at discrete frequencies. To include the effects of gas radiation, models are needed for the calculation of the coefficients governing absorbed and emitted energy.

4.2 Radiative transfer equation

The general radiative transfer equation for an absorbing, emitting and scattering medium is given by:

$$\frac{dI(\vec{r}, \vec{s})}{ds} + (a + \sigma_s)I(\vec{r}, \vec{s}) = an^2 \frac{\sigma T^4}{\pi} + \frac{\sigma_s}{4\pi} \int_0^{4\pi} I(\vec{r}, \vec{s}') \Phi(\vec{s} \cdot \vec{s}') d\Omega' \quad (4.1)$$

In equation (4.1) \vec{r} and \vec{s} are the position of the medium and the direction of the radiative heat transfer. \vec{s}' is the scattering direction vector. a , n and σ_s are the absorption coefficient, refractive index and scattering coefficient, respectively, σ is the Stefan-Boltzmann constant.

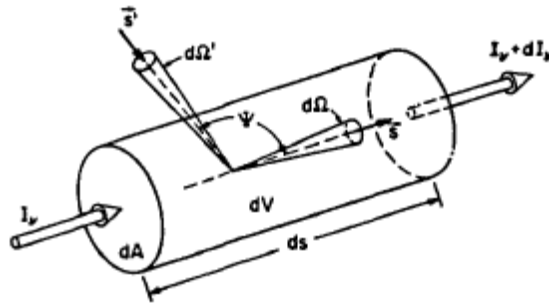


Figure 4.1: Radiative heat transfer in an absorbing, emitting and scattering medium [21]

Figure 4.1 shows the control volume used to derive equation (4.1). The first term on the left hand side of equation (4.1) represents the change in radiation intensity, I , per unit length along the path ds . The second term on the left hand side represents loss of energy due to absorption and scattering.

The first term on the right hand side represents the contribution by emission. In developing this particular expression, Kirchoff's law for radiation has been applied, hence the gas emission coefficient is replaced by its absorption coefficient, a , and the refractive index, n . Kirchoff's law is further described in Incropera and DeWitt [22]. The increase in energy by scattering of radiation into the control volume is counted for by the integral on the right hand side of equation (4.1). Radiation scattered into the control volume comes along the vector \vec{s}' and over the solid angle $d\Omega'$. Ψ is the scattering angle between \vec{s} and \vec{s}' . The phase function, $\Phi(\vec{s} \cdot \vec{s}')$, represents the probability that radiation is scattered into the control volume. A thorough derivation of the radiative transfer equation is given by Viskanta and Mengüç [21]

The effects of scattering can be significant in radiating media containing considerable amounts of particles, e.g. in the flue gas of coal combustion, or gases with large molecules. However, in the case of lean combustion of a methane/hydrogen mixture, the effect of scattering in the flue gas is negligible [21].

As can be seen, the general expression for radiative heat transfer, equation (4.1), is dependent on both position (\vec{r}) and direction (\vec{s}). This dependence makes radiation modeling a tedious task. Over the years several different methods have been developed. The most widespread radiation model for engineering problems is the zonal method, usually known as Hottel's zonal method, [23]. When using a zonal method, the surfaces and volumes are divided into a number of zones. Each zone is assumed to be isothermal and with a uniform distribution of radiation properties. Direct exchange factors between each zone are used to determine the radiative heatflux to and from every zone. The radiative heat transfer equation is reduced to a set of non-linear algebraic equations that is solved using matrix inversion techniques. In engineering calculations, the considered domain is divided into a limited number of zones, making the method quite fast.

The most accurate simulation model available for the radiative transfer equation is the Monte Carlo simulation technique. The Monte Carlo model is a purely statistical method, and in its simplest form the method is based on generating random numbers to represent the path of energy carrying photons. The solution of the radiative heat transfer problem can, in theory, be exact by utilizing Monte Carlo techniques, but the computational cost becomes immense [21]. Monte Carlo techniques are usually not used directly in engineering problems, but radiation models are often benchmarked against Monte Carlo simulations.

The zonal method and Monte Carlo method represent the radiative transfer equation in a non-differential form, and are therefore not suited for implementation in CFD codes [24]. One way of modeling the radiative transfer equation is by series expansion of the variables in spherical harmonics, using so-called Legendre polynomials. This results in a series of models, known as the P-N models [25]. The models are classified by the number of terms included in the model, the simplest model, P-1, uses only the four first terms of the series. Usually only the odd-numbered models are used, as the even-numbered models can result in mathematical singularities at directions parallel to boundaries [21]. Other models are based on finite volume techniques and angular discretization of solid angles.

Fluent offers five different radiation models, all with their advantages and disadvantages. The simplest model is an algebraic relation, while the more detailed models add one more conservation equation to the equation set. A short summary of each radiation model is given in the list below, a more thorough description of the model used in this work is given later.

Rosseland	The simplest radiation model in Fluent. In this model no extra transport equations are solved, as the radiative transfer equation is rewritten into an algebraic relation.
P-1	The radiative transfer equation is modeled as a separate differential equation. The CPU demand is relatively low, while accuracy is high even for complicated geometries.
Discrete Transfer	The model features a «ray tracing» technique where the radiation leaving a surface in a range of solid angles are approximated by a single ray. If a high number of rays are considered, the model is very CPU-intensive.
Surface-to-surface	In this model only surface radiative processes are considered, thus it is not applicable to cases with a participating medium (e.g. a radiating gas). The surface-to-surface model requires view factors between surfaces to work. If these are computed internally in Fluent, the model is very CPU intensive.
Discrete Ordinates	The most versatile of the radiation models available in Fluent. The model requires discretization of the solid angle through which radiation is considered. With coarse discretizations the model is quite computationally efficient, but increasing the fineness of discretization increases the CPU-demand.

Choice of radiation model is based, among others, on the geometry of the computational domain, and the composition of the medium considered. The desired level of detail in the final solution will also play an important role. The surface-to-surface radiation model is quickly ruled out, as the effects of the flue gas in the cracker would be omitted. Computation of view factors with as many participating surfaces could also be a quite time consuming task. To choose a radiation model, the optical thickness of the problem at hand should be calculated. Optical thickness is a dimensionless value given as:

$$\tau_{opt} = (a + \sigma_s)L \tag{4.2}$$

In equation (4.2) L is a characteristic length of the computational domain (for a circular combustion chamber, L would be the diameter of the chamber). In the following computations, the characteristic length of the firebox is taken as four times the volume of the firebox, divided by the surface area⁴, which gives a value of 2.52 m for the characteristic length. For optical thicknesses larger than 1, the P-1 and Rosseland models are the most efficient models. If the optical thickness is even larger, from 3 and upwards, the Rosseland model is the cheapest and most efficient. For optically thin problems, where τ_{opt} is less than 1, the Discrete Ordinates (DO) and Discrete Transfer models are the only applicable [14].

⁴This is analogous to a hydraulic diameter for a duct flow.

The absorption coefficient used in the above equations can be calculated from optics through Beer-Lambert's law to be:

$$a = \frac{-1}{L_M} \ln(1 - \varepsilon_g) \quad (4.3)$$

In equation (4.3), the total gas emissivity, ε_g is given by the contributions from water vapour and carbon dioxide. To correct for the presence of nonradiating gases in the mixture, a correction factor, $\Delta\varepsilon$, is introduced. The total gas emissivity is thus obtained from [22]:

$$\varepsilon_g = \varepsilon_{H_2O} + \varepsilon_{CO_2} - \Delta\varepsilon \quad (4.4)$$

and the mean beam length, L_M defined as:

$$L_M = 4C \frac{V}{A} \quad (4.5)$$

where V is the total gas volume, and A its surface area. C is a constant with a value of 0.9 [21].

Using numerical values from Incropera and DeWitt⁵ [22] for ε_{H_2O} , ε_{CO_2} and $\Delta\varepsilon$ in equation (4.4), ε_g is calculated. Then the gas absorption coefficient, a, and the optical thickness is calculated from equation (4.3) and equation (4.2), respectively. The scattering coefficient, σ_s is assumed to be zero throughout these calculations. Calculated values at different temperatures are given in Table 4.1

Table 4.1: Emissivities, absorption coefficient and optical thickness for various temperatures

T_g [K]	ε_{H_2O}	ε_{CO_2}	$\Delta\varepsilon$	ε_g	a	τ_{opt}
600	0.25	0.13	0.022	0.358	0.195	0.492
900	0.22	0.16	0.022	0.358	0.195	0.492
1200	0.16	0.17	0.045	0.285	0.148	0.372
1500	0.13	0.13	0.045	0.215	0.107	0.269
1800	0.12	0.11	0.045	0.185	0.090	0.227
2100	0.09	0.08	0.045	0.125	0.059	0.148

With the calculated value for optical thickness being less than 1, the choice of radiation models is between the discrete ordinates and the discrete transfer models. As the discrete ordinates model is valid for all optical thicknesses, and allows for use of detailed models for computing gas absorption coefficients, this model is chosen.

4.3 Discrete Ordinates radiation model

When the DO radiation model is activated in Fluent, equation (4.1) is considered a field equation and is written as:

$$\nabla \cdot (I(\vec{r}, \vec{s})\vec{s}) + (a + \sigma_s)I(\vec{r}, \vec{s}) = an^2 \frac{T^4}{\pi} + \frac{\sigma_s}{4\pi} \int_0^{4\pi} I(\vec{r}, \vec{s}')\Phi(\vec{s} \cdot \vec{s}')d\Omega' \quad (4.6)$$

Each octant of the angular space 4π is discretized into $N_\theta \times N_\phi$ solid angles, or control angles. N_θ and N_ϕ are the number of control angles used to discretize the angular space. As shown on Figure 4.2(a), θ and ϕ refer to the polar and azimuthal angles respectively.

⁵Gas emissivities are given in charts taken from Hottel «Radiant-Heat Transmission» 1954

To account for the fact that radiation can be both incoming and outgoing over one solid angle, referred to as angle overhang, the control angles are further divided into smaller areas. This technique is called pixelation, and is shown in Figure 4.2(b). In this work the default values for both angular discretization and pixelation are used, hence N_θ and N_ϕ are both 2 and the pixel resolution is 1×1 .

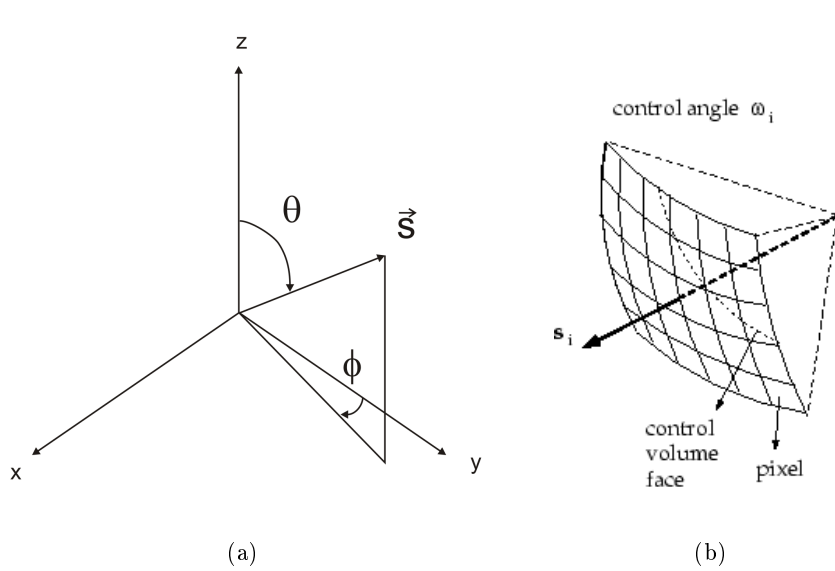


Figure 4.2: Angular coordinate system (a); Pixelation of control angle (b) [14]

4.3.1 Gas radiation

Gas radiation is strongly dictacted by the radiation properties of the gas, cf equation (4.6). The DO model offers the widest range in detail level of all the radiation models when it comes to such properties. The lowest level of detail is to simply assume that all radiation properties are constant. By assuming that the properties are temperature dependent, higher level of detail is achived. The highest level of detail in the DO model arise from employing a band model. When using a band model, the entire radiative spectrum, or Planck distribution, is divided into distinct bands, bounded by an upper and lower wave length. This is a much more realisitc model for gas radiation than to assume a constant emmissivity, as a gas usually only emits radiation over a fraction of the entire wave length domain. Band emission is shown in Figure 4.3, here the bell shaped curve denoted $I_{b\lambda}/I_{b\lambda,max}$ represents a normalized Planck distribution. The peaks distributed along the abscissa represent the bands at which a H_2O/CO_2 mixture actually absorb and emit radiation. The dotted and drawn lines for these bands represent two different band models, namely the wide band and narrow band models respectively [21].

From Figure 4.3 it is evident that to assume a constant absorption coefficient is a very inaccurate approach. A compromise between the overly simplified gray gas assumption, and the computationally expensive band models, is the so called Weighted-sum-of-gray-gases Model (WSGGM) of Coppalle and Vervisch [26]. The model is developed for high temperature flames, and is applicable to radiation in combusting flows. When using the WSGGM, the total emissivity for a mixture containg I absorbing gases over the pathlength, s , is taken as:

$$\varepsilon_g = \sum_{i=0}^I a_{\varepsilon,i}(T)(1 - e^{-a_i p s}) \quad (4.7)$$

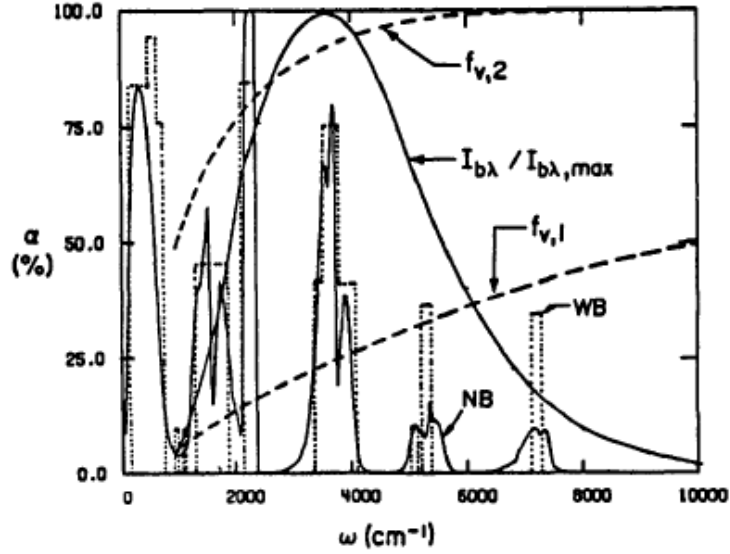


Figure 4.3: Absorptivity of $\text{H}_2\text{O}/\text{CO}_2$ mixture $T = 1000 \text{ K}$, $p = 1 \text{ atm}$, $p_{\text{H}_2\text{O}}/p_{\text{CO}_2} = 0.1$ [21]

Where $a_{\varepsilon,i}$ is the emissivity weighting coefficient of the i th gas, and κ_i its absorption coefficient. In Fluent numerical values for these two parameters are taken from Coppalle and Vervisch [26] and Smith et al. [27]. Both values depend on gas composition, and $a_{\varepsilon,i}$ is also dependant on temperature. Scaling rules for κ_i apply when the total pressure is below 0.9 or above 1.1 atm. When using the WSGGM it is assumed that the gas absorptivity is equal to gas emissivity. Unless the optical thickness of the problem is very low and there are large temperature differences between walls and gas, this assumption holds [14]. The pathlength, s , can be taken as the characteristic length, L_M of the problem, or as the characteristic cell size. However, by using the characteristic cell size, absorptivity becomes grid dependent. The recommended approach is therefore to use the characteristic length as the pathlength, s [14].

In the CFD simulations conducted in this work, the absorption coefficient is taken as a piecewise linear function of temperature. The numerical values used are those in Table 4.1

4.3.2 Wall radiation

Thus far only radiation from the participating media has been considered. However radiation to and from surfaces is just as important when it comes to radiative energy transfer. Interior walls have adjacent fluid or solid zones on both sides, while exterior walls have an adjacent solid or fluid zone on only one side. In this work only radiation from interior walls are considered, as the radiation from the outer surfaces of the cracker is assumed to be negligible due to the low temperature of the surface.

Walls are treated as opaque, i.e. no radiation is transmitted through the wall, and reflection can be either diffuse, i.e. non-dependent on direction, or specular, i.e. normal to incident radiation, or somewhere in between. A schematic of radiation at an opaque wall is shown in Figure 4.4.

Figure 4.4 shows how the incident radiation, $q_{in,a}$ on one side of an opaque wall is reflected partly diffusively and partly specularly. The amount of specular reflection is depending on the diffuse

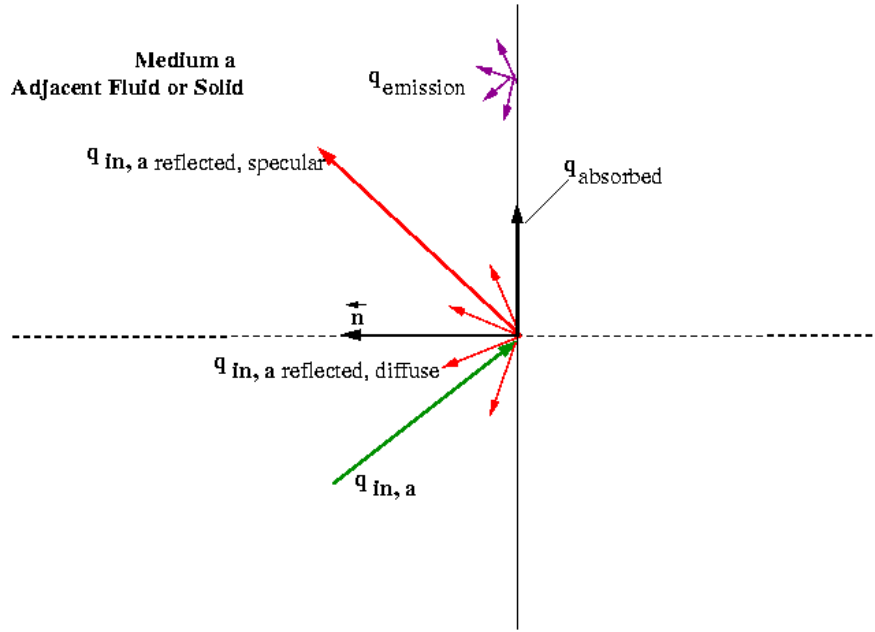


Figure 4.4: Radiation at an opaque wall [14]

fraction, f_d , which is a user specified 0-1 normalized value. Depending on the absorptivity, part of the incident radiation is absorbed in the wall. With q_{in} being the incident radiation to the opaque wall, Fluent computes the following quantities:

Emission from the wall surface	$n^2 \varepsilon_w T_w^4$
Diffusively reflected energy	$f_d(1 - \varepsilon_w)q_{in}$
Specularly reflected energy	$(1 - f_d)q_{in}$
Absorption at the wall surface	$f_d \varepsilon_w q_{in}$

As can be seen from the list above, there is no absorption in the specular component of reflected energy at an opaque wall. In addition, Kirchhoff's law has been used to link wall absorptivity to wall emissivity. By assuming a gray, diffuse ($f_d = 1$) surface, the net radiative flux leaving the surface, q_{out} , is:

$$q_{out} = \underbrace{n^2 \varepsilon_w \sigma T_w^4}_{\text{Emitted}} + \underbrace{(1 - \varepsilon_w)q_{in}}_{\text{Reflected}} \quad (4.8)$$

and the net absorbed energy at the surface is:

$$q_{abs} = \varepsilon_w q_{in} \quad (4.9)$$

To include non-opacity, i.e. transmission of radiation through the wall, the semi-transparent boundary condition should be employed. As transmissivity of the materials considered here is generally very low, all surfaces are regarded as opaque. The idealization of purely diffuse surfaces will also be made. The emissivity of the refractory and reaction coil can be entered into Fluent at various level of detail. The simplest form is to assume perfectly gray surfaces, i.e. that the surfaces have a constant emissivity independent of temperature, wave lengths or other factors. Non-gray treatment of walls results in the discretization of radiative heat flux into bands of width $\Delta\lambda$. At each band the emissivity is set to a constant value.

5 Process side simulation

The CFD simulations compute the temperature distribution in the firebox based on the fired heat and a given heatflux profile. Using the same heatflux profile the thermal dehydrochlorination of EDC in a tubular reactor can be simulated by integrating a set of conservation equations.

5.1 Governing equations

The simplest conservation equations for a tubular reactor is the one-dimensional PFR equations. Plehiers et al. have set forth a set of model equations for PFRs [28]. This set of equations have later been used by both Choi et al. [2] and Park et al. [29] in simulation of EDC cracking. By using the ideal gas equation of state and neglecting the tube bends, Plehiers et al. equations can be rewritten. This is shown in more detail in Appendix C, the resulting equations are given below.

$$\frac{dF_k}{dx} = R_k \frac{\pi d_t^2}{4} \quad (5.1)$$

$$\frac{dT}{dx} = \frac{1}{\sum F_k c_{p,k}} \left[q''(x) \frac{4}{d_t} + \sum_{i=1}^I r_i (-\Delta H_{rx,i}) \right] \quad (5.2)$$

$$\frac{du}{dx} = \frac{-1}{(\rho u - \frac{p}{u})} \left[\frac{p}{T} \frac{dT}{dx} - \frac{p}{MW_{mix}} \frac{dMW_{mix}}{dx} + \frac{2f}{d_t} \rho u^2 \right] \quad (5.3)$$

In the above equations F_k is the molar flow of component k given in kmol/s, T is the absolute temperature of the process fluid given in K, and u is the process fluid velocity in m/s. The parameters MW_{mix} , R_k , ν_{ki} and r_i are defined as follows:

$$MW_{mix} = \left[\sum_{k=1}^K \frac{Y_k}{MW_k} \right]^{-1} \quad (5.4)$$

$$R_k = \sum_{i=1}^I \nu_{ki} r_i \quad (5.5)$$

$$\nu_{ki} = \nu''_{ki} - \nu'_{ki} \quad (5.6)$$

$$r_i = k_{fi} \prod_{k=1}^K [X_k]^{\nu'_{ki}} - k_{ri} \prod_{k=1}^K [X_k]^{\nu''_{ki}} \quad (5.7)$$

The molecular weight derivative in equation (5.3) does not introduce molecular weight as a state variable. The derivative can be written out by using the definition of molecular weight [19]:

$$\frac{dMW_{mix}}{dx} = -MW_{mix}^2 \sum_{k=1}^K \frac{1}{MW_k} \frac{dY_k}{dx} = \frac{-MW_{mix}^2}{\rho u} \sum_k R_k \quad (5.8)$$

The model describes a reaction system where K species are involved in I reactions. Equations (5.1 - 5.7) are presented in a way suitable for computer programming. In equation (5.2) $q''(x)$ is the heat flux in position x given in kW/m² and d_t is the inner diameter of the tubular reactor. f in equation (5.3) is a straight tube friction factor, for simplicity it is held constant at 0.01. Several

correlations for this friction factor can be found in White [30]. The value of 0.01 for f is based on Prandtl's model for the friction factor in smooth tubes, equation (5.9), and a Reynolds number of about 10^6 .

$$\frac{1}{f^{1/2}} = 2.0 \log(Re_D f^{1/2}) - 0.8 \quad (5.9)$$

As equation (5.9) is implicit with respect to f , and is therefore not easily implemented in a computer code. Explicit models exist, but Prandtl's model shows that even by a 10000-fold increase in Reynolds number, the friction factor only drops by a factor of 5. The error by assuming constant f is therefore quite small. A Moody chart confirms that for high Reynolds numbers, the friction factor becomes constant [30].

To include a chemical reaction mechanism in the model, the mechanism must be written in vector/matrix form as:

$$\sum_{i=1}^K \nu'_{ki} [X_k] \Leftrightarrow \sum_{i=1}^K \nu''_{ki} [X_k] \quad (5.10)$$

In equations (5.6) and (5.10), ν'_{ki} and ν''_{ki} denote the stoichiometric coefficients of the reactant and product side of the reaction equation, respectively. $[X_k]$ is the vector containing the molar concentration of each of the species going into the reaction mechanism. The Matlab model can integrate reaction mechanisms ranging from one reaction to several reactions, over 75 elementary reactions containing over 50 species have been tested. Since the change in concentrations for radical species may be several orders of magnitude higher than for stable species, the equation set becomes very stiff as the number of radical species considered is increased. Special numerical integrators are needed to avoid instability in the solution of the equation set. In this work the *ode15s* integrator, which is part of the *ODE* suite, in Matlab is used. The *ode15s* integrator is based on numerical differentiation formulas by Klopfenstein and Reiher [31], and allows integration of stiff as well as non-stiff ordinary differential equations with up to fifth order accuracy.

In this work, a simple reaction mechanism based on reaction (2.6) is used. The stiffness of the equation set is reduced as no radical species are considered. According to Park, the velocity equation, equation (5.3) may also be a stiff equation, due to the friction terms [29]. The *ode15s* integrator is therefore used nonetheless. The reaction rate constant is obtained by combining the simple four step mechanism from Howlett [32] with elementary reaction rates from Choi et al. [2]. The resulting expression for the reaction rate constant is given in Arrhenius form as:

$$k_g = 1.2 \cdot 10^{12} \cdot T^{-0.05} \cdot e^{\frac{-23348}{T}} \quad (5.11)$$

With such a simple expression for the reaction, only the main components of the system can be studied. However, as the radical reactions are left out, the stiffness of the system, and hence the simulation time is greatly reduced. Enthalpy of formation and specific heats for the species considered are taken from Ranzi et al. [8].

5.2 Coupling Fluent and Matlab

The Fluent and Matlab models can both compute the outer surface temperature of the reaction coil. In Matlab the outer surface temperature is computed using a combination of Newton's law of cooling and Fourier's law for heat conduction.

5.2.1 Calculation of outer surface temperature

As can be seen from the differential equations above, temperature is chosen as one of the state variables for the PFR. In the Fluent simulations of the firebox side of the cracker, the outer wall temperature of the coil is computed. However, the temperature used in the PFR equations is the process fluid temperature, not the wall temperature. As the PFR model is one-dimensional, a mean temperature over the tube's cross section should be used. A mean fluid temperature at a given cross section, A_c , can be defined by means of the thermal energy, \dot{E}_t , transported by the fluid through this area:

$$\dot{E}_t = \int_{A_c} \rho u c_v T dA_c \quad (5.12)$$

By defining a mean fluid temperature, T_m , as:

$$\dot{E}_t = \dot{m} c_v T_m \quad (5.13)$$

An overall expression for mean fluid temperature is obtained by combining equation (5.12) and equation (5.13):

$$T_m = \frac{\int_{A_c} \rho u c_v T dA_c}{\dot{m} c_v} \quad (5.14)$$

The mean temperature can be inserted into Newton's law of cooling, and thereby links the mean temperature to the inner surface temperature, T_s :

$$q'' = h(T_s - T_m) \quad (5.15)$$

By introducing Fourier's law for heat conduction through the pipe wall and assuming a linear temperature profile through the tube wall, the relation between outer surface temperature and mean fluid temperature inside the pipe can be written as:

$$T_m = T_o - q'' \left(\frac{t_w}{\lambda_w} + \frac{1}{h} \right) \quad (5.16)$$

In equation (5.16) T_o is the outer surface temperature of the pipe, t_w is the pipe wall thickness and λ_w the thermal conductivity of the pipe material. The tube wall thickness, t_w is 8 mm, the thermal conductivity for the coil material is given in Table D.2.

The convective heat transfer coefficient, h , is depending on boundary layer conditions, and is therefore a function of surface geometry, the fluid motion, and various thermophysical and transport properties [22]. Modeling is thus required in order to get a numerical value for h . A common way to determine h is to use the Nusselt number, defined for an internal flow as:

$$Nu_D \equiv \frac{hD}{\lambda_f} \quad (5.17)$$

From equation (5.17), h can be determined using the Dittus-Boelter equation:

$$Nu_D = 0.023 Re_D^{4/5} Pr^n \quad (5.18)$$

With the n in equation (5.18) being 0.4 for heating ($T_s > T_m$), and 0.3 for cooling ($T_s < T_m$). Equation (5.18) is proven, experimentally, to hold for fully developed turbulent flow with the following limitations:

$$\left[\begin{array}{l} 0.7 \leq Pr \leq 160 \\ Re_D \gtrsim 10000 \\ \frac{L}{D} \gtrsim 10 \end{array} \right]$$

Because the Prandtl number of the gases considered in the reactor is around 0.7 for all temperatures encountered, cf. Table D.3, the first limitation should hold. The second limitation dictates a fully developed turbulent flow regime. To control that none of the two first limitations are violated during calculations, they should be carefully monitored. The last limitation dictates that the length of the tube considered (L) should be more than 10 times bigger than the diameter of the tube (D). In the case of the reaction coil, with an overall length of approximately 150 m and a diameter of 13.4 cm, the ratio of length to diameter is above 1000.

λ_f in equation (5.17) denotes the thermal conductivity of the fluid, and is calculated from:

$$\lambda_f = \sum_i^N \chi_i \lambda_i \quad (5.19)$$

Where λ_i is the thermal conductivity of the i th species. This simple mixing rule results in an overprediction of the mixture's thermal conductivity [33]. However, for the system examined here it is believed to be a sufficient approximation. The other thermophysical properties of the process fluid are also calculated using similar mixing rules. As thermal conductivity for gases is nearly independent of pressure, thermal conductivity data for one atmosphere is used [22]. The Prandtl number, Pr , is also taken as independent of pressure. With thermal conductivity and Prandtl number known, the last parameter needed in order to calculate the convective heat transfer coefficient is the Reynolds number. For an internal flow, the Reynolds number is defined as:

$$Re_D \equiv \frac{uD}{\nu} \quad (5.20)$$

In equation (5.20), u is the fluid velocity, D the inner tube diameter and ν the kinematic viscosity. The velocity is taken from the velocity profile computed by equation (5.3) and D is 0.134 m. The viscosity of a gas is strongly influenced by temperature, but only moderately by pressure [30]. Viscosity is therefore taken as a function of temperature only. Numerical data for the dynamic viscosity of EDC, VCM and HCl are taken from the Heat Exchanger Handbook [34]. The kinematic viscosity is obtained by division by the density, which is obtained through the ideal gas equation of state. All values used to calculate the Nusselt number, and therefore the convective heat transfer coefficient, h , are varying with temperature only. The numerical values used for these properties are listed in appendix D.

5.3 Procedure for coupling Fluent and Matlab simulations

Kaggerud suggests a method for integrating the process side simulations in Matlab with the firebox side simulations from Fluent [15]. This method uses the outer wall temperature to calculate the fluid temperature, and using this fluid temperature to simulate the extent of the cracking reaction. When a simulation of the reaction is finished, equation (5.2) should be used to calculate a new heat flux profile. This approach leads to a number of challenges in the simulations. For instance, the

convective heat transfer coefficient, h , in equation (5.16) is depending on the reactor temperature. Thus, calculation of the fluid temperature, T_m , requires knowledge of the temperature itself. There are ways of overcoming this implicit formulation of fluid temperature. Differentiating equation (5.16) would yield an alternative expression for the fluid temperature gradient as a function of the outer wall temperature gradient, the heatflux gradient and the derivative of the total heat transfer coefficient. Since this would require an approximated expression for both outer wall temperature and heatflux gradients, the integration method suggested by Kaggerud is discarded.

Instead a method based on solving the equation set given by equations (5.1 - 5.7) is used in this work. The first step in this method is to conduct a Matlab simulation using an assumed heatflux profile, in this work the profile is obtained from EDC CRACK. The results from this simulation is easily compared to existing data, such as measured fluid temperatures in the actual cracker and conversion level of EDC. Allready during these Matlab simulations, which have a much shorter running time than the Fluent simulations, the heatflux profile can be tuned to match measured data. With the heatflux profile, fluid temperature distribution and velocity in the reactor, the outer wall temperatures can be calculated using equation (5.16). The next step is to export the heatflux profile to Fluent, and run a CFD simulation on the firebox side of the cracker. This CFD simulation will result in a outer wall temperature on the coil. The outer wall temperature from Fluent can then be compared to that from Matlab, if the two are equal (within some margin of error), and the conversion of EDC agrees with the assumed level, the solution is converged. If the two temperature profiles are not equal, the tuning options are the flue gas inlet temperature or the heatflux profile.

5.3.1 Preparing Fluent data for Matlab calculations.

As the Matlab model is one dimensional, the raw data exported from Fluent need to be processed before they can be compared to the Matlab data. The main difference between the two models is that the Matlab model sees the reaction coil as a long straight⁶ tube, whereas in Fluent the coil is modeled as 11 separate tubes. Figure 5.1 shows how the coil is represented in both models.

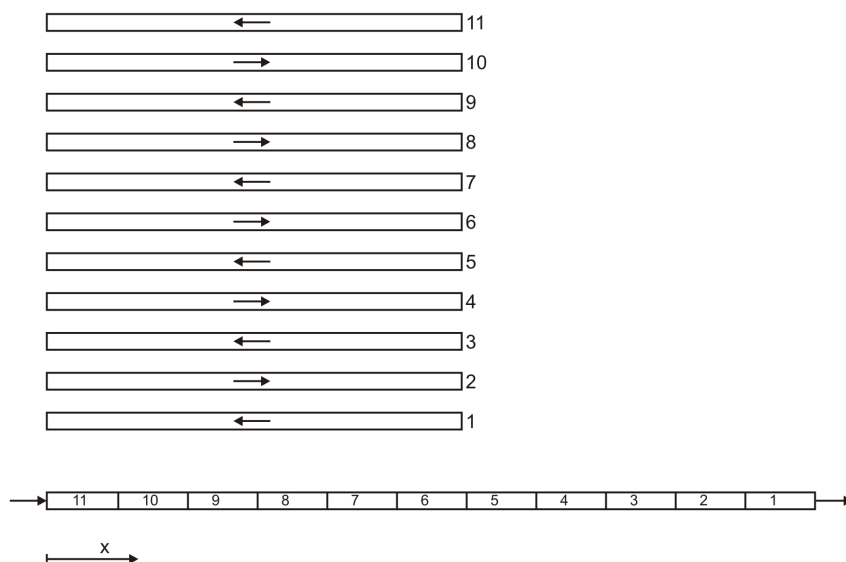


Figure 5.1: Coil representation in Fluent (upper) and Matlab (lower) .Flow direction is indicated by arrows

⁶Pressure drop in the pipe bends can be included in the model

As can be seen from Figure 5.1, the flow in the odd-numbered tubes is in the negative x-direction. This means that in order to arrive at the straight tube representation used in Matlab, the values calculated in Fluent need to be flipped end to end for the odd numbered tubes. The same rule apply when importing data to Fluent; the direction of the flow inside a given tube must be taken into account.

Temperature data are exported from Fluent as XY-plots written to a file. The file contains one vector with x-coordinates and one with the corresponding temperature. There is one such file for each of the 11 tubes in the model. The data in these files are imported to a spreadsheet in MS-Excel where a matrix with the form shown in Table 5.1 is constructed. The data for each tube is sorted ascending with respect to x-coordinate. Temperature variations over the cross section of the tubes are removed by taking the arithmetic average of the temperature at a given x-coordinate, this is done in Matlab. The output from these processing steps is a one dimensional outer surface temperature profile suitable for comparison with the process side simulation model.

Table 5.1: Structure of MS Excel spreadsheet containing temperature profiles

Tube 1		Tube 2		Tube 3		...	Tube 11	
x ₁	T ₁	x ₁	T ₁	x ₁	T ₁		x ₁	T ₁
x ₂	T ₂	x ₂	T ₂	x ₂	T ₂		x ₂	T ₂
⋮	⋮	⋮	⋮	⋮	⋮		⋮	⋮
x _{N₁}	T _{N₁}	x _{N₂}	T _{N₂}	x _{N₃}	T _{N₃}		x _{N₁₁}	T _{N₁₁}

In Table 5.1 the indices N_1 , N_2 etc represent the number of data points for each of the tubes. These numbers are not necessarily the same for all tubes, resulting in blank spaces in the worksheet. When read into Matlab, such blank spaces are represented as «Not-a-Number» or «NaN». As NaN-entries are undesirable when running operations on a matrix, the NaN's are replaced by zeroes in the Matlab routine.

5.4 Simulation setup

In their simulations Choi et al. use 6th order polynomial fitting to measured plant data to obtain the temperature profile along the reaction coil. This is shown in Figure 5.2 [2].

From the temperature profile shown in Figure 5.2 and heat of reaction, Choi et al. estimate the heat flux profile along the coil. The estimated heat flux profile is then used when integrating the governing equations for the PFR. In this work, an adapted version of the method used by Choi et al. is used. Polynomial fitting is not done to the temperature profile, but to the heatflux profile calculated by EDC Crack. The heatflux, $q''(x)$, in equation (5.2) is thus given as an analytical function of position. The heatflux profile is shown in Figure 5.3, and the initial values used are given in Table 5.2. The circles in Figure 5.3 represent the average heatflux in EDC Crack of each tube in the coil. Based on the heat flux profile shown in Figure 5.3 the total heat delivered to the reaction coil is 2.5 MW which is in very good agreement with the heat of reaction calculated earlier, cf. Table 2.2.

Caution should be excersised when using high order polynomials to represent data. While the fit of the polynomial within the range of tha data might be excellent, extrapolations might lead to errors of several orders of magnitude even at short distances.

As can be seen from Table 5.2, there is a small fraction of VCM and HCl in the molar flow entering the reaction coil. This does not agree with the assumption of Choi et al. and Park et al. that the cracking reaction does not start until the process temperature is above 430°C [2,29]. EDC Crack,

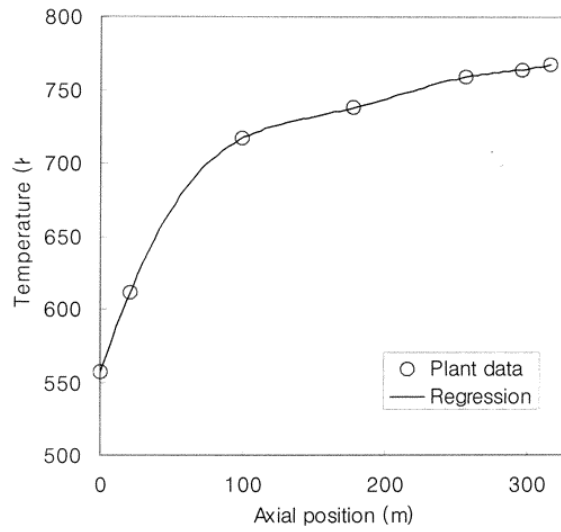


Figure 5.2: Temperature profile used by Choi et al. for EDC cracking simulations [2]

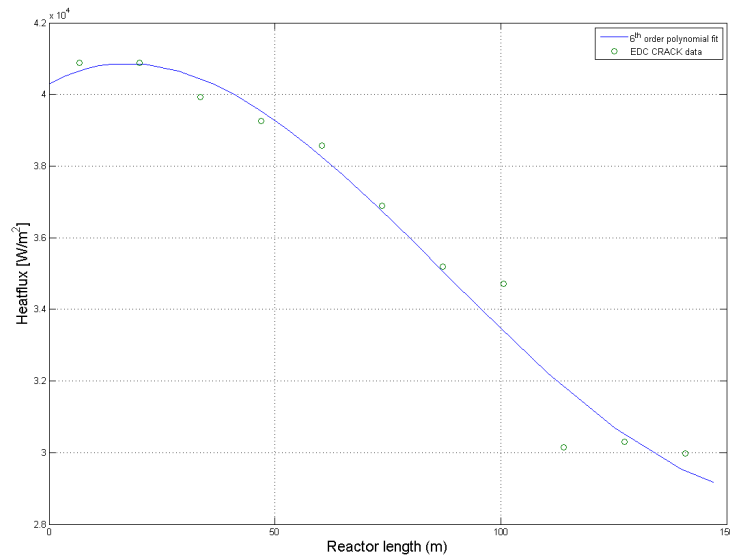


Figure 5.3: Heatflux profile used for process side simulation. Polynomial fitting (drawn line) and EDC Crack data (circles)

Table 5.2: Initial values for Matlab simulation

Property	Initial value	Unit
Velocity	13	m/s
Temperature	696	K
Molar flow, EDC	0.0597	kmol/s
Molar flow, VCM	0.0018	kmol/s
Molar flow, HCl	0.0018	kmol/s

on the other hand calculates a conversion of EDC of 5% out of the shock coil, this value is also used in this work. The total molar flow of EDC is tuned to a capacity of 9 tonnes of VCM produced per coil per hour. The inlet temperature is obtained by interpolating the data given in Table 2.1, the

temperature is approximately 20°C lower than the temperature calculated by EDC Crack in the same position.

6 Results

The results in this work include both Matlab simulations and Fluent simulations. As they are not integrated with each other, they are presented separately.

6.1 Matlab simulation with EDC Crack heatflux profile

As described earlier the first step in the simulation of the EDC cracker is a process side simulation with a prescribed heatflux profile. By using the heatflux profile given in Figure 5.3, and the initial values in Table 5.2, the governing equations can be integrated using Matlab. The running time of the Matlab simulation is about 10 seconds on a 2.60 GHz Pentium 4 personal computer. The computed fluid temperature, measured fluid temperature in the cracker and the outer surface temperature corresponding to the computed fluid temperature are shown in Figure 6.1

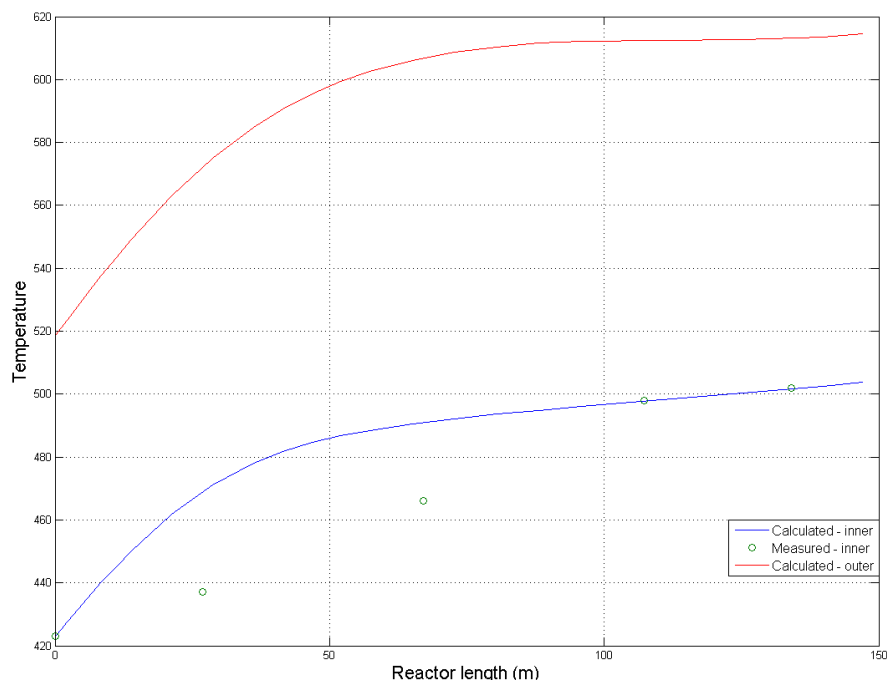


Figure 6.1: Temperature profiles; Fluid temperature, calculated (drawn blue), fluid temperature, measured (green circles) and calculated outer surface temperature (drawn red)

The reported fluid temperature (drawn blue line) follows a very smooth curve. The fluid temperature rises by approximately 60°C over the first 40 meters of the reactor. Then the temperature profile flattens out, and over the last 100 meters of the reactor, the temperature only increases by about 20°C. The outer surface temperature (drawn red line) is calculated from equation (5.16) with the heatflux given in Figure 5.3, and the total heat transfer coefficient calculated as described in Section 5. The outer surface temperature follows a profile very similar to the fluid temperature with the temperature rising quickly over the first 40-50 m and then flattening out towards the end.

Numerical values for the state variables at the outlet of the reaction coil is given in Table 6.1.

Table 6.1: Values of state variables at the outlet of the reaction coil

Property	Final value	Unit
Velocity	23.14	m/s
Temperature	776.77	K
Molar flow, EDC	0.0308	kmol/s
Molar flow, VCM	0.0307	kmol/s
Molar flow, HCl	0.0307	kmol/s

The mass fractions of EDC and VCM corresponding to the temperature profile shown in Figure 6.1 are shown in Figure 6.2.

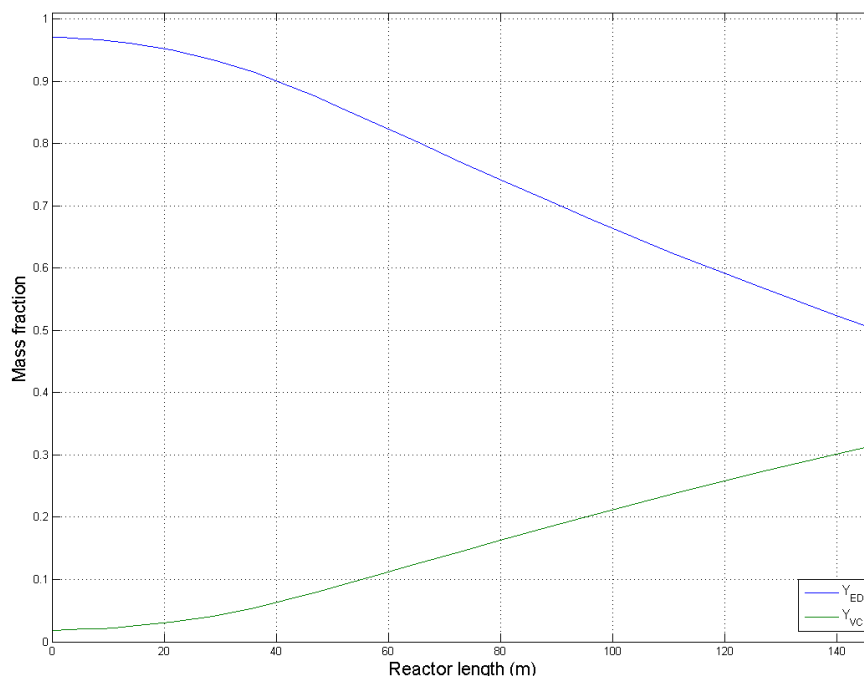


Figure 6.2: Mass fractions of EDC (blue) and VCM (green)

As can be seen from the above figure, the cracking reaction is predicted to be rather slow over the first 40 meters of the coil. Only 10% of the fed EDC is converted at this stage, but as the temperature increases, as do the rate of reaction, and at the outlet the conversion level of EDC is almost exactly 50 wt-%. As only the three main components, EDC, VCM and HCl, are considered in the model, the molar flows of VCM and HCl are equal in every position in the coil. At 50 wt-% conversion of EDC, the mole fractions of each of the three species are all 33% at the reactor outlet.

During the Matlab simulation, the numerical values for the Prandtl and Reynolds numbers are monitored. Subject to round off, the Prandtl number is greater than or equal to 0.7 at all positions along the reactor. The Reynolds number decreases from approximately $1.65 \cdot 10^6$ at the reactor inlet to $0.7 \cdot 10^6$ at the outlet. The Dittus-Boelter equation, equation (5.18), is therefore applicable at all stages along the coil. Furthermore, the simplification of assuming a constant friction factor, f , and calculating this at a Reynolds number of 10^6 , is a satisfactorily approximation.

Since the results from the first simulation correspond well to the measured plant data, the heatflux profile from EDC CRACK is imported into Fluent to conduct a firebox side simulation with the same profile.

6.2 CFD simulation with EDC Crack heatflux profile

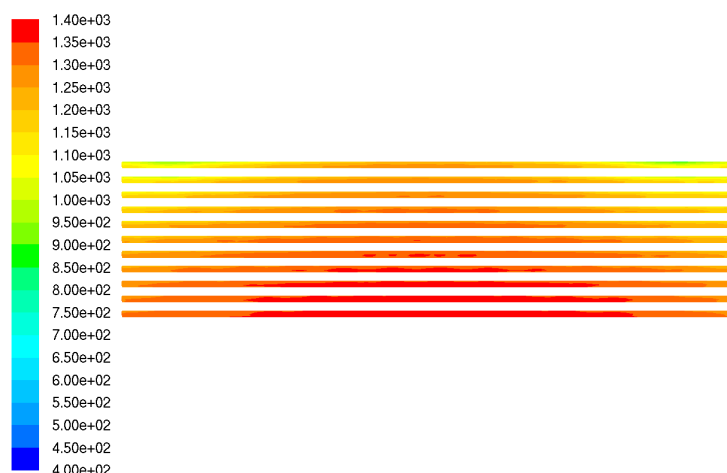
The CFD simulations were run with the convergence criteria, under-relaxation factors and models described earlier. Residuals of the equations for velocities, turbulence properties (k and ε) and flue gas species were all reduced below their given convergence criteria in approximately 100-200 iterations. The continuity equation needed about 1000 iterations to do the same. The energy and DO equations needed a significantly higher amount of iterations. Some minor adjustments of the under-relaxation factors for both equations were also made, they were varied within the range of 0.9 to 1.0. Running on 16 parallel compute nodes, the time per iteration was about 20-25 seconds.

CFD simulations of the EDC cracker with the original boundary conditions listed in Table 3.1 and with modified boundary conditions were conducted. The heatflux profile from EDC Crack has been used in all simulations.

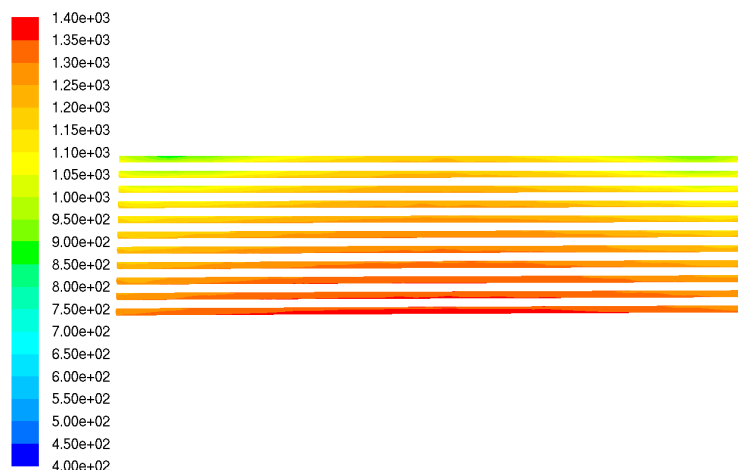
6.2.1 Original boundary conditions

The CFD model is run with the original boundary conditions shown in Table 3.1. In this case a heat sink was added in the upper part of the cracker to represent the heat absorbed in the shock coil. The resulting temperature distributions along the reaction coil seen both from the burner wall and the center of the firebox are shown in Figure 6.3.

As can be seen from Figure 6.3, the temperature along the reaction coil is higher towards the center of the coil than near the ends. Generally, the temperature is higher on the lower tubes than on the higher. In addition, temperature is higher on the part of the tube facing the burner wall than the part facing the center of the firebox. A one-dimensional temperature profile representing the coil's outer wall temperature is calculated using the Matlab routine described earlier. The resulting profile is shown in Figure 6.4



(a)



(b)

Figure 6.3: Temperature distribution along the reaction coil (K); Seen from burner wall (a); Seen from center of the firebox (b)

As can be seen from the one-dimensional temperature profile in Figure 6.4, the temperature along the reaction coil is 300-400 K higher than that calculated from the Matlab simulation, cf. Figure 6.1. In Figure 6.4 each of the «bumps» represent one tube of the coil, starting from the top one at the left and to the lowest at the right. The trend from the thermographic measurements that the temperature is higher at the center of the tube than on the ends, and that there are significant temperature gradients along the reaction coil, are clearly shown in Figure 6.4.

Figure 6.5(a) shows the temperature distribution in a plane perpendicular to the coil in the center of the cracker. Figure 6.5(a) shows the flow direction in a segment of the same plane.

From Figure 6.5(a) it is clear that the flue gas temperature in the firebox is quite uniform with a temperature of about 1500 K. The four «lips» with a higher temperature originate from the four upper burner rows. The temperature distribution in the refractory wall can be observed in the right, rectangularly shaped, part of Figure 6.5(a). The temperature is lowered in the upper part of the cracker due to the addition of a heat sink in the shock zone. The area weighted average of the temperature as it exits the cracker at the top is reported to be 1107.6 K. The vector field in Figure 6.5(b) shows that the velocity of the flue gas in the firebox is relatively low, most have a

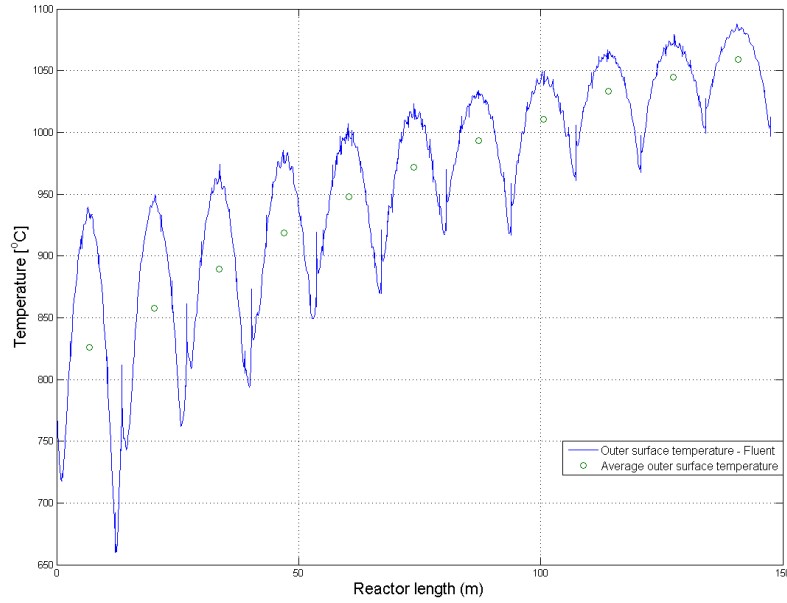


Figure 6.4: One dimensional temperature distribution (drawn) and average values (circles) calculated using Matlab routine

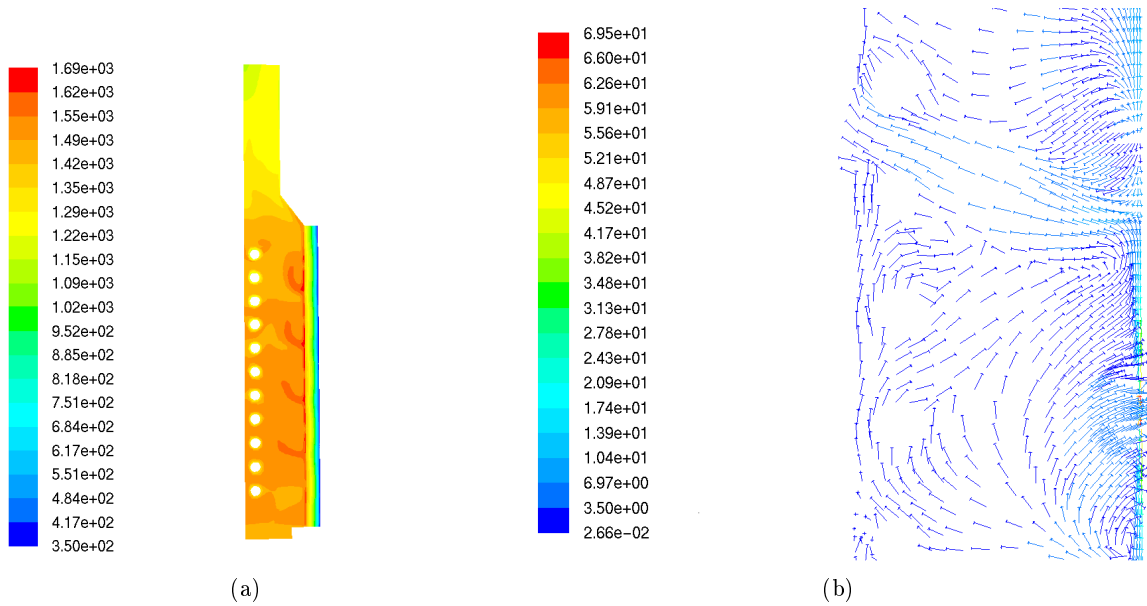


Figure 6.5: Flue gas temperature distribution in the center of the firebox (K) (a); Flow field in the center of the firebox (m/s) (b)

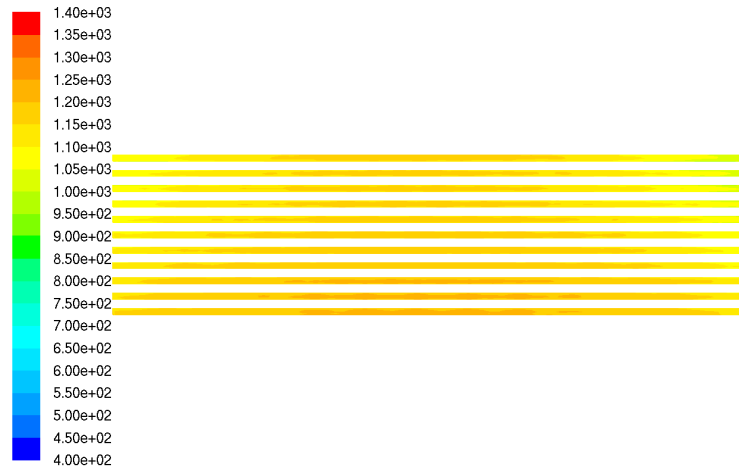
velocity no higher than 1-5 m/s. Out of the burner outlets the velocity is higher, with the velocity being 30-40 m/s. One can also clearly observe that there are large recirculation zones of flue gas near the wall. The velocity profiles are similar for all the cases considered in this work, vector fields are therefore not shown for the other cases.

6.2.2 Modified boundary conditions

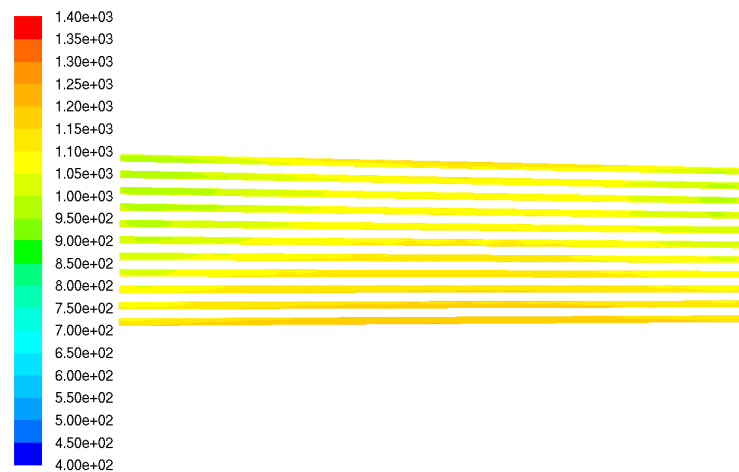
As described earlier, the boundary conditions at the mass flow inlet are adjusted to account for the non-adiabatic nature of the firebox and increased amount of excess air.

6.2.3 Inlet temperature 1800 K

The first simulation with modified boundary conditions was run with the mass flow increased to 3.3 kg of flue gas per second and the inlet temperature lowered to 1800 K. At these conditions, the delivered heat to the cracker is nearly unchanged, as mass flow increases while temperature decreases. Flue gas composition was kept unchanged. In this simulation no heat sink was added in the top of the cracker, hence the shock coil was not represented. The resulting temperature distribution along the reaction coil, seen both from the burner wall and the center of the firebox are shown in Figure 6.6.



(a)



(b)

Figure 6.6: Temperature distribution along the reaction coil (K); Seen from burner wall (a); Seen from center of the firebox (b)

A flue gas temperature profile similar to that in Figure 6.5(a) is shown in Figure 6.7 for an inlet temperature of 1800 K.

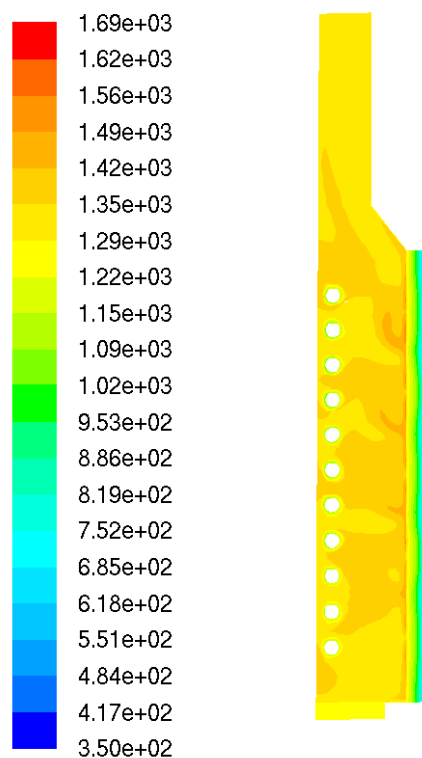


Figure 6.7: Flue gas temperature profile (K) in a plane perpendicular to the reaction coil. Inlet temperature 1800 K

As can be seen from Figure 6.7, the flue gas temperature is quite uniform, with a value of around 1300 K in the firebox. As no heat sink is added in the upper part of the cracker, the temperature level is maintained up to the outlet. The area weighted average temperature at the outlet is reported to be 1321 K. With an even lower inlet temperature, the same trend in flue gas temperature distribution is observed. The temperature is uniform over the firebox cross section, but as the inlet temperature is lowered, the general temperature level is lowered accordingly. With a inlet temperature of 1700 K, the average temperature at the outlet is 1214 K.

Using the Matlab routine to calculate the one-dimensional temperature profile results in the Profile shown in Figure 6.8

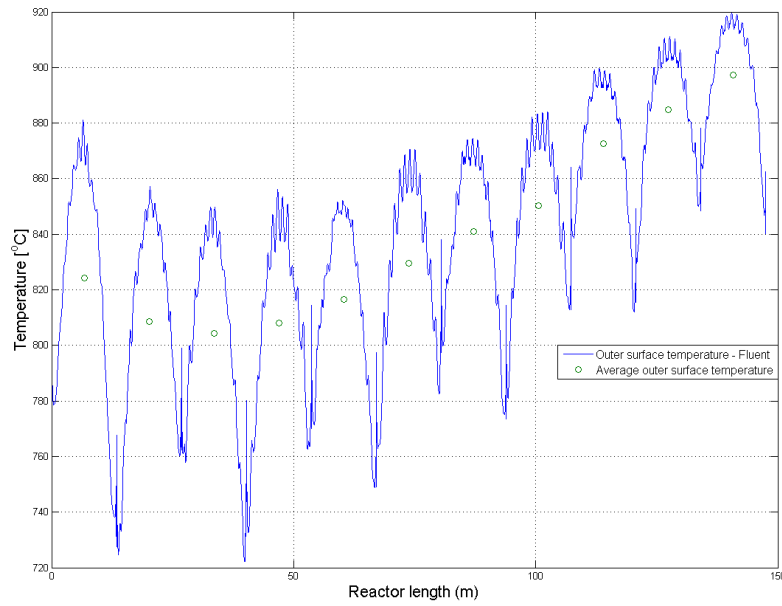
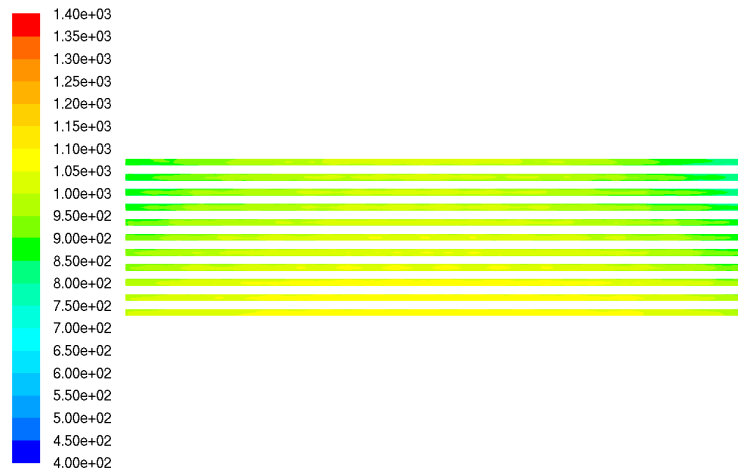


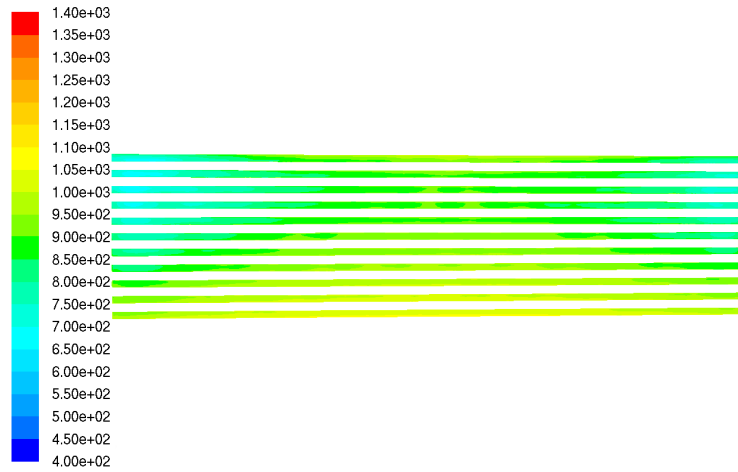
Figure 6.8: One dimensional temperature distribution (drawn) and average values (circles) calculated using Matlab routine

6.2.4 Inlet temperature 1700 K

To further investigate the effect of the non-adiabatic nature of the firebox, the temperature was reduced further to 1700 K. By keeping the mass flow constant at 3.3 kg/s, the total effect delivered to the cracker is lower in this case than in the foregoing cases. Temperature distribution along the coil is shown in Figure 6.9.



(a)



(b)

Figure 6.9: Temperature distribution along the reaction coil (K); Seen from burner wall (a); Seen from center of the firebox (b)

Using the Matlab routine to calculate the one-dimensional temperature profile results in the Profile shown in Figure 6.10

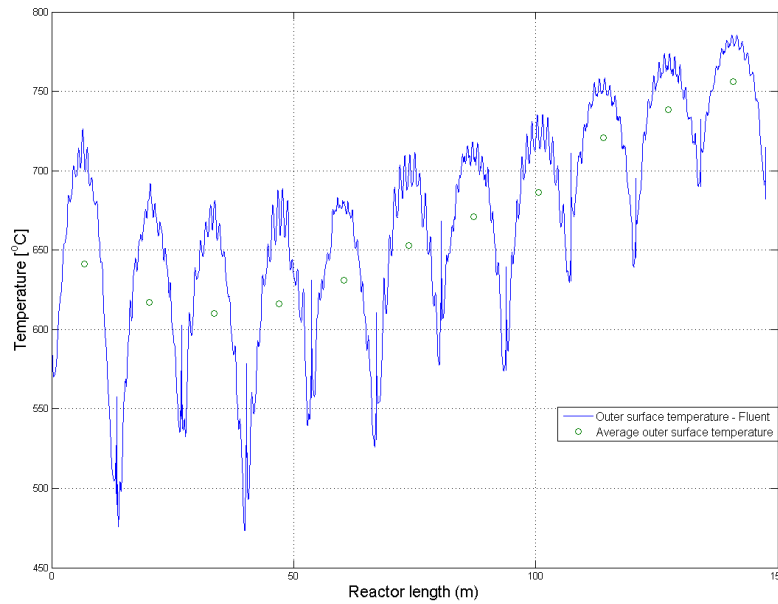
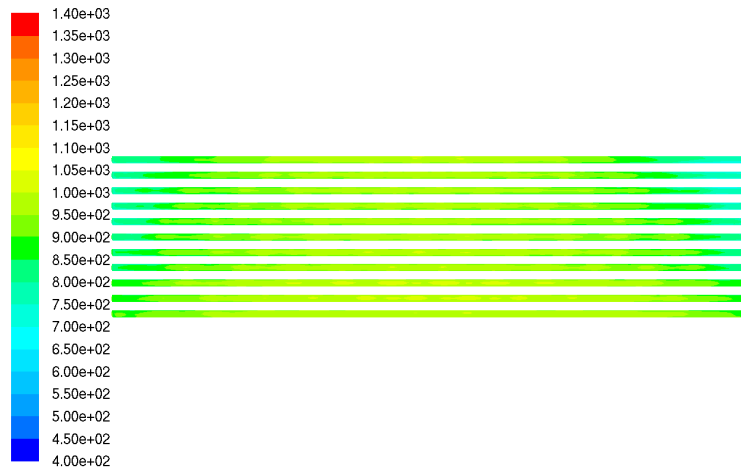


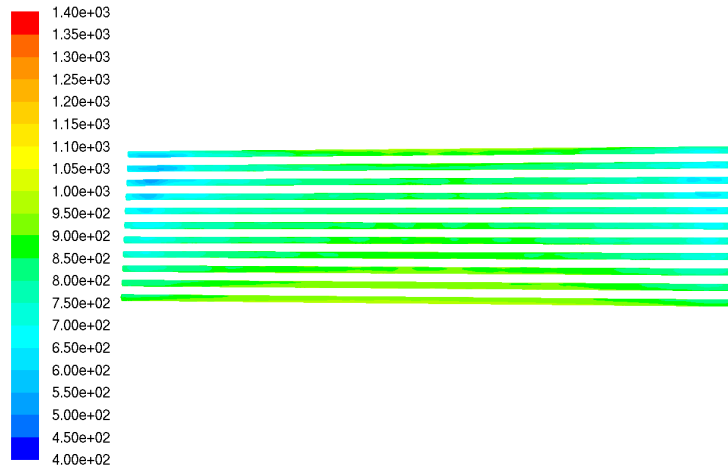
Figure 6.10: One dimensional temperature distribution (drawn) and average values (circles) calculated using Matlab routine

6.2.5 Modified firing profile

In all the other simulated cases, the mass flow of flue gas was kept equal on each burner row. In the actual cracker, the firing is harder in the top three rows than on the lower. The distribution follows a pattern with 22% of the fired heat on each of the top three burner rows, 18% on the second to lowest, and 16% on the lowest. The mass flow of flue gas through the burners are adjusted accordingly, the inlet temperature and total mass flow rate are still 1700 K and 3.3 kg/s respectively. Temperature distribution along the coil is shown in Figure 6.11.



(a)



(b)

Figure 6.11: Temperature distribution along the reaction coil (K); Seen from burner wall (a); Seen from center of the firebox (b)

The temperature distribution of the flue gas is shown in Figure 6.12. As can be seen from the figure, the temperature level in the firebox is around 1100-1200 K. Some small areas with a higher temperature can be seen on the right in the figure, these represent the burner outlets. With the modified firing profile, the temperature at the outlet is reported to 1196 K.

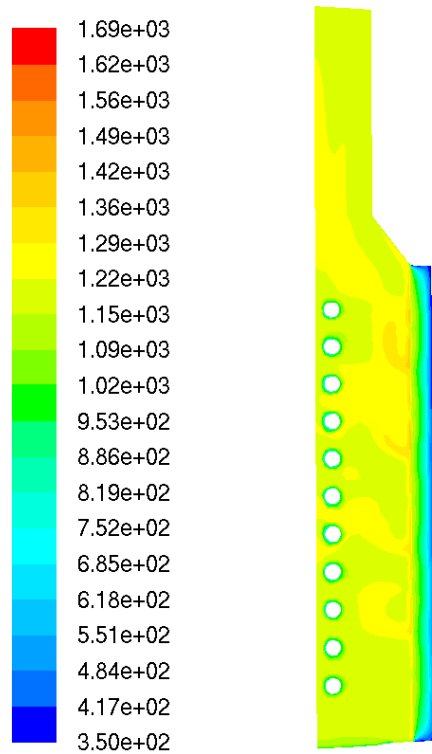


Figure 6.12: Flue gas temperature profile (K) in a plane perpendicular to the reaction coil. Inlet temperature 1700 K and modified firing profile.

Using the Matlab routine to calculate the one-dimensional temperature profile results in the Profile shown in Figure 6.13

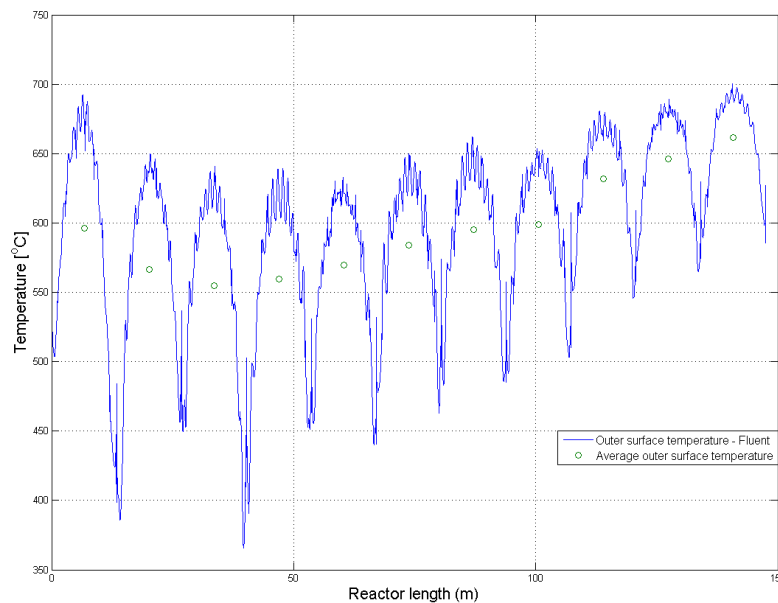


Figure 6.13: One dimensional temperature distribution (drawn) and average values (circles) calculated using Matlab routine

6.3 Refractory

Refractory temperature distributions for the four cases presented above are given in Figure 6.14.

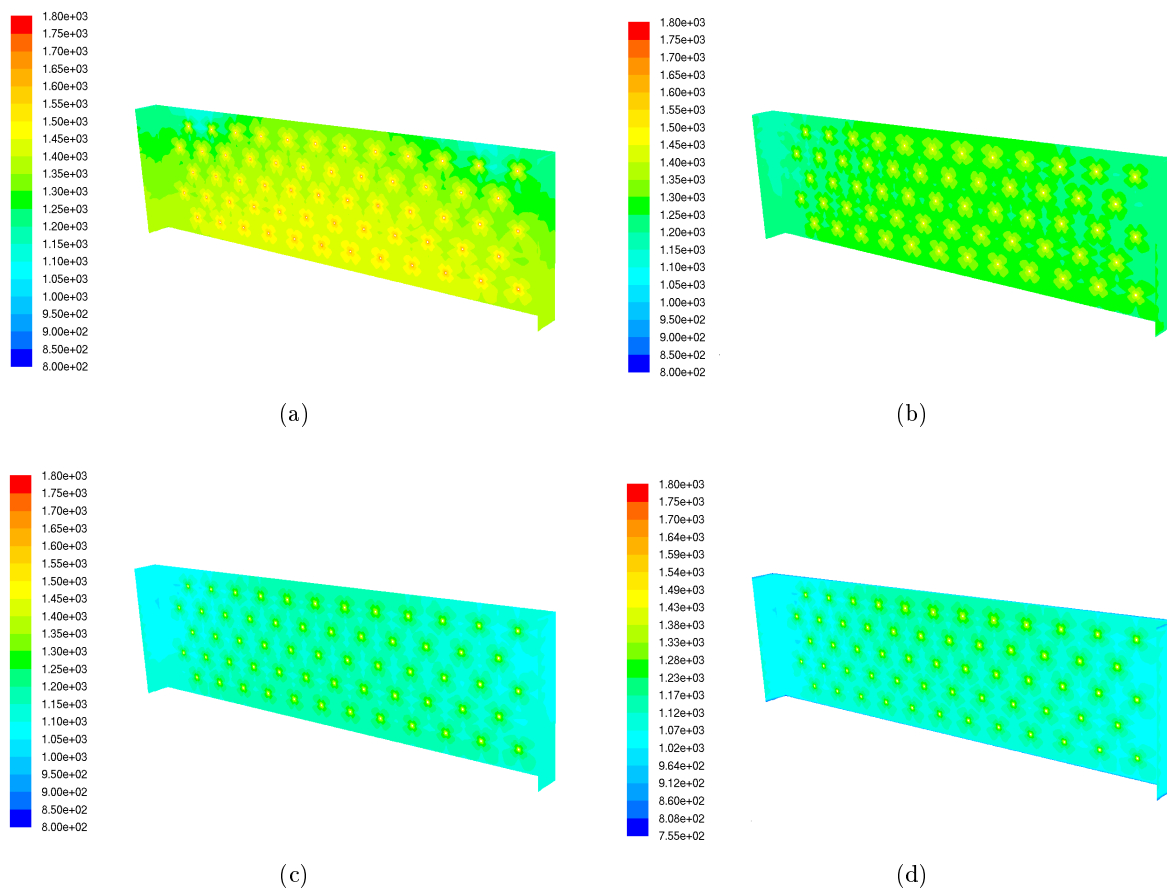


Figure 6.14: Temperature distribution on the inner wall of the refractory (K); Original boundary conditions (a); Inlet temperature 1800 K (b); Inlet temperature 1700 K (c); Inlet temperature 1700 K and modified firing profile(d)

In the Figure 6.14, the evenly spaced areas with higher temperature represent the area around the burners. As can be seen the temperature distribution becomes more and more uniform as the temperature is lowered. The area weighted average temperature of the refractory and burner brick is 1356 K and 1454 K, respectively in the first case (Figure 6.14(a)). While in the case with a modified firing profile, the corresponding values are 1101 K and 1219 K. The heat loss through the refractory wall is nearly unaffected by the variations in inner wall temperature; the highest heat loss is encountered in the original case (78.3 kW), while the heat loss is lowest in the case with an inlet temperature of 1700 K and even firing (62.7 kW). The numerical values for the heat transfer rate through the refractory wall are taken directly from Fluent.

7 Discussion

Both firebox- and reaction side simulations have been conducted. Only the Matlab model can compute the process fluid temperature, and only the Fluent model can compute the temperature distribution in the flue gas and refractory of the cracker.

7.1 Reaction coil temperature

The computed temperature profile based on the heatflux profile given in Figure 5.3 is shown in Figure 6.1. The inlet temperature to the reaction coil is based on interpolation within measured temperature points in the cracker. Hence it is not an explicitly known temperature. Near the outlet of the cracker, the temperature profile agrees with measured data. In the upper part of the reactor, however, the computed temperature is about 5% higher than the measured temperature. This could be due to an incorrect measurement of temperature, after all one of the temperature measurement probes (TI-2020) gives a reading approximately 100°C lower than the expected temperature. The temperature measurement could also be biased by a local «cold spot» on the reaction coil, high local coke formation or other factors. However, from the EDC crackers operated by Hydro Polymers at Rafnes, the same deviation in measured and simulated (EDC Crack) data is observed [35]. The temperature measurements are therefore believed to be correct. The difference between measured and computed temperatures must therefore be sought explained by other factors. The most likely contributors to lowering the process fluid temperature are endothermic chemical reactions. It has been observed in lab scale tests that the dehydrochlorination of EDC can start at temperatures as low as 275°C, and a conversion level of EDC of 15 wt-% at 400°C is observed [36]. Borsa also reports that impurities in the EDC feed, such as Cl₂, FeCl₂ and CCl₄, will initiate the cracking reaction at lower temperatures [37]. If this is transferable to full scale reactors, the cracking reaction does not start in the lower tubes of the shock coil, but perhaps as far up as the fourth or fifth tube. The effect of low temperature cracking and byproducts formation could be verified by running a process side simulation for both the shock- and reaction coil with a detailed reaction mechanism, such as the one presented by Choi et al. or the very comprehensive mechanism presented by Borsa [2,37].

The outer surface temperature is computed from the fluid temperature, heatflux profile and total heat transfer coefficient. As can be seen from Figure 5.3, the EDC Crack heatflux profile has a drop in heatflux of about 4.5 kW/m² between the fourth and the third tube from the bottom. Very little is known about the algorithms used in EDC Crack to calculate these heatflux profiles, but as the program is very small (less than 1.4 MB) it is reason to believe that some sort of coarse zonal method is used for radiative heat transfer. The heatflux profile used in the Matlab simulations is the drawn line in Figure 5.3, and as can be seen from the figure the heatflux profile does not represent the heatflux for tube three and four from the bottom well. On the fourth tube the heatflux is too low and on the third it is too high. A higher heatflux may result in a higher conversion rate and/or a higher process fluid temperature. Accordingly, there is some uncertainty in the temperature profile over the last four tubes, or last 50 meters, of the coil. As polynomial fitting is used to represent the heatflux profile in the Matlab model, the large difference in heatflux between tube four and three is smoothed out. This smoothing of the heatflux profile will result in a smoothing of the fluid-, and thereby also the outer wall- temperature. The effects of this step in heatflux between the third and fourth tube can also be seen in Figure 7.1, where the averages of the one dimensional temperature profiles computed for various inlet conditions are shown. In the legend of Figure 7.1, the temperature in K refers to the inlet temperature of the flue gas. The drawn lines are the same as that shown in Figure 6.1. Up until 100 m, the temperature profile has a smooth shape, and if the profile had been extrapolated, the shape of the temperature profile would flatten out over the last 50 m of the reactor, similar to the profile computed in Matlab. With the change in heatflux

between the third and fourth tube, the temperature does not flatten out, but starts to increase in stead.

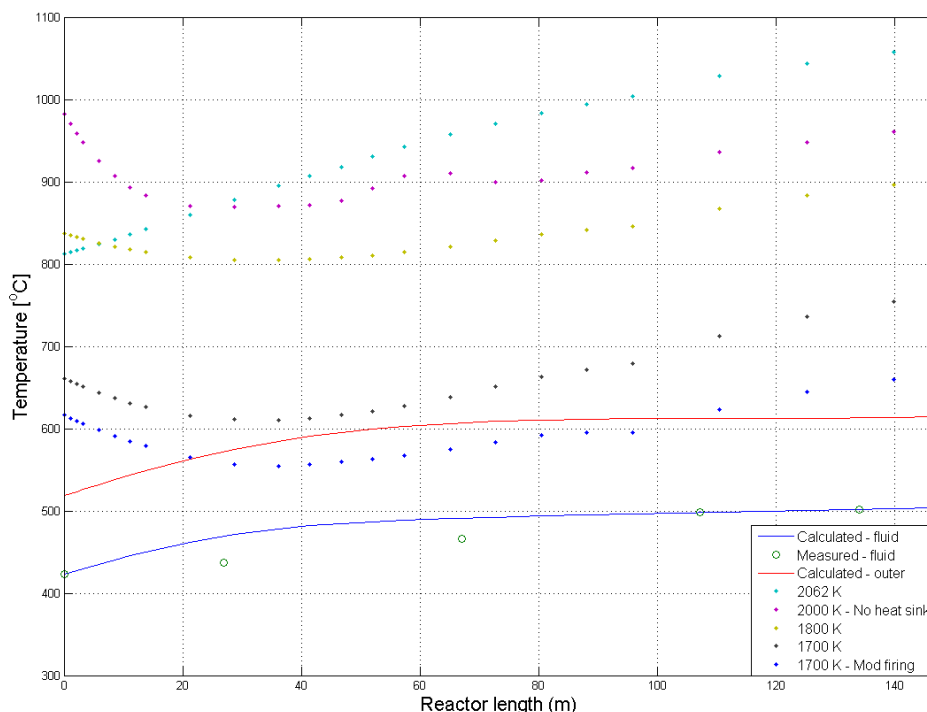


Figure 7.1: Outer surface temperature of the reaction coil at different inlet conditions; 2062 K and heat sink (light blue); 2000 K and no heat sink (purple); 1800 K and no heat sink (yellow); 1700 K and no heat sink (black); 1700 K, no heat sink and modified firing profile (blue). Process side simulation temperatures; Measured fluid temp (green circle), computed fluid temperature (drawn blue), and calculated outer surface temperature (drawn red)

When comparing the calculated temperature profile to the thermographic reference data, there is a large difference between these two profiles. From the thermographic report, the temperature on the third pipe from the bottom is reported to be between 620 and 700°C. The Matlab model computes a temperature in the same position of approximately 610°C. There are many possible factors explaining this difference. First of all, the Matlab temperature profile is an average outer surface temperature, whereas the thermographic measurements give the temperature along a narrow line only. In the Matlab profile all differences in temperature between the part of the tube facing the burner wall and the part facing the center of the firebox are smoothed out. The thermographic data show that the difference between the burner facing and the center facing parts of the tube can be as much as 50-60°C. Furthermore, the thermographic measurements were conducted at a time when the cracker was nearly due for de-coking, and the coil was therefore significantly coked. Coke is a very poor thermal conductor, and therefore leads to a higher outer surface temperature than if the process tubes were clean.

A comparison between computed outer surface temperature on the part of the coil facing the burner wall (front) and the part facing the center of the firebox (back) with the thermographic data for the same tube is given in Figure 7.2. The Fluent data are taken from the case with an inlet temperature of 1700 K and modified firing profile.

From the figure it is clearly shown how the Fluent model computes a significant difference in temperature between the burner side and center side of the coil tubes. It is also clear that the

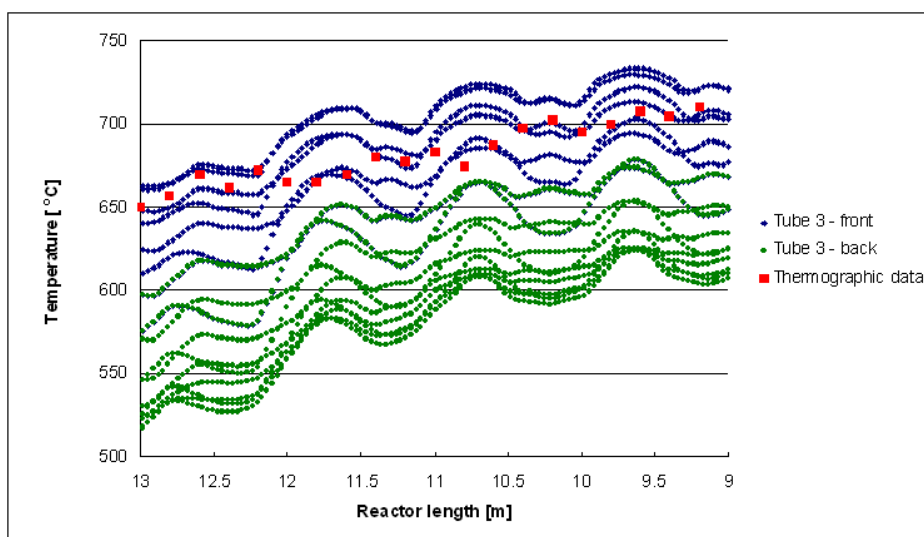


Figure 7.2: Fluent temperatures on the burner side (blue) and center side (green) of the third tube from the bottom of the firebox. Thermographic data on the burner side of the same tube (red squares)

thermographic measurements do not contradict the outer surface temperature profile calculated by Matlab. The measured data are reported along a line on the part of the tube facing the burner wall, cf. Figure 2.4. These data fit well within the computed temperature on the front of the tube from Fluent. The arithmetic mean of the computed data, however, is affected by the lower temperature on the back of the tube and this is probably also the case in the actual cracker. The thermographic measurements show a difference of more than 50°C between front and back of a given tube, hence the average temperature over the entire cross section of the coil tubes is considerably lower than the temperature shown in the thermographic report.

7.1.1 Molar flow

The process simulation model computes molar flow of each species as a function of position, x . In postprocessing, these molar flows are converted into mass- or mole fractions to ease the result presentation. From Figure 6.2 it can be seen that the conversion level of EDC is 50 wt-%, this is equal to the assumed conversion level of EDC out of the firebox. A comparison between the mass fractions of EDC and VCM and temperature profiles in the reactor from Matlab and EDC Crack is given in Figure 7.3.

EDC Crack computes a higher temperature in the first 20 meters of the reactor, with the reported mean temperature over the first tube in the reaction coil being 459°C . This results in a slightly higher conversion rate of EDC in the start of the reactor. This is made visible by the fact that the mass fraction of EDC is about 5% lower in the first 80 meters of the reactor in the EDC Crack simulations than in the Matlab simulations. The two models have an almost identical conversion level of EDC at the reactor outlet. The temperature used in the Matlab simulations is more in line with the measured temperature in the cracker, but as there is no temperature measurement at the start of the reaction coil, the inlet temperature is an estimate. Since the Matlab model used in this work and the reactor model used in EDC Crack are very likely to be almost identical, it is not remarkable that the two models produce such similar results. EDC Crack also include the

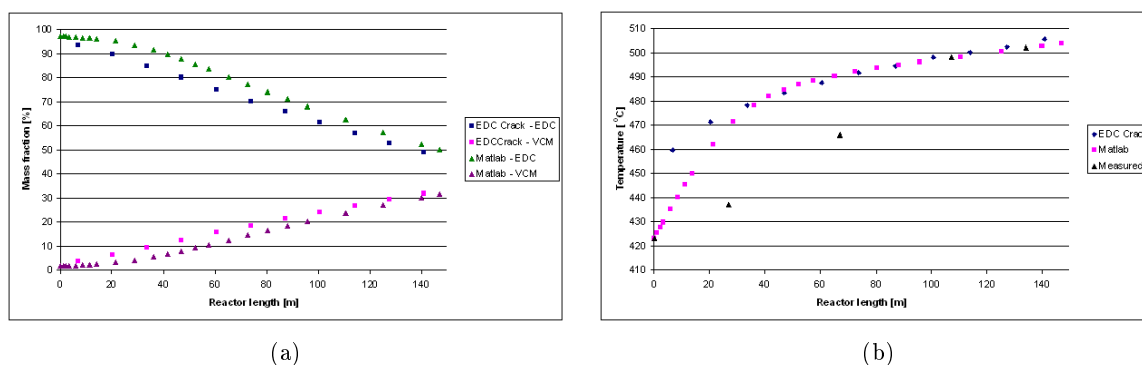


Figure 7.3: Comparison between EDC Crack and Matlab models; Mass fractions of EDC and VCM (a); Reactor temperature, measured temperatures also included (b)

calculation of radicals and byproducts, but these only make up about 1% of the total molar flow in the model.

7.2 Firebox properties

The first Fluent simulation had a flue gas inlet temperature of 2062 K, the resulting temperature distribution along the reaction coil are seen in Figure 6.3 and Figure 6.4. When comparing the computed temperature profile from this simulation with the one computed by Matlab, it is clear that the general temperature level in the cracker is too high. This is seen both from the temperature profile in Figure 6.4, where the temperature is 3-400 K higher than the temperature distribution computed in Matlab, and that the flue gas exit temperature is 200 K higher than expected. The shape of the temperature profile, however, resembles that computed by Matlab. This indicates that the method used for simulating the firebox is working, but that the temperature level of the incoming flue gas is too high. By lowering the temperature and increasing the mass flow of flue gas, a more realistic representation of the firebox is sought. By lowering the inlet temperature, the overall temperature level in the firebox is also lowered. The temperature distribution along the reaction coil is lowered accordingly. As can be seen from the one-dimensional temperature profiles in Figure 6.8, 6.10 and 6.13, the temperature level along the coil is rapidly reduced as the flue gas inlet temperature is lowered. The profiles also predicts that the temperature on the first two tubes from the top is higher than on the third. Simulations run with a flue gas inlet temperature of 2000 K and no heat sink in the top of the cracker show the same tendency in the coil's temperature distribution, cf. Figure 7.1. This shows that the tubes in the shock coil are influenced by radiation from the firebox to such an extent that the temperature on the top two tubes in the reaction coil is reduced. Furthermore this shows that a model for the firebox of the EDC cracker where the shock coil is left out altogether, is not a fully adequate model.

7.2.1 Flue gas temperature

The flue gas exit temperature can give a good indication of the overall temperature distribution in the cracker. Flue gas exit temperature is taken as the area weighted average of the temperature at the pressure outlet at the top of the CFD model. The Matlab simulations show that the EDC Crack heatflux profile is a good representation of the actual cracker, and the flue gas exit temperature is therefore the only tuning parameter left. For the three cases with lower inlet temperature and increased mass flow, the temperature out of the pressure outlet should be compared with the temperature out of the firebox in Table 2.2, 1007°C or 1280 K. The case with a higher inlet tempera-

ture and a shock zone representation should be compared to the temperature out of the shock zone, 636°C or 909 K. Since the mass flow of flue gas used in the calculations behind the temperatures in Table 2.2 is 3.3 kg/s, the original case temperature is not directly comparable to these. With a lower mass flow of flue gas, the outlet temperature from the shock zone is about 20°C higher than that given in Table 2.2. A comparison between the theoretical outlet temperature of Table 2.2 and computed temperature out of the pressure outlet in the CFD model, shows that the temperature level in the first case is too high. As the reported area weighed average temperature is 1107 K, the temperature is almost 200 K too high. The two cases with an inlet temperature of 1700 K have a temperature out of the pressure outlet lower than the expected value, 1214 K and 1196 K for the case with even and modified firing respectively. For the case with an inlet temperature of 1800 K, the outlet temperature is 1321 K, which is only 40 K higher than the theoretical temperature.

Stefanidis et al. ran CFD simulations on a steam cracking furnace with detailed combustion mechanisms [38]. The fuel and equivalence ratio suggests an adiabatic flame temperature⁷ well above 2100 K. With a combustion mechanism consisting of 35 elementary reactions among 16 species, and by employing the Eddy Dissipation Concept of Gran and Magnussen [39] for combustion, the highest encountered temperature in the computational domain is 1918K [38]. The burners in their model were long flame burners, thus the results are not directly comparable to those obtained in this work. However, this suggests that to assume that the combustion products are at the adiabatic flame temperature results in an overprediction of temperature level. Most of the difference between actual temperature and adiabatic temperature is probably due to radiation from the reaction zone. In this zone, the temperature, and therefore the radiative heatflux from the gas, is at its highest. As the cracker is operated in steady state, the radiative heat transfer from the reaction zone, will lead to a reduced temperature in this area.

By setting the flue gas inlet temperature, the amount of heat delivered to the cracker is given. This amount of heat can be tuned to match the heat released from combustion of fuel at given conditions. A major shortcoming in omitting the combustion reaction in the way it has been done in this work, is that the only way of affecting the temperature level in the computational domain, is to lower the flue gas temperature, or increase the mass flow of flue gas. Furthermore, neither the flue gas temperature, nor the combustion zone temperatures, are explicitly known or easily measured. This results in a simulation model where the boundary conditions are not known, but can only be represented by estimates. If, on the other hand, the combustion reaction had been included in the model, boundary conditions would be much more accurate. The temperature and pressure of the fuel gas at the inlet to the cracker are known from plant measurements, as is the consumption of fuel. Excess air can be tuned to match the measurements of CO₂ and O₂ in the top of the cracker. With the combustion reaction included, the flue gas temperature would be calculated based on the fuel gas consumption and the heat absorbed in the reaction coil. This means that all internal heat exchange between hot combustion products and cold combustion reactants, and the radiation from the flame zone to the firebox volume would be computed during simulations.

The measurements of O₂ and CO₂ indicate that the amount of excess air is about 25%. The burners, however, are said to operate at 10% excess air, and simulations by Bech and Manger [40] and statements from the burner provider, Selas, support this [6]. Selas also states that 10% excess air gives the best performance of the burners. The excess air is probably caused by leaks in the cracker. Due to the high velocities of the flue gas and buoyancy effects, there is a significant negative pressure in the firebox [41]. This, in turn, will draw air through any small opening available, resulting in lowering of the overall temperature level. The effect of increasing the excess air level from 10 to 25% is illustrated in the case with an flue gas inlet temperature of 1800 K. In this case, the delivered heat to the cracker is nearly equal to that of the first case. As can be seen from Figure 7.1 the temperature level of the reaction coil is reduced by as much as 100-150 K, just by increasing the mass

⁷Calculated with HPFLAME

flow of flue gas, while maintaining the delivered effect. This shows that leaks in the cracker result in a substantial loss of energy, and that there is a potential for reducing the energy consumption, or increasing the throughput, by reducing these leaks.

7.2.2 Flow pattern

The flow pattern in a section of the cracker is shown in Figure 6.5(a). From this figure it is evident that the high velocity flow of flue gas out of the burner outlets leads to recirculation of flue gas from the firebox volume and into the close vicinity of the burner outlets. This ejector effect is important, because the hot combustion products are the only means of igniting the fuel/air mixture that enters the cracker through the burner outlets. In the simulations conducted on a single burner by Kaggerud, similar recirculation zones were predicted to form downstream of the burner outlets [15]. Figure 7.4 shows the flow field at the burner outlet for combustion of a mixture of 90% methane and 10% hydrogen with 10% excess air.

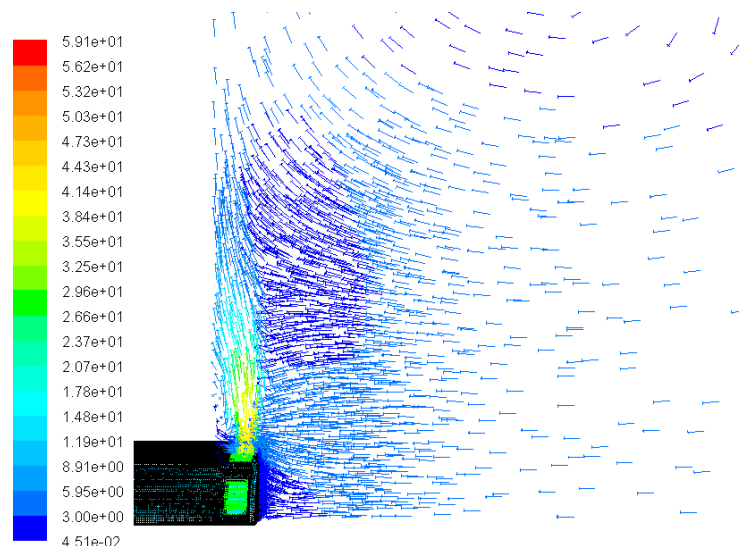


Figure 7.4: Flow field in the close vicinity of the burner. CFD simulation of a single burner, with a fuel composition of 90% methane and 10% hydrogen [15]

Figure 7.4 clearly shows the ejector effect of the high velocity fuel/air mixture on the hot flue gas in the cracker. The hot combustion products are mixed with the cold fuel/air mixture, and the fuel is ignited. In fact the ejector effect in the simulations of a single burner was so powerful that a large mass flow from the pressure outlet 50 cm downstream of the burner was induced [15]. A consequence of this back flow is that the temperature fields in the simulations of one single burner conducted by Kaggerud are likely to be biased by the 2000 K used as a boundary condition for the pressure outlet. From the simulations conducted in this work it is shown that even in the case where the flue gas inlet temperature was set to above 2000 K, the temperature of the flue gas that circulates back into the combustion zone will only be about 1500 K.

7.2.3 Refractory temperature

As can be seen from the four temperature distributions shown in Figure 6.14, the temperature at the inner wall of the cracker's refractory is highly dependent on the flue gas inlet temperature. Between the highest and lowest inlet temperature, the temperature difference is over 200 K. With radiation

depending on T^4 , lowering of the surface temperature from 1356 K to 1101 K results in the radiative heatflux from the surface being more than halved, with all other parameters held constant.

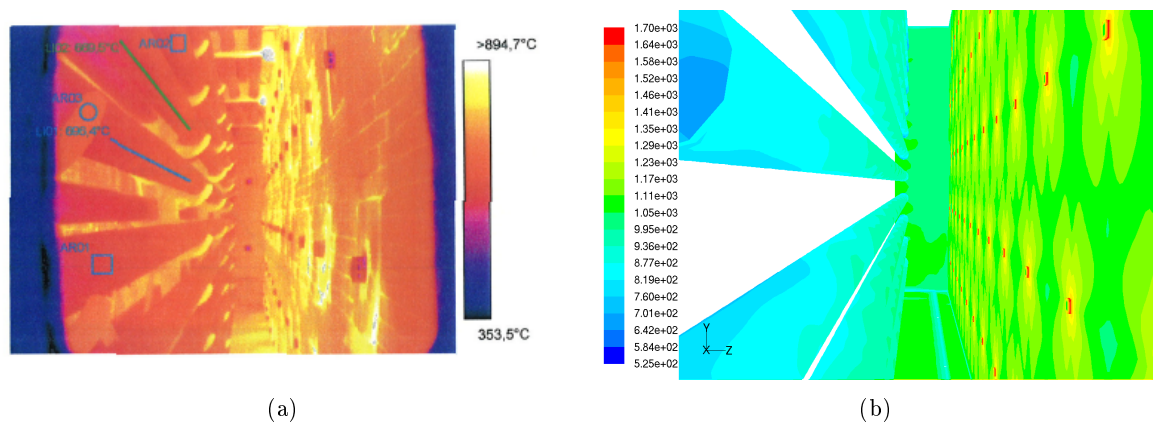


Figure 7.5: Temperature distribution along the reaction coil and refractory; Thermographic picture [42] (a); Fluent simulations with inlet temperature 1700 K and modified firing (b)

Figure 7.5 shows a thermographic picture and a temperature profile computed by Fluent over the same segment of the EDC cracker. The refractory wall temperature in the thermographic picture and the Fluent simulation show the same trend. With fairly uniform temperature distribution over the refractory wall, but with the temperature significantly higher in the burner tiles enclosing the burners. The thermographic measurements show that the temperature of the refractory is about 800-900°C. This agrees with the simulated data with a inlet temperature of 1700 K and modified firing profile, where the average refractory temperature is 1101 K or 828°C. The burners are shown in Figure 7.5(a) as the circular tubes protruding from the wall, and the square tubes in Figure 7.5(b). The main difference between the computed and measured data is that the burners themselves appear to be much colder than the refractory in the measured data, while they are much hotter in the simulations. This is caused by the cooling effect of the cold fuel/air mixture on the burner tube in the actual cracker. This effect can also be observed in the simulations of a single burner conducted by Kaggerud, where the part of the burner that protrudes into the cracker volume is approximately 300 K cooler than the flue gas [15]. With the flue gas inlet temperature at 1700 K, the burner is not cooled, but heated by the incoming gas.

7.3 Sources of computational instability

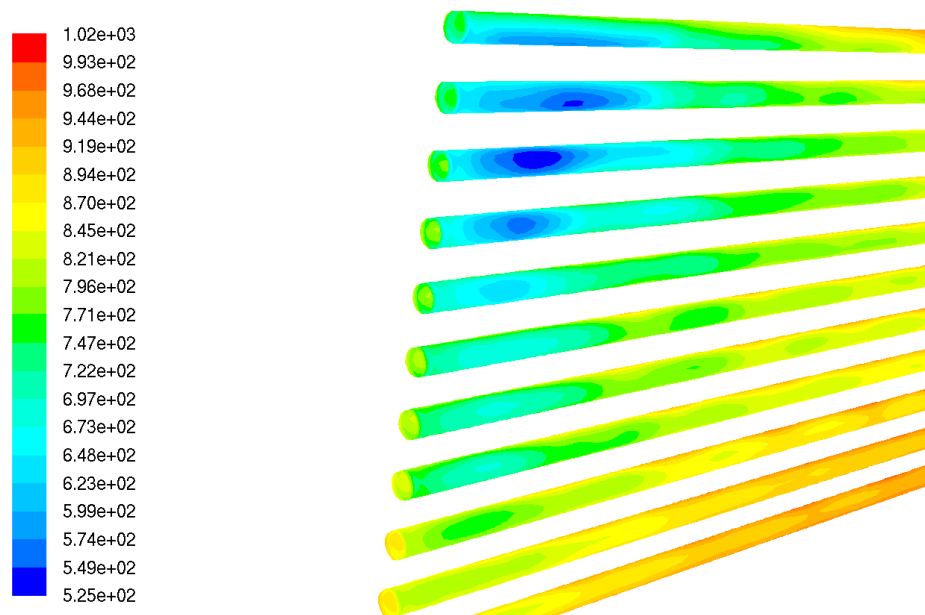


Figure 7.6: Cold spots on the center facing side of the reaction coil

In the cases with lowered flue gas inlet temperature, the Fluent calculations became unstable when a heat sink was added in the shock section of the cracker. Instability was observed by the fact that the temperature was limited to the minimum allowable temperature in several thousand cells in the computational domain. Figure 7.6 shows a section of the reaction coil that is facing the center of the firebox. As can be seen there are significant cold spots on the outer surface. The figure is taken from the simulation with a modified firing profile. Similar cold spots are observed at the same location on all simulations with the EDC Crack heatflux profile. With the original boundary conditions, the cold spots are not equally pronounced compared to the cases with a lower inlet temperature, but they are present nevertheless. The source of these cold spots is probably a combination of the one-dimensional heatflux profile and the fact that the center facing part of the reaction coil is shielded from direct radiation from the refractory walls. The one-dimensional heatflux profile dictates that the heatflux is even over the entire cross section of the tube. As the view factor between the center facing part of the tube and the refractory is near zero, there is no direct radiation from the refractory to this part of the coil. The result is that energy that is not available at the shadow side, is attempted transferred to the coil. This will eventually lead to a too low temperature in these areas. Conduction in the tube wall will even out some of these temperature differences, but as can be seen from Figure 7.6 the temperature differences can be quite large over short distances of the tube. According to the printouts from Fluent during the calculations, the temperature was first limited in the areas shown as cold spots in Figure 7.6. Thus, the evenly imposed heatflux profile is believed to be, at least partially, the reason for computational instability in the simulations.

The default minimum allowable temperature in Fluent is 1 K, and the computed temperature was even lower than this. With such a low minimum temperature in a case with high temperatures, the risk of computational instability is high. If the temperature in one cell decreases below the minimum temperature, a large heatflux is induced from the neighbouring cells, and consequently the temperature is reduced in these cells too. Even by increasing the minimum temperature to 340 K, which should be sufficiently low, as the outer wall temperature is set to 350 K, the temperature was limited to the minimum temperature in several thousand cells. In the same manner as before,

the temperature was first limited to the minimum temperature at the shadow side of the coil.

The unstable behavior of the simulation model at the conditions mentioned above indicate that to represent the shock coil only by including a single volumetric heat sink is a too simple approximation. To avoid modifying the entire grid, one could separate out more than one zone. By defining non-porous volumes that represent the each of the tubes in the shock section, a model that represent the entire firebox and shock section could be made without having to make a entirely new mesh.

8 Conclusions and further work

The objective of this work has been to develop a coupled simulation model for the firebox- and process side of the EDC cracker operated by Hydro Polymers in Stenungsund. Two separate models are used, a Matlab model that simulates the cracking reaction and a CFD model that simulates the heat transfer from combustion of fuel gas to the reaction coil. Different cases have been run in the CFD model to match the simulated data with measured data.

The reactor model used in the Matlab simulations is a simple one-dimensional model combined with the ideal gas equation of state and a simple global reaction mechanism. Nevertheless, the Matlab model can, with a given heatflux profile, predict the extent of the cracking reaction and the temperature profile in the reactor to a satisfactorily level of detail. The reported conversion level of EDC agrees very well with the assumed conversion level out of the firebox of the EDC cracker in Stenungsund. The reported reactor temperature is about 5% higher than the measured temperature over the first 40-50 meters of the coil, but the last two temperature measurements are met by the model. This suggests that the endothermic cracking reaction starts at lower temperatures than expected, and this suggestion is supported by lab-scale tests. With thermodynamical data for all species, and reaction rate constants for all reactions between them, a reaction mechanism of any size can be entered into the Matlab model. Detailed reaction mechanisms can be used to investigate the effect of impurities in the feed on EDC conversion, monitor byproduct formation, and even be combined with coking models to predict coke formation in the cracker. There are of course limitations due to the one-dimensional formulation of the conservation equations in the PFR model. The effects of hot- or cold spots along the cracker will be smoothed out because of averaging over the cross section. The result is that the profiles for temperature, velocity and process fluid compositions will only represent the average value at a given position. Based on the results in this work, and the work conducted by Choi et al. and Park et al. the reactor model can, however, be regarded as fully representative for the reaction coil in an EDC cracker.

The firebox model developed in Fluent gives a good representation of the geometry of the EDC cracker in Stenungsund. With a heatflux along the coil temperature distributions in the flue gas, the refractory, and along the reaction coil can be computed. The assumption that the heatflux is even over the entire cross section of the coil, resulted in cold spots on the shadow side of the coil. These are probably due to the fact that the imposed heatflux profile dictates that energy, that is not available at the shadow side, should be transferred to the coil. Simulations without a shock coil representation showed that this is not a fully representative model, as the temperature on the upper tubes of the coil becomes too high. On the other hand, the cold spots on the shadow side of the coil led to computational instability in the cases with lowered flue gas inlet temperature and a shock coil heat sink. A thorough model for the EDC cracker can thus not be made without including the shock coil, but in a more detailed way than using a single volumetric heat sink.

Considering the simplifications that have been made in the CFD model of the cracker, the results from the simulations are quite interesting. With a given heatflux, the model computes a temperature profile along the coil that is very similar in shape to both that computed by the Matlab reactor model, and the temperatures measured through thermography. The same fluctuations in outer surface temperature on the coil are observed in the CFD model as in the thermographic data.

A summary of the most important results of the different simulation cases are given in the list below.

Original Boundary conditions Shows that to assume that the flue gas is at its adiabatic flame temperature in the combustion zone is a gross overprediction of temperature level. The outer surface temperature of the coil is 3-400 K higher than expected, and refractory and flue gas exit temperatures are both approximately 200 K too high.

Increased mass flow and lower temperature The first case with modified boundary conditions, show that the effects of air drawn into the cracker by other means than through the burners (e.g. leaks) results in a substantial reduction of coil temperature. Between the case with original boundary conditions and this case, the delivered heat to the cracker is nearly unchanged, but the coil temperature is 100-150 K lower in the latter case.

Further investigations of non-adiabatic operation By lowering the flue gas inlet temperature even further, the effects of non-adiabatic operation could be observed. From the case with an inlet temperature of 1800 K to the one with 1700 K, the coil temperature was reduced with almost 200 K. The mass flow of flue gas was the same in both simulations. This reduction in temperature clearly shows the effect of temperature being raised to a power of four in the radiative heat transfer equation.

Modified firing profile The last simulation case had a firing profile modified to match the one used in the actual cracker, the total mass flow and temperature of the flue gas was unchanged from the 1700 K case. With harder firing in the top of the cracker, the temperature along the coil was affected the most in the lower parts of the cracker. The middle part of the coil (40 to 100 meters) seems to be unaffected by the lack of a shock coil representation and the step in heatflux profiles from the fourth to third (from the bottom) tube. In this section the average temperature profile from Fluent and that from Matlab are similar in the case with a modified firing profile.

The summary above shows that the CFD model can be used to represent the EDC cracker in Stenungsund, but that there is need for knowledge of the temperature in the combustion zone to make the model accurate. As there is no apparent way of obtaining the temperature level in the combustion zone, other than the upper limitation given by the adiabatic flame temperature, the conclusion must be that to represent the burners by flue gas alone is not sufficient. A simulation that establishes the temperature level of the gas in the combustion zone should be conducted. This can either be done with the computational network already established through this work, in a two-dimensional case, or in a three-dimensional segment of the mesh used in this work.

The different simulations with varying flue gas inlet temperature show that it is possible to use the flue gas inlet temperature in order to tune the simulation model. However, with the CFD model being like it is, only trial and error can be used to determine the values for the inlet temperature. This trial and error method is not the form of integration, or interaction that is aimed at. With the current model, the heatflux profile along the reaction coil must be known prior to running a Fluent simulation. With other words one has to assume that a key parameter in the cracker, namely the heatflux to the reaction coil, is known in order to compute the temperature distribution. Park et al. run a two dimensional CFD simulation in their work [29]. Polynomial fitting to measured process fluid temperature in the reaction coil is used to get an analytical expression of temperature

as a function of position. This fluid temperature and a convective heat transfer coefficient are used as boundary conditions on the inner surface of the coil tubes. With temperature and heat transfer coefficient as the boundary condition, the heatflux to the reaction coil at the given firing conditions can be computed by Fluent. This approach seems more favourable for integrating the two models, inasmuch as there is no need for knowledge of the heatflux along the coil, only an expression for temperature. However, it is still not a coupled simulation of the process- and firebox side of the cracker, since knowledge of a key parameter is needed prior to running simulations.

To arrive at a model that can fully describe the EDC cracker and be used for optimization of its operation, a coupling of the two models is required. With the Matlab model yielding results that agree with measured and assumed data, it is believed that the one-dimensional PFR model is sufficient for modeling the cracking reaction. There are different ways of coupling the two models, some suggested methods, together with some comments about them, are listed below.

Communication through files An automated version of the coupling used in this work. After a Fluent or Matlab simulation has been run, data are written to files. User Defined Functions (UDF) are used to read and write such files in Fluent. This coupling does not require any change in the models, but reduces the number of steps in the communication between the two, as there is no need for manual data preparation.

PFR model as C-code Computer routines written in the programming language C can be fully integrated in Fluent. By writing an integrator in C, the governing equations for the cracking reaction can be solved within Fluent. By using this approach, there is no longer the need to import heatflux profiles to Fluent, as the cracking reaction is included in the model and thus represents the heat sink. As the coil is represented as 11 straight, independent, tubes in the model used in this work, special routines must be written to ensure that the process model is continuous.

Extend grid and include the coil By meshing not only the tube wall of the coil, but also the process fluid zone, the entire cracking reaction can be simulated in one Fluent model. This approach will be computationally demanding, but can probably yield quite accurate results.

The first suggestion is only an improvement of the method used thus far, it just involves less manual interaction. In this method, the temperature profiles from both models must be compared to each other, and the conversion level of EDC compared to its assumed value of 50 wt-%. In the two other methods, convergence can only be monitored through the EDC conversion level, and the temperature level of the flue gas must be adjusted accordingly.

References

- [1] J. Brandrup, E. H. Immergut, and E. A. Grulke. *Polymer Handbook*. John Wiley & sons, fourth edition, 1999.
- [2] B.S. Choi, J.S. Oh, S.W. Lee, H. Kim, and J.H. Yi. Simulation of the effects of ccl4 on the ethylene dichloride pyrolysis process. *INDUSTRIAL & ENGINEERING CHEMISTRY RESEARCH*, 40:4040–4049, 2001.
- [3] A.G. Borsa, A.M. Herring, J.T. McKinnon, R.L. McCormick, S. Yamamoto, Y. Teraoka, and Y. Natori. Characterization of coke formed in vinyl chloride manufacture. *INDUSTRIAL & ENGINEERING CHEMISTRY RESEARCH*, 38:4259–4267, 1999.
- [4] Hydro Polymers. Flow sheets and technical drawings, received from Gunde Persson, Hydro Polymers Stenungsund [01.02.2007].
- [5] Operational data for the HPS EDC cracker 01.07 - 01.10.05. Recieved from P. Saxegaard [26.01.07].
- [6] Terje Fuglerud Hydro's Oil and Energy Research Centre, Porsgrunn - personal communication.
- [7] M.J. Moran and H.N. Shapiro. *Fundamentals of engineering thermodynamics*. John Wiley & sons, third edition, 1998. pp. 124f, 756.
- [8] E. Ranzi, M. Dente, M. Rovaglio, T. Faravelli, and S.B. Karra. Pyrolysis and chlorination of small hydrocarbons. *CHEMICAL ENGINEERING COMMUNICATIONS*, 117:17–39, 1992.
- [9] J.A. Manion. Evaluated enthalpies of formation of the stable closed shell c1 and c2 chlorinated hydrocarbons. *JOURNAL OF PHYSICAL AND CHEMICAL REFERENCE DATA*, 31:123–172, 2002.
- [10] C.L. Yaws. *Chemical properties handbook : physical, thermodynamic, environmental, transport, safety, and health related properties for organic and inorganic chemicals*. McGraw-Hill handbooks. McGraw-Hill, 1999. E-book available through NTNU.
- [11] K. Stigeborn. Månadsrapport VCM produktion Februari 2007. Monthly operational report from the VCM plant at Hydro Polymers Stenungsund. Available through the company intranet. In Swedish.
- [12] G.W. Lauesen. Infrarød termografi kontroll hos Hydro Polymers Stenungsund. Crackerovn R-201. Thermographic control at HPS [16.03.2007]. In Norwegian.
- [13] Fluent Inc. Gambit 2.3 user's guide. <http://www.fluentusers.com>.
- [14] Fluent Inc. Fluent 6.3 user's guide. <http://www.fluentusers.com>.
- [15] T.H. Kaggerud. CFD Modeling of an EDC-cracker. Project report, The Norwegian University of Science and Technology, 2006.
- [16] B.E. Launder and D.B Spalding. The numerical computation of turbulent flows. *COMPUTER METHODS IN APPLIED MECHANICS AND ENGINEERING*, 3:269–289, 1974.
- [17] I.S. Ertesvåg. *Turbulent Strøyming og Forbrenning*. Tapir akademisk forlag, 2000. In Norwegian. pp. 45f.
- [18] L. Wahlqvist. Brännare krackugn HPS VCM fabrikk. Descriptions of burners at HPS. Telefax to E. Manger [20.06.2002]. In Swedish.

- [19] S. R. Turns. *An introduction to combustion*. McGraw-Hill, second edition, 2000. pp. 200f.
- [20] Petter Saxegaard. HPS furnace with expanded adiabatic volume. EDC CRACK simulation printout [20.05.2006].
- [21] R. Viskanta and M.P. Menguc. Radiation heat-transfer in combustion systems. *PROGRESS IN ENERGY AND COMBUSTION SCIENCE*, 13:97–160, 1987.
- [22] F.P. Incropera and D.P. DeWitt. *Fundamentals of Heat and Mass transfer*. John Wiley & sons, fifth edition, 2002. pp. 477f, 738f, 821f, 917f.
- [23] H.C. Hottel and E.S. Cohen. Radiant heat exchange in a gas-filled enclosure - allowance for nonuniformity of gas temperature. *AICHE JOURNAL*, 4:3–14, 1958.
- [24] L. Teleaga, M. Seaid, I. Gasser, A. Klar, and J. Struckmeier. Radiation models for thermal flows at low mach number. *JOURNAL OF COMPUTATIONAL PHYSICS*, 215:506–525, 2006.
- [25] G.W. Faris. P-n approximation for frequency-domain measurements in scattering media. *APPLIED OPTICS*, 44:2058–2071, 2005.
- [26] A. Coppalle and P. Vervisch. The total emissivities of high-temperature flames. *COMBUSTION AND FLAME*, 49:101–108, 1983.
- [27] T.F. Smith, Z.F. Shen, and J.N. Friedman. Evaluation of coefficients for the weighted sum of gray gases model. *JOURNAL OF HEAT TRANSFER-TRANSACTIONS OF THE ASME*, 104:602–608, 1982.
- [28] P.M. Plehiers, G.C. Reyniers, and G.F. Froment. Simulation of the run length of an ethane cracking furnace. *INDUSTRIAL & ENGINEERING CHEMISTRY RESEARCH*, 29:636–641, 1990.
- [29] Y. Park, B.S. Choi, and J. Yi. Simulation of imbalance reduction between two reactors in an ethylene dichloride cracker. *CHEMICAL ENGINEERING SCIENCE*, 60:1237–1249, 2005.
- [30] F.M. White. *Fluid Mechanics*. McGraw Hill, fifth edition, 2003. pp. 24f, 362, 366.
- [31] L.F. Shampine and M.W. Reichelt. The matlab ode suite.
http://www.mathworks.com/access/helpdesk/help/pdf_doc/otherdocs/ode_suite.pdf
[14.09.2006].
- [32] K.E. Howlett. The pyrolysis of 1-2-dichloroethane. *TRANSACTIONS OF THE FARADAY SOCIETY*, 48:25–34, 1952.
- [33] Y.S. Touloukian, P.E. Liley, and S.C. Saxena. *Thermal conductivity. Nonmetallic liquids and gases*, volume 3 of *Thermophysical properties of matter*. IFI/Plenum, second edition, 1977.
- [34] G.F. Hewitt (ed). *Heat exchanger handbook 2002*. Begell House, 2002.
- [35] Petter Saxegaard Hydro’s Oil and Energy Research Centre, Porsgrunn - personal communication.
- [36] A. Grønvold. EDC Cracking: Low temperature cracking in the evaporator and cracking tube in the pilot unit. Internal Memo, 2004.
- [37] A.G. Borsa. *Industrial plant/laboratory investigation and computer modelling of 1,2-dichloroethane pyrolysis*. PhD thesis, Colorado School of Mines, 1999.
- [38] G.D. Stefanidis, B. Merci, G.J. Heynderickx, and G.B. Marin. CFD simulations of steam cracking furnaces using detailed combustion mechanisms. *COMPUTERS & CHEMICAL ENGINEERING*, 30:635–649, 2006.

- [39] I.R. Gran and B.F. Magnussen. A numerical study of a bluff-body stabilized diffusion flame. part 2. influence of combustion modeling and finite-rate chemistry. *COMBUSTION SCIENCE AND TECHNOLOGY*, 119:191–217, 1996.
- [40] K. Bech and E. Manger. EDC Cracking HPS: Proposal of improved burner design. Internal Memo, 2005.
- [41] Eirik Manger Hydro Aluminium Research Centre, Porsgrunn - personal communication.
- [42] G.W. Lauesen. Infrarød termografi kontroll hos Hydro Polymers Stenungsund. Crackerovn R-201. Thermographic control at HPS [27.04.2007]. In Norwegian.
- [43] T. Poinso and D. Veynante. *Theoretical and Numerical Combustion*. Edwards, second edition, 2005. p 2.
- [44] Technical data sheets for refractory materials, received from Gunde Persson, Hydro Polymers Stenungsund [01.02.2007].
- [45] Special Materials Corporation. Inconel 600 Technical Bulletin. <http://www.specialmetals.com/documents/Inconel%20alloy%20600.pdf> [27.03.2007].

A Acronyms

CFD Computational Fluid Dynamics

DO Discrete Ordinates

EDC Ethylene Dichloride

HCl Hydrogen chloride

PFR Plug Flow Reactor

PVC Polyvinyl Chloride

RANS Reynolds Averaged Navier Stokes

UDF User Defined Functions

VCM Vinyl Chloride Monomer

WSGGM Weighted-sum-of-gray-gases Model

B Basic equations

Combustion involves reactions between different species, and describing a combusting flow involves both the chemical reactions between the species and the flow itself. In fluid mechanics, the Navier-Stokes equations are used to give a mathematical description of, usually non-reacting, fluid flows. For such a non-reacting system 5 equations need to be solved. However, when reacting systems are described with the Navier-Stokes equations, each of the N species considered in the reacting flow gets its own equation, resulting in a total of $5+N^8$ equations [43].

B.1 Reynolds averaged Navier-Stokes equations

The development of the time averaged Navier-Stokes equations given below uses Cartesian tensor notation. In a three dimensional Cartesian coordinate system, $[x \ y \ z]$, the indices i and j represent the direction in the coordinate system. Tensor notation makes the equations more compact and comprehensible. However, one should be aware that a second order tensor, such as τ_{ij} , has 9 elements.

Continuity:

$$\frac{\partial \rho}{\partial t} + \frac{\partial}{\partial x_j}(\rho u_j) = 0 \quad (\text{B.1})$$

Conservation of momentum:

$$\frac{\partial}{\partial t}(\rho u_i) + \frac{\partial}{\partial x_j}(\rho u_i u_j) = -\frac{\partial p}{\partial x_i} + \frac{\partial \tau_{ij}}{\partial x_j} + \rho f_i \quad (\text{B.2})$$

Conservation of species:

$$\frac{\partial}{\partial t}(\rho Y_k) + \frac{\partial}{\partial x_j}(\rho Y_k u_j) = \frac{\partial}{\partial x_j} \left(\rho \mathcal{D} \frac{\partial Y_k}{\partial x_j} \right) + R_k \quad (\text{B.3})$$

Conservation of energy:

$$\frac{\partial}{\partial t}(\rho E) + \frac{\partial}{\partial x_j}[u_j(\rho E + p)] = \frac{\partial}{\partial x_j} \left(\lambda \frac{\partial T}{\partial x_j} - \sum_{i=1} h_j J_j + u_j \tau_{ij} \right) + S_h \quad (\text{B.4})$$

In equation (B.2) the last term ρf_i is the contribution from distant forces, such as gravity. This term is often neglected. The stress tensor τ_{ij} can take different forms depending on the fluid. Fick's law of mass diffusion has been introduced in the first term on the right hand side of equation (B.3). To avoid an unwieldy expression for the mass diffusivity coefficient, \mathcal{D} , it has been taken as equal for all species. The energy equation (B.4), is the equation solved in Fluent. The terms in brackets on the right hand side are heat transfer by conduction, species diffusion and viscous dissipation, respectively. The last term on the right hand side is a source term, accounting for any internal sources of energy, such as reactions and radiation.

To give a manageable set of equations for turbulent flow, equations (B.1 - B.4) must be rewritten into equations for mean values. The development of the Reynolds averaged equation for conservation of momentum will be given below, and to derive the full set of Reynolds averaged Navier-Stokes

⁸Actually $5+(N-1)$ equations should be sufficient, the last (bulk) species can be calculated by an algebraic relation.

equations (often referred to as RANS) the same method is applied. The density is taken as constant throughout the development.

Step 1 - Introduce Reynolds averaging to each property in the equation

$$u = \bar{u} + u' \quad , \quad p = \bar{p} + p' \quad , \quad \tau_{ij} = \bar{\tau}_{ij} + \tau'_{ij} \quad , \quad f_i = \bar{f}_i + f'_i$$

This gives the slightly different form of equation (B.2):

$$\frac{\partial}{\partial t}(\rho(\bar{u}_i + u'_i)) + \frac{\partial}{\partial x_j}(\rho(\bar{u}_i + u'_i)(\bar{u}_j + u'_j)) = -\frac{\partial(\bar{p} + p')}{\partial x_i} + \frac{\partial(\bar{\tau}_{ij} + \tau'_{ij})}{\partial x_j} + \rho(\bar{f}_i + f'_i) \quad (\text{B.5})$$

Step 2 - Take the average of each term in the equation

Equation (B.5) becomes:

$$\frac{\partial}{\partial t}(\rho(\overline{\bar{u}_i + u'_i})) + \frac{\partial}{\partial x_j}(\rho(\overline{\bar{u}_i \bar{u}_j} + \overline{\bar{u}_i u'_j} + \overline{\bar{u}_j u'_i} + \overline{u'_i u'_j})) = -\frac{\partial(\overline{\bar{p} + p'})}{\partial x_i} + \frac{\partial(\overline{\bar{\tau}_{ij} + \tau'_{ij}})}{\partial x_j} + \rho(\overline{\bar{f}_i + f'_i}) \quad (\text{B.6})$$

Step 3 - Simplify the equation

To simplify equation (B.6), the following rules of averaging are employed (shown here for two generic variables, Φ and Ψ):

$$\overline{\bar{\Phi}} = \bar{\Phi} \quad , \quad \overline{\bar{\Phi}'} = 0 \quad , \quad \overline{\bar{\Phi}\bar{\Psi}} = \bar{\Phi}\bar{\Psi} \quad , \quad \overline{\bar{\Phi}'\bar{\Psi}'} \neq 0$$

This means that terms including only one fluctuation, e.g. $\overline{\bar{u}_i u'_j}$ becomes zero. This leads to the Reynolds averaged equation for conservation of momentum:

$$\frac{\partial}{\partial t}(\rho\bar{u}_i) + \frac{\partial}{\partial x_j}(\rho\bar{u}_i\bar{u}_j) = -\frac{\partial\bar{p}}{\partial x_i} + \frac{\partial}{\partial x_j}(\bar{\tau}_{ij} - \overline{u'_i u'_j}) + \rho\bar{f}_i \quad (\text{B.7})$$

Similarly, the continuity equation and transport equations for species and energy can be expressed in Reynolds averaged form:

Continuity:

$$\frac{\partial\bar{u}_j}{\partial x_j} = 0 \quad \text{and} \quad \frac{\partial\bar{u}'_j}{\partial x_j} = 0 \quad (\text{B.8})$$

Conservation of species:

$$\frac{\partial}{\partial t}(\rho\bar{Y}_k) + \frac{\partial}{\partial x_j}(\rho\bar{Y}_k\bar{u}_j) = \frac{\partial}{\partial x_j}(\rho\mathcal{D}\frac{\partial\bar{Y}_k}{\partial x_j} - \rho\overline{Y'_k u'_j}) + \bar{R}_k \quad (\text{B.9})$$

Conservation of energy⁹:

$$\frac{\partial}{\partial t}(\rho E) + \frac{\partial}{\partial x_i}[\bar{u}_i(\rho E) + \bar{p}] = \frac{\partial}{\partial x_j} \left[\lambda \frac{\partial\bar{T}}{\partial x_j} - \overline{u'_j T'} + \overline{u'_j \tau'_{ij}} \right] + \bar{S}_h \quad (\text{B.10})$$

⁹This equation is partially rewritten into a temperature equation.

B.2 Closure of the equations

By Reynolds averaging the equations, they are rewritten as equations for average properties, and can be solved numerically. However, each equation involves a correlation between two fluctuations; $-\overline{\Phi'\Psi'}$. These correlations are unknown and the set of equations now includes more unknowns than equations. This means that the set of equations needs to be closed in order to be solved.

A much used way of closing the equations is to employ the k- ε model, where the two parameters average turbulence energy, k, and dissipation of turbulence energy, ε , are modeled through transport equations.

The most widely used k- ε model was presented in its final form by Launder and Spalding in 1974 [16], and this version is often referred to as the standard k- ε model. The equations and constants going into the model are given below.

The turbulent energy, k, is defined as:

$$k \equiv \frac{1}{2} \overline{u'_i u'_i} \quad (\text{B.11})$$

The Reynolds stresses are modeled as:

$$-\rho \overline{u'_i u'_j} = \mu_t \left(\frac{\partial \overline{u}_i}{\partial x_j} + \frac{\partial \overline{u}_j}{\partial x_i} \right) - \frac{2}{3} \rho k \delta_{ij} \quad (\text{B.12})$$

Transport equations for turbulence energy, k, and turbulence energy dissipation, ε are expressed as¹⁰:

$$\frac{\partial}{\partial t}(\rho k) + \frac{\partial}{\partial x_j}(\rho k \overline{u}_j) = \frac{\partial}{\partial x_j} \left(\left(\mu + \frac{\mu_t}{\sigma_k} \right) \frac{\partial k}{\partial x_j} \right) + \mu_t \left(\frac{\partial \overline{u}_i}{\partial x_j} + \frac{\partial \overline{u}_j}{\partial x_i} \right) \frac{\partial \overline{u}_i}{\partial x_j} - \rho \varepsilon \quad (\text{B.13})$$

$$\frac{\partial}{\partial t}(\rho \varepsilon) + \frac{\partial}{\partial x_j}(\rho \varepsilon \overline{u}_j) = \frac{\partial}{\partial x_j} \left(\left(\mu + \frac{\mu_t}{\sigma_\varepsilon} \right) \frac{\partial \varepsilon}{\partial x_j} \right) + C_{\varepsilon 1} \frac{\varepsilon}{k} \mu_t \left(\frac{\partial \overline{u}_i}{\partial x_j} + \frac{\partial \overline{u}_j}{\partial x_i} \right) \frac{\partial \overline{u}_i}{\partial x_j} - C_{\varepsilon 2} \frac{\varepsilon}{k} \rho \varepsilon \quad (\text{B.14})$$

The turbulent viscosity is modelled as:

$$\mu_t = C_\mu \rho \frac{k^2}{\varepsilon} \quad (\text{B.15})$$

The different constants in the equations have values of:

$$C_\mu = 0.9 \quad , \quad C_{\varepsilon 1} = 1.44 \quad , \quad C_{\varepsilon 2} = 1.92 \quad , \quad \sigma_k = 1.0 \quad , \quad \sigma_\varepsilon = 1.3 \quad (\text{B.16})$$

This model closes the Reynolds-averaged equation for momentum. However the correlations $-\overline{Y'_k u'_j}$ and $-\overline{u'_j T'}$ from equation (B.9) and (B.10) respectively have yet to be resolved. A common way of modeling these correlations is to use gradient models, and this is the approach used in Fluent.

¹⁰Launder and Spalding actually takes density as constant in their model equations, yielding slightly different equations than equation (B.13) and (B.14) where density is also allowed to vary but not fluctuate.

When using a gradient model, the correlations are modelled as:

$$-\overline{Y'_k u'_j} = \frac{\nu_t}{\sigma_Y} \frac{\partial \overline{Y_k}}{\partial x_j} \quad (\text{B.17})$$

$$-\overline{u'_j T'} = \frac{c_p \mu_t}{\sigma_h} \frac{\partial T}{\partial x_j} \quad (\text{B.18})$$

In equations (B.17) and (B.18) the coefficients σ_Y and σ_h are called turbulent Schmidt number and turbulent Prandtl number respectively, both coefficients are assigned values between 0.7 and 0.9¹¹. ν_t is the kinematic turbulent viscosity, $\frac{\mu_t}{\rho}$.

The term $\overline{u'_j \tau'_{ij}}$ in equation (B.10) is, in Fluent, modeled with an effective stress tensor, $(\tau_{ij})_{\text{eff}}$ defined as for a Newtonian fluid:

$$(\tau_{ij})_{\text{eff}} = \mu_t \left(\frac{\partial \overline{u_j}}{\partial x_i} + \frac{\partial \overline{u_i}}{\partial x_j} \right) - \frac{2}{3} \mu_t \frac{\partial \overline{u_i}}{\partial x_i} \delta_{ij} \quad (\text{B.19})$$

The correlation $\overline{u'_j \tau'_{ij}}$ is modeled as:

$$\overline{u'_j \tau'_{ij}} = \overline{u_j} (\tau_{ij})_{\text{eff}} \quad (\text{B.20})$$

The motivation for using gradient models for the remaining correlations is that the k- ϵ -model gives a description of the turbulent motion in the flow, and it is this same turbulent motion that transports both energy, momentum and species.

¹¹Fluent uses 0.7 and 0.85 as the default values for the turbulent Schmidt number and turbulent Prandtl number.

C Plug Flow Reactor model

In this work a combination of Plehiers PFR model, and the model found in Turns is used [19,28]. Plehiers equation set was originally used for simulations of an ethane cracking furnace, but have later been used for simulations of EDC crackers by both Choi et al. and Park et al. [2,29].

C.1 Original equation set

As state variables Plehiers uses temperature, pressure and molar flux. Choi rewrites the pressure equations into a velocity equation, and the equation set used by both Choi and Park is therefore:

$$\frac{dF_k}{dx} = R_k \frac{\pi d_t^2}{4} \quad (\text{C.1})$$

$$\frac{dT}{dx} = \frac{1}{\sum_{k=1}^K F_k c_{p,k}} \left[q''(x) \pi d_t + \frac{\pi d_t^2}{4} \sum_{i=1}^I r_i (-\Delta H_{rx,i}) \right] \quad (\text{C.2})$$

$$\rho u \frac{du}{dx} = -\frac{dp}{dx} - \left[\frac{2f}{d_t} + \frac{\zeta}{\pi r_b} \right] \rho u^2 \quad (\text{C.3})$$

In the above equations, F_k is the molar flux of component F in a given position x . The two last terms on the right hand side of equation (C.3) is the pressure drop due to friction in the straight tubes and pipe bends, respectively

C.2 Modified equation set

The equation set presented by Plehiers is well suited for computer programming, however a few modifications are made to simplify the calculations.

The pressure gradient in equation (C.3) is evaluated using the ideal gas equation of state;

$$\frac{dp}{dx} = \frac{d}{dx} \left(\frac{\rho RT}{MW} \right) \quad (\text{C.4})$$

By using the chain rule of derivation it can be shown that the pressure gradient can be expressed as [19]:

$$\frac{dp}{dx} = p \left[\frac{1}{\rho} \frac{d\rho}{dx} + \frac{1}{T} \frac{dT}{dx} - \frac{1}{MW} \frac{dMW}{dx} \right] \quad (\text{C.5})$$

To avoid adding more state variables to the equation set, the density gradient can be expressed by means of the velocity gradient. This is done by using the mass conservation equation for a PFR [19]:

$$\frac{d(\rho u A)}{dx} = 0 \quad (\text{C.6})$$

With constant tube diameter, the area of the PFR is constant and hence:

$$\frac{1}{\rho} \frac{d\rho}{dx} = -\frac{1}{u} \frac{dv_x}{dx} \quad (\text{C.7})$$

By assuming that the pressure drop in the pipe bends is negligible, the PFR equation set used in this work becomes:

$$\frac{dF_k}{dx} = R_k \frac{\pi d_t^2}{4} \quad (\text{C.8})$$

$$\frac{dT}{dx} = \frac{1}{\sum F_k c_{p,k}} \left[q''(x) \frac{4}{d_t} + \sum_{i=1}^I r_i (-\Delta H_{rx,i}) \right] \quad (\text{C.9})$$

$$\frac{du}{dx} = \frac{-1}{(\rho u - \frac{p}{u})} \left[\frac{p}{T} \frac{dT}{dx} - \frac{p}{MW_{mix}} \frac{dMW_{mix}}{dx} + \frac{2f}{d_t} \rho u^2 \right] \quad (\text{C.10})$$

The molecular weight gradient introduced in the above equations, does not result in an additional state variable, as the gradient can be expressed as:

$$\frac{dMW_{mix}}{dx} = -MW_{mix}^2 \sum_{k=1}^K \frac{1}{MW_k} \frac{dY_k}{dx} = -\frac{MW_{mix}^2}{\rho u} \sum_k R_k \quad (\text{C.11})$$

D Thermophysical data

Thermophysical data for refractory materials, coil material and process fluid are needed at various stages of the simulations. In this appendix the thermophysical data used in this work is listed.

D.1 Refractory materials

Thermophysical data for the refractory materials are taken from datasheets made available by the suppliers [44]. For steady state calculations, density and thermal conductivity need to be given in Fluent. New materials representing the three refractory materials have been added to the Fluent materials list. In addition the surface emissivity for the materials making up the inner surface of the cracker is added as a boundary condition. In Table D.1 the density, which is taken as constant, and the thermal conductivity at different temperatures are given for the refractory materials.

Table D.1: Thermophysical data for refractory materials

MPK - 125						Unit
Density	670					kg/m ³
Temperature	473	673	873	1073	1273	K
Thermal conductivity (T)	0.18	0.2	0.22	0.24	0.26	W/mK
Emissivity (T)	0.8	0.8	0.8	0.8	0.8	1
Skamolex						
Density	245					kg/m ³
Temperature	473	673	873			K
Thermal conductivity (T)	0.07	0.09	0.10			W/mK
Rodarox						
Density	2800					kg/m ³
Temperature	973	1473				K
Thermal conductivity (T)	1.90	1.70				W/mK
Emissivity (T)	0.8	0.8				1

D.2 Coil material

According to the original technical drawings of the cracker, the entire coil, including convection- and shock coil, are made from the alloy Inconel 600. This high nickel alloy is widely used in processes where its heat and corrosion resistance is needed. An extensive overview of its technical- and thermophysical properties are given by Special Metals Corporation [45]. For a range of temperatures, thermal conductivity and total normal emissivity are given in Table D.2.

Table D.2: Thermophysical data for Inconel 600 [45]

Temperature (K)	Thermal Conductivity (W/mK)	Total normal emissivity
373	15.9	-
473	17.3	-
573	19	-
673	20.5	-
753	-	0.85
773	22.1	-
873	23.9	-
923	-	0.87
973	25.7	-
1073	27.5	-
1088	-	0.9
1253	-	0.95
1363	-	0.98

The density and specific heat of the alloy are taken as constant. Numerical values are 8470 kg/m^3 and 444 J/kgK respectively. As for the refractory material, surface emissivity is given as a boundary condition at the wall surface.

D.3 Process fluid properties

In the cracking reaction modeling only EDC, VCM and HCl are considered. To calculate the heat transfer coefficient in the fluid, a few thermophysical properties must be known. Viscosity, thermal conductivity and Prandtl number are all assumed to be independent of pressure, and only depending on temperature. The numerical values are taken from Heat Exchanger Design Handbook [34].

Table D.3: Thermophysical properties for process gases

EDC									Unit
Temperature	273	298	373	473	573	673	773	873	K
Viscosity	8.46	9.20	11.38	14.21	16.95	19.64	22.27	24.85	$\mu\text{Pa}\cdot\text{s}$
Thermal conductivity	7.33	8.58	12.75	19.21	26.55	34.64	43.35	52.59	mW/mK
Prandtl number	0.86	0.84	0.79	0.76	0.72	0.69	0.67	0.64	1
VCM									Unit
Temperature	273	298	373	473	573	673	773	873	K
Viscosity	9.35	10.24	12.80	16.01	19.01	21.83	24.50	27.03	$\mu\text{Pa}\cdot\text{s}$
Thermal conductivity	10.49	12.11	17.38	25.18	33.68	42.69	52.10	61.81	mW/mK
Prandtl number	0.73	0.73	0.73	0.73	0.72	0.71	0.69	0.68	1
HCl									Unit
Temperature	273	298	373	473	573	673	773	873	K
Viscosity	13.40	14.64	18.30	23.02	27.51	31.73	35.63	39.17	$\mu\text{Pa}\cdot\text{s}$
Thermal conductivity	13.10	14.41	18.15	22.76	26.95	30.78	34.28	37.49	mW/mK
Prandtl number	0.82	0.81	0.81	0.81	0.83	0.84	0.87	0.89	1

D.4 Flue gas properties

The flue gas is a mixture of water vapour, carbon dioxide, nitrogen and oxygen. In addition there are trace amounts of other species, such as carbon monoxide, nitrous oxides and some radicals. Only the main species are considered in this work, as the minor species are not believed to have a significant effect on the total heat transfer rate in the cracker. The radiative properties of the flue gas is given in the Section 4. Specific heat and thermal conductivity for the flue gas is given in Table D.4. The values are obtained from the Chemical Properties Handbook [10] for specific heats and Incropera and DeWitt [22] for thermal conductivity. The flue gas is assumed to be an ideal gas mixture, and its properties are calculated using a standard mixing law.

Table D.4: Specific heat and thermal conductivity of flue gas at different temperatures

Temperature [K]	Specific heat [kJ/kgK]	Thermal conductivity [W/mK]
500	1.126	0.039
900	-	0.060
1000	1.282	-
1100	-	0.070
1200	1.327	-
1300	-	0.081
1500	1.391	-
1800	1.454	-
2000	1.495	-

The viscosity and mass diffusivity are assumed to be constant and equal to $4.5 \cdot 10^{-5}$ kg/ms and $2.88 \cdot 10^{-5}$ m²/s respectively. The viscosity is the value for the flue gas at 1000°C with values from Incropera and DeWitt [22]. The mass diffusivity is the default value as given by Fluent. The density is calculated using the ideal gas equation of state.